Electrical Crosstalk

in

Multilayer Ceramic Substrates

by

In Kyeong Yoo

Dissertation submitted to the Faculty of the

Virginia Polytechnic Institute and State University

in partial fulfillment of the requirements for the degree of

Doctor of Philosophy

in

Materials Engineering Science

APPROVED:

L.C. Burton, Chairman

F.W. Stephenson, Co-Chairman

R.W. Hendricks

S. Onishi

A.A. Elshabini-Riad

A.L. Ritter

September, 1990

Blacksburg, Virginia

Electrical Crosstalk in Multilayer Ceramic Substrates

by

In Kyeong Yoo

L.C. Burton, Chairman F.W. Stephenson, Co-Chairman

Materials Engineering Science

(ABSTRACT)

Electrical crosstalk is becoming increasingly important as size shrinks and component densities increase in hybrid circuits. This occurs especially in multilayer thick film circuits. Crosstalk studies at high frequencies apply transverse electromagnetic (TEM) or quasi-TEM mode. However, the TEM mode theory is not applicable at low frequencies and low frequency-crosstalk is still a concern for circuit designers.

In this research, crosstalk equations were derived in a simpler way, which can be used for low frequency applications such as automotive electronics. Test patterns were designed in both single and multilayer substrates in order to study crosstalk parameters such as line separation, line width, ground distance, ground type, and multilayer thickness. The mutual inductance and the mutual capacitance were calculated in order to use them in predicting crosstalk for particular transmission line geometrical structures. A conventional technique was used for the mutual inductance, and a new conformal mapping technique was developed for the mutual capacitance.

Frequency dependence of crosstalk was confirmed by the equations developed. There is good agreement between the experimental mutual inductance and mutual capacitance and the calculated values. Finally, crosstalk prediction (simulated by combining crosstalk equations with calculated mutual parameters) fits well with the measured values.

Acknowledgements

The author would like to express his sincerest gratitude to Dr. L.C. Burton and Dr. F.W. Stephenson for their contributions and suggestions throughout this research effort. Their time and support are deeply appreciated. The author would also like to extend his thanks to Dr. R.W. Hendricks, Dr. S. Onishi, Dr. A.A. Elshabini Riad, and Dr. A.L. Ritter for their helpful suggestions and for serving on his committee. The author wishes to acknowledge financial support from E.I. DuPont de Nemours & Co., Inc. and Ford Motor Co., the Virginia Center for Innovative Technology and sponsors of the Hybrid Microelectronics Program at Virginia Tech, namely: AAI Corporation, Allied Signal Corporation, Analog Devices, C&P Telephone, General Electric Foundation, Motorola and Texas Instruments.

Special thanks are due to my family. Kyesook, my wife and Dongjoon, my son for their support and encouragement throughout this research effort. I would also like to express my special thanks to Gary Kunselman for his grammar corrections. Finally I would like to express my sincere thanks to Monty Hayes and Eric Ellis for their assistance with laboratory maintenance during my tenure in graduate school.

Table of Contents

List of Illustrations

Chapter I

Introduction

Recent trends in electronic systems are related to the reduction of device size combined with increased complexity in terms of the number of components as well as their function. This is the same trend found in thick film technology. Higher circuit densities can be achieved by using a multilayer system in combination with thick film devices. The simplest multilayer can be made by printing and firing dielectric layers sequentially. However, this multiple firing leads to imprecise dielectric thickness control and, above all, the number of layers is limited because conductor properties such as conductivity change after multiple firings. In order to improve these two problems, co-fired Al_2O_3 processing was developed. In this processing, circuits are printed on each alumina substrate separately, and then layers are collated, laminated, and co-fired. This technique gives high print resolution, good dielectric thickness control, surface smoothness, and an unlimited number of layers. Unfortunately, the process requires a high firing temperature, so that only modest conductivity metals such as W and Mo/Mn can be used.

One state-of-the-art multilayer system which combines the positive advantages of the above two processes is low temperature co-fired Green Tape™. In this technique, green dielectric tape, used for each separate layer, can be fired at a low firing temperature (850°C). This Green Tape™ shrinks in three dimensions after firing. Fortunately, however, since the shrinkage tolerance is relatively small (12.0±0.2%), such shrinkage can be taken into account in circuit design[1]. Another green tape system is called Tape-On-Substrate™ (TOS), in which green tape is

laminated onto an alumina substrate and fired. Each TOS substrate is fired separately. Even though relatively few layers are fabricated in this technique, it shows shrinkage in the *z*-direction only and dielectric thickness is still easily controlled (2.7 μm after firing)[1].

While these multilayer systems may guarantee high circuit density, they do have potential problems such as low heat dissipation, and electrical crosstalk. When a heat source exists somewhere in the multilayer ceramic, heat dissipation is difficult because the source is surrounded by bulky ceramic. Crosstalk, a form of signal interference, occurs between adjacent transmission lines due to the close conducting line separation in complex circuits. When a transmission line exists close to another line, the second line can pick up a signal from the first due to the mutual capacitance and mutual inductance that exists between them. This induced current signal may result in the circuit malfunctioning, especially in digital circuits. The Federal Communications Commission (FCC) Rules and Regulations (Part 15, Subpart J) requires of any commercial product marketed in the United States that "generates and uses timing signals or pulses at a rate in excess of 10,000 pulses (cycles) per second and uses digital techniques" must not radiate signals in excess of certain levels in the frequency range of 30 MHz to 1 GHz[2]. Emissions injected from the product into the commercial power mains also have to meet a similar requirement in the frequency range of 450 kHz to 30 MHz. Clock frequencies in excess of 10 kHz in digital electronic products are also regulated. Therefore, virtually all digital electronic products are subject to the FCC regulations. In order to satisfy the reliability of multilayer electronic devices which are subject to FCC regulations, the

circuit designer needs to be able to predict crosstalk for a given circuit design before manufacturing.

Several software programs are available to predict crosstalk for given transmission line structures (discussed further in Chapter II). These calculate mutual parameters (mutual inductance and mutual capacitance) using numerical techniques which assume that the skin effect is well developed at high frequencies (> 1 GHz)[3]. Such software is therefore not applicable to low frequency applications such as automotive electronics (< 100 MHz). IBM has developed its own software (ASTAP: The Advanced Statistical Analysis) which is a general-purpose network-analysis program. C.R. Paul[4] used ASTAP to predict crosstalk at frequencies lower than 100 kHz. However, he still applied relationships between inductance and capacitance which are valid only at high frequencies. He used this relationship to predict mutual inductance using mutual capacitance which was computed by numerical methods. This approximation was acceptable for transmission lines which are widely separated, as much as 30 mils. But, his prediction may be invalid when line spacing becomes narrower than 30 mils. Generally speaking, a rigorous crosstalk model at low frequency has yet to be developed.

A typical transmission line structure which gives rise to crosstalk is the parallel transmission line, sometimes called coupled lines. A coupled transmission line system consists of at least two ordinary transmission lines which have some form of coupling between them such that a voltage and/or current signal in one line will induce a voltage and/or current signal in the other line. There are two generic types of coupled lines in multilayer circuits: side-coupled and broad-coupled. Depending

on the characteristics of the ground, transmission lines can be classified into several structures. Fig. 1.1 shows some examples of parallel transmission lines and grounding configurations.

In order to analyze coupled lines, voltage is measured at both terminals of the second line. Fig. 1.2 shows crosstalk test diagrams where far-end and near-end crosstalk voltages (V_F and V_N) are defined in accordance with measurement position. Each line is terminated by a resistor (R_B, R_N, and R_F). R_S is the source resistance of the signal generator and V_S is the source voltage. Fig. 1.3 shows the equivalent test circuit, where the self-inductance and self-capacitance of each line, and the mutual inductance and the mutual capacitance between them are indicated. When coupled lines are analyzed, equivalent circuits such as Fig. 1.3-a and/or Fig. 1.3-b are used. In Fig. 1.3-a, a perfect ground without resistance and inductance is assumed. In reality, however, ground resistance and ground inductance should be considered for rigorous analysis, and Fig. 1.3-b is better suited for that case. Two mutual parameters exist between coupled lines in Fig. 1.3-a, but the mutual inductance term is actually loop inductance which consists of the partial mutual inductance and self-inductance of each line. Fig. 1.3-b shows these partial inductances and produces better models for crosstalk analysis. In the next section, crosstalk model and prediction will be reviewed briefly.

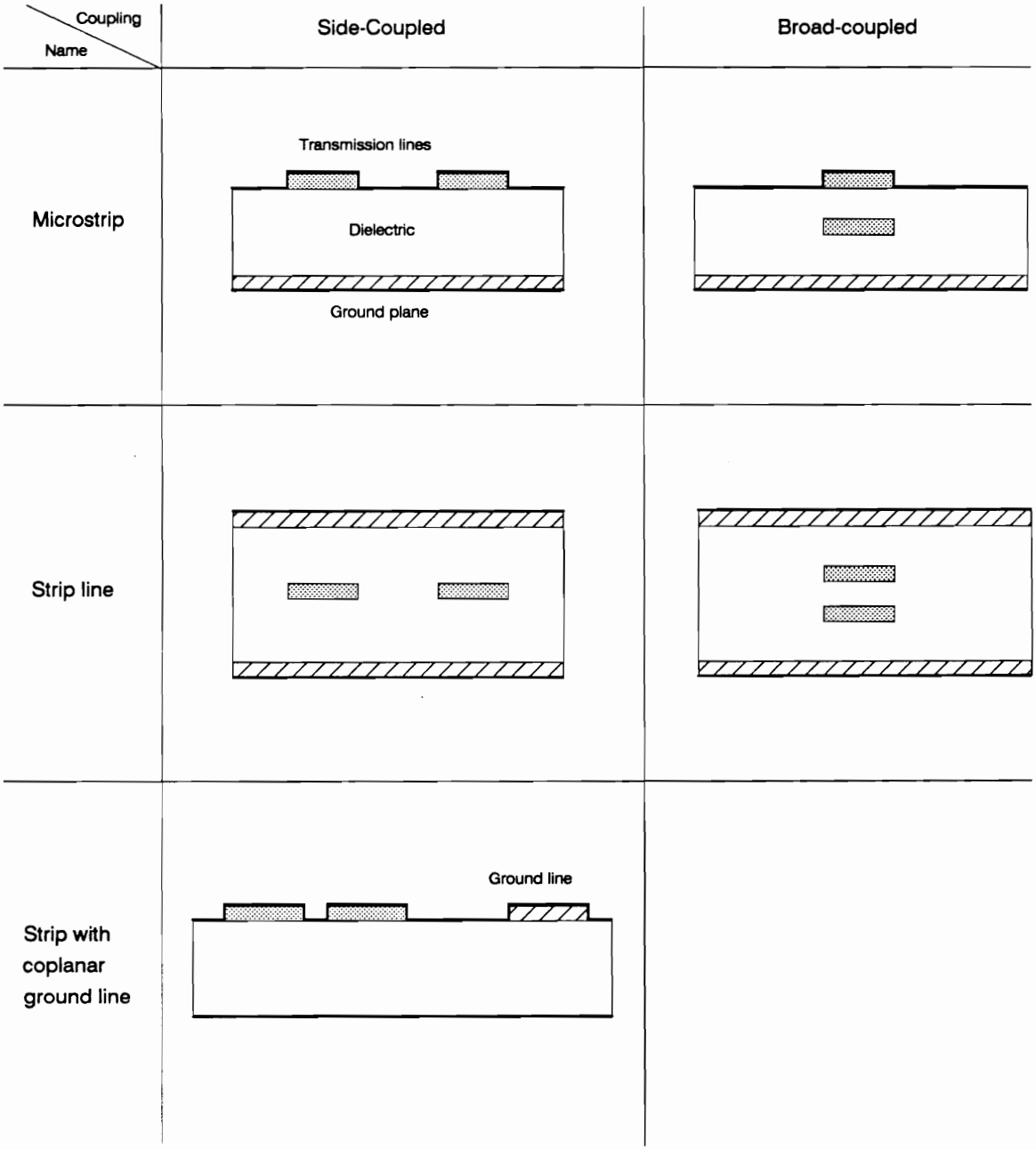

Fig. 1.1 Five structures for coupled parallel transmission lines

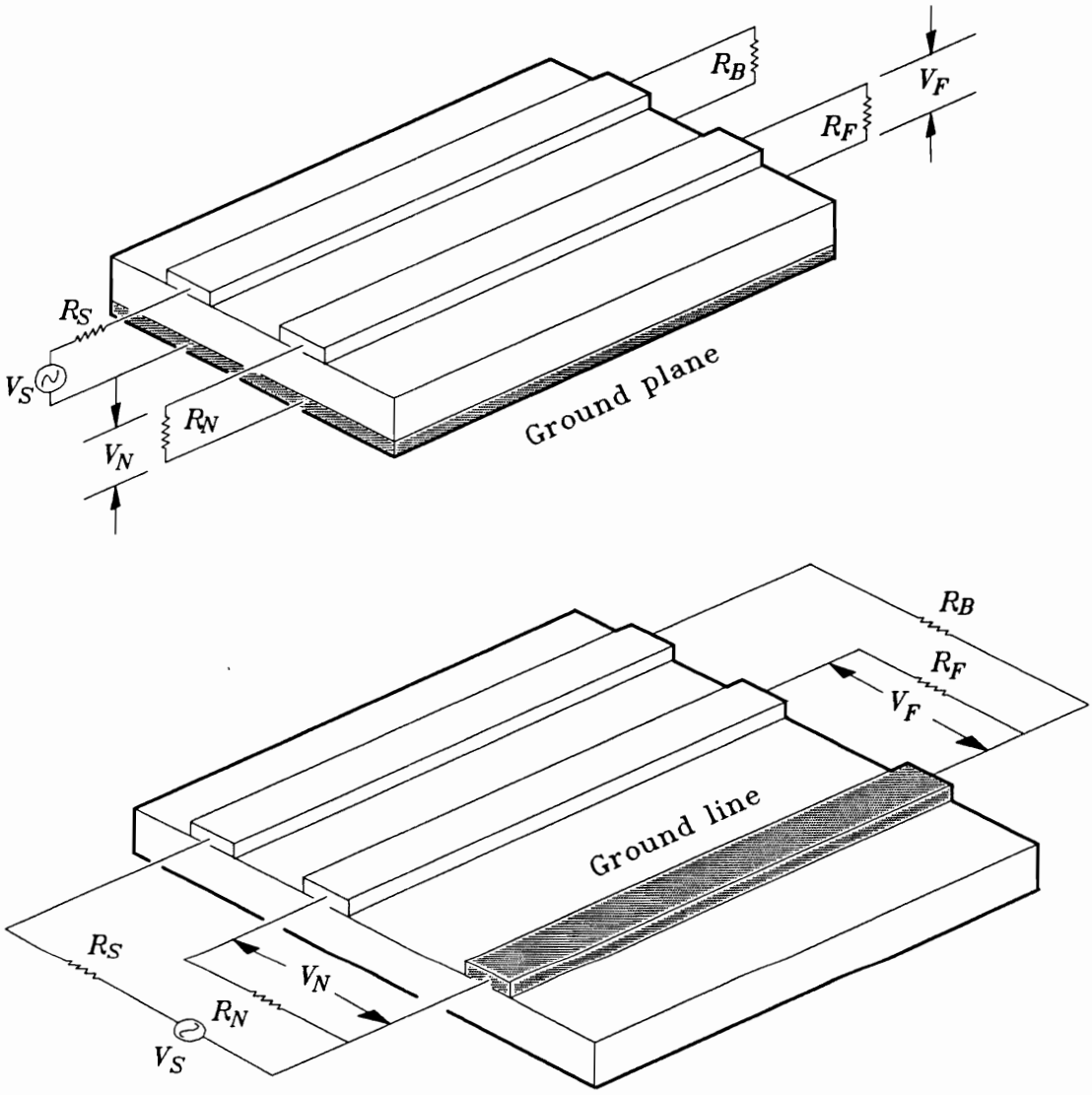

Fig. 1.2 Crosstalk test circuit diagrams with ground plane and ground line structures. Components are discussed in text.

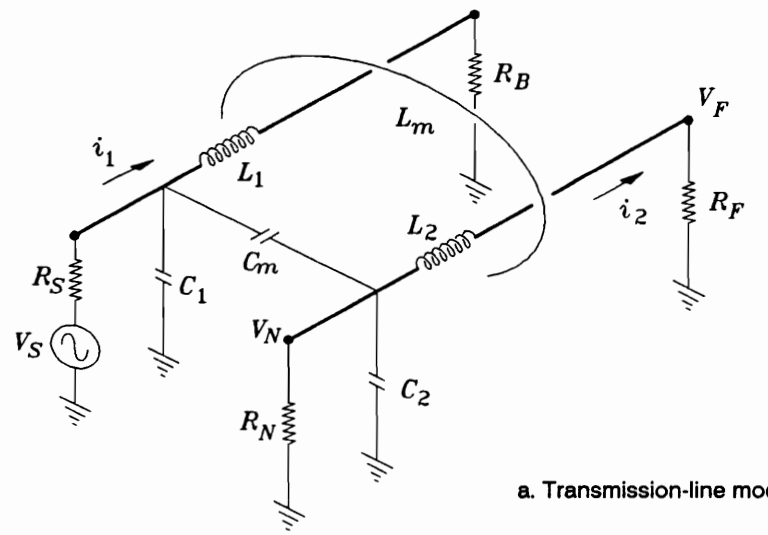

a. Transmission-line model

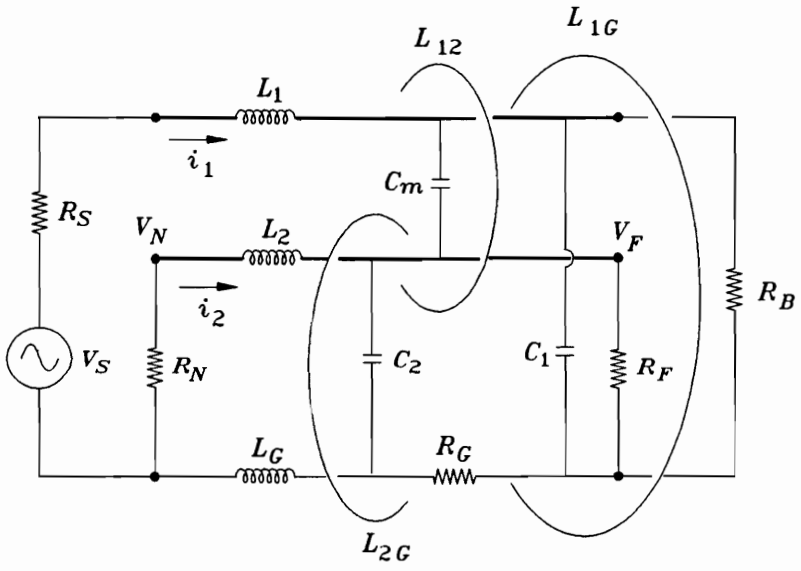

b. Lumped circuit model

Fig. 1.3 Equivalent circuits for coupled lines : a. shows loop inductance L_m and b. shows partial mutual inductances (L_{12}, L_{1G}, and L_{2G}) and considers ground inductance (L_G) and ground resistance (R_G).

Chapter II

Literature Review

§ 2.1 General overview

The simplest coupled transmission line consists of two conductors with a common return ground conductor. This type of coupled transmission line will be the main topic of discussion in this dissertation. Coupled transmission lines are identified in several ways, as shown by the examples below (input signal is applied to line 1).

Line 1	Line 2[5, 6]
generator	receptor[7]
active line	quiescent line[8]
active line	passive line[9]
driven conductor	idle conductor[10]
drive line	sense/pickup line[11]
interfering line	victim line[12]
source line	receptor line[13]

Analysis of coupled lines has been studied in several ways. In 1947, two symmetric parallel wire lines immersed in a homogeneous medium were studied by M. Cotte[14]. He derived a general solution using "telegrapher's equations" with transverse electromagnetic (TEM) propagation. L.J. Greenstein and H.G. Tobin studied multiple cable-coupled interference, and found a rigorous solution for

crosstalk using a Laplace transform technique[15]. With the subsequent increase in digital circuit speeds and denser component packing, crosstalk problems have spread to backplane wiring, circuit boards, etc.. I. Catt obtained the same results as Cotte's solutions using Laplace transform technique for two coupled transmission lines[16]. For practical computer wiring, D.B. Jarvis introduced a weak coupling approximation called "loose-coupling theory" (which neglects the effect of line 2 on line 1)[6]. "Close-coupling theory", in contrast to Jarvis' analysis, considers the effect of line 2 on line 1[9]. A qualitative description of the nature of the crosstalk signals for pulse-driven interconnecting lines was presented by A. Feller et al[11]. They made an attempt to separate the coupling into independent capacitive- and inductive-coupling, and then to superimpose their solutions. In their studies, a general expression for the transient crosstalk signal voltage between lines in a nonhomogeneous medium was derived. V.K. Tripathi, in 1975, developed general solutions for asymmetric coupled transmission lines in an inhomogeneous medium[17]. He discussed a solution for symmetric coupled lines in a homogeneous medium as a special case of a general solution. In the above cases, crosstalk analysis for transmission lines was studied with TEM or "quasi-TEM" propagation assumptions for high frequency applications. In 1967, R.J. Mohr reported crosstalk studies at low frequencies, where TEM mode can not be assumed[12]. C.R. Paul developed a solution for three conductor lines (one being a common ground line) in homogeneous media using matrix chain parameters[7, 18]. The general solution was complicated, and a low-frequency approximation was used to simplify the expressions. A.J. Rainal reported a crosstalk model which could be applied to arbitrary pulse, periodic, and random signals[10].

Once crosstalk equations are established, the next step is to predict crosstalk

from given line geometries and terminations. In order to predict crosstalk, mutual parameters must be determined. In this light, analysis of mutual capacitance has been made by using conformal mapping[19] and numerical methods[20-23]. If mutual capacitance is known, mutual inductance can be obtained from the relationship:

$$[L][C] = \frac{1}{c^2} \tag{2.1}$$

where $[L]$ is the inductance matrix, $[C]$ is the capacitance matrix, and c is the wave velocity in the medium[3]. S. Okugawa calculated mutual capacitance using numerical methods and used this value to predict crosstalk between microstrip transmission lines by employing Jarvis' loose-coupling theory[24]. N. Schibuya and K. Ito simulated crosstalk of wiring on printed circuit boards using close-coupling theory for the crosstalk model, with numerical techniques for determining mutual capacitance[9]. They developed software called NESSY and CALCAP for this purpose. With a similar technique, A. Djordjević et al developed software for time-domain response of multiconductor transmission lines, but their techniques were only useful for applications in microwave range[25]. C.R. Paul used IBM's ASTAP software to predict crosstalk of land patterns (having coplanar ground line) at frequencies lower than 500 MHz[4, 26]. However, he still used the relationship in Eq.(2.1) to predict mutual inductance, which is not acceptable at low frequencies.

In this chapter, some crosstalk anaysis at low frequencies and calculation techniques for mutual parameters will be briefly reviewed.

§ 2.2 Crosstalk models

R.J. Mohr derived coupling equations for wire lines over a ground plane[12]. He assumed wires in which lengths are short compared with a half wavelength, and terminating resistances are significantly smaller than the characteristic impedance of the wires, the net coupling thus being magnetic, which is related to L_m. Without electric coupling (which is related to C_m), the mesh equation of the active line is:

$$j\omega L_m I_1 = (R_N + R_F + j\omega L_2) I_2 \tag{2.2}$$

where I_1 is the current on line 1 and ω is angular frequency (also see Fig. 1.3-a). From this equation, near-end crosstalk is given by:

$$V_N = j\omega L_m I_1 \frac{R_N}{R_F + R_N} \frac{1}{1 + j\omega L_2/(R_F + R_N)} \tag{2.3}$$

When frequency increases sufficiently, $1 \ll j\omega L_2/(R_F+R_N)$, and the resultant crosstalk V_N becomes linearly proportional to frequency.

Mohr's simple crosstalk expression is useful at low frequencies (wire length is shorter than a half wavelenght), but mutual capacitance still cannot be neglected when the distance between coupled lines is small. C.R. Paul studied terminal voltages of a transmission line consisting of three conductors immersed in a homogeneous medium[7]. He derived the following per-unit-length transmission line equations for the structure shown in Fig. 1.3-b :

$$\begin{aligned}
\frac{dV_1}{dx} &= -j\omega L_1 I_1 - j\omega L_m I_2 \\
\frac{dV_2}{dx} &= -j\omega L_m I_1 - j\omega L_2 I_2 \\
\frac{dI_1}{dx} &= -j\omega (C_1 + C_m) V_1 + j\omega C_m V_2 \\
\frac{dI_2}{dx} &= -j\omega C_m V_1 - j\omega (C_2 + C_m) V_2
\end{aligned} \tag{2.4}$$

Paul discussed the sinusoidal steady-state behavior of the line using matrix chain parameters[18] for the transmission-line equations. The matrix chain parameters provide a solution to these transmission line equations by relating the voltage and current at the far-end to the voltage and current at the near-end. At low frequencies, he found general solutions for near and far-end crosstalk voltages (V_N and V_F, respectively).

$$\begin{aligned}
V_N &= j\omega l \left[\frac{R_N}{R_F + R_N} L_m \frac{1}{R_S + R_B} + \frac{R_N R_F}{R_F + R_N} C_m \frac{R_B}{R_S + R_B} \right] V_S \\
V_F &= -j\omega l \left[\frac{R_F}{R_F + R_N} L_m \frac{1}{R_S + R_B} - \frac{R_N R_F}{R_F + R_N} C_m \frac{R_B}{R_S + R_B} \right] V_S
\end{aligned} \tag{2.5}$$

From Eq. 2.5 linear frequency dependence of crosstalk for both far-end and near-end can be found. It is possible that V_F may be identically zero for all frequencies when the first and second terms are equal. When coupled transmission lines are designed for this condition, they are called directional couplers[5, 27]. When terminal resistances have the condition that $R_B = R_N = R_F = Z_o$, where Z_o is the characteristic impedance of the transmission line, the crosstalk equation of Eq. 2.5 forms the result of Jarvis[6], Feller et al[11], and Rainal[10].

$$V_N = \frac{1}{2}\left[\frac{L_m}{Z_o} + Z_o C_m\right] \int_0^l \frac{dV_S}{dt}\, dx$$

$$V_F = -\frac{1}{2}\left[\frac{L_m}{Z_o} - Z_o C_m\right] \int_0^l \frac{dV_S}{dt}\, dx \qquad (2.6)$$

where $j\omega V_S$ is replaced by dV_S/dt and l, by integration of dx.

§ 2.3 Mutual capacitance

A conformal mapping technique for the determination of mutual capacitance will be reviewed in this section. The conformal transformation which maps the upper half of the z-plane onto the interior of a rectilinear polygon in the w-plane was advanced independently and more or less simultaneously by the German mathematician, H.A. Schwarz[28], and the Italian mathematician, E.B. Christoffel[29]. The perimeter of the polygon in the w-plane coincides with the real axis of the z-plane. Fig. 2.1-a shows this transformation, where the upper half infinite z-plane is mapped into the polygon on the w-plane. Mutual capacitance for two coplanar

parallel conducting strips with equal and opposite charges can be obtained using their technique. When microstrip conductor boundaries are given by $\pm a$ and $\pm b$ (as shown in Fig. 2.1-b), four real axis bends of $\pi/2$ form a rectangular box (Fig. 2.1-b) which encloses an area of uniform field bounded by A^*, B^*, A, and B. Thus, mutual capacitance can be obtained from these simple parallel plates as $C_m = e\,\overline{AB}/\overline{A^*A}$, where e is permittivity. S.B. Cohn calculated the mutual capacitance of a shielded coupled-strip transmission line in 1955[19]. He discussed fringing capacitance for zero thickness strips and finite thickness strips (Fig. 2.2-a). In his discussions, the mutual capacitance can be treated as an "odd-mode fringing capacitance between two strip lines" as shown in Fig. 2.2-b. Even though exact mutual capacitance was not discussed, several persons developed useful conformal mapping functions for self capacitance and characteristic impedance of transmission lines[29-35]. K.G. Black and T.J. Higgins calculated the self capacitance of a microstrip on a ground plane at ultra high frequencies[29]. A.A. Oliner calculated the self capacitance of strip lines[30]. H.A. Wheeler discussed wave resistance (equivalent to characteristic impedance) of parallel strips (broad coupled line) and microstrips on a ground plane using conformal mapping approximation[31]. C.P. Wen studied self capacitance of a surface strip transmission line with infinite coplanar waveguides[32] (Fig. 2.3-a). C. Veyres and V.F. Hanna developed conformal mapping techniques to calculate capacitance of strips with finite coplanar ground planes[33] (Fig. 2.3-b).

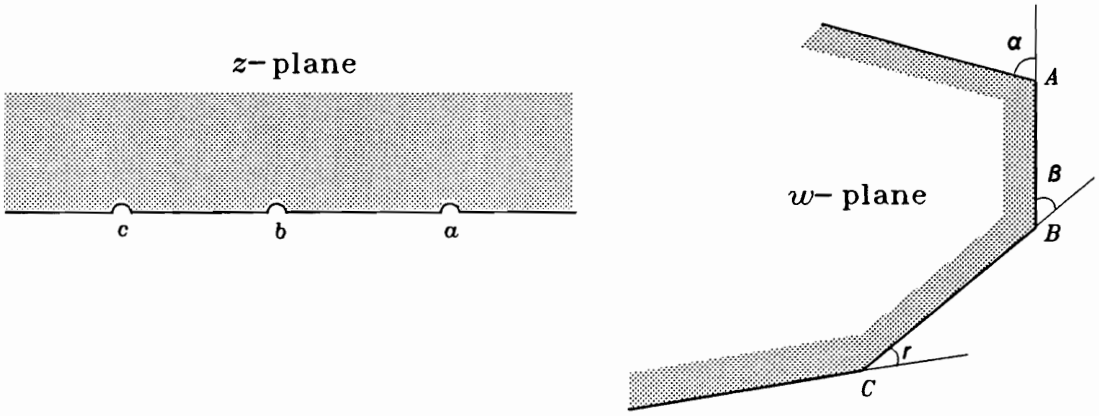

a. General transformation

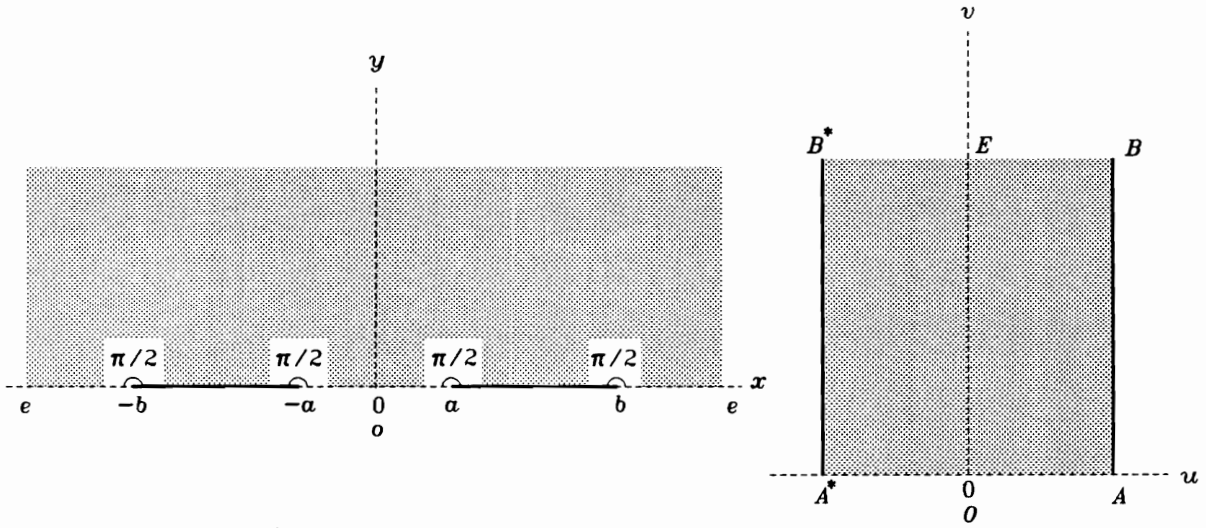

b. $\pi/2$ bends

Fig. 2.1 Schwarz−Christoffel conformal mapping

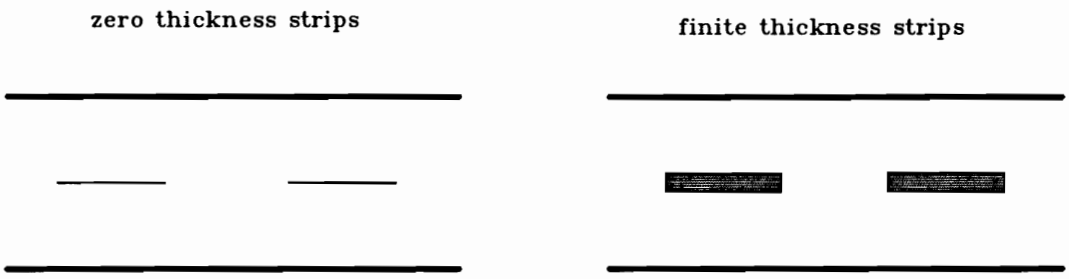

a. Coupled-strip-line cross sections

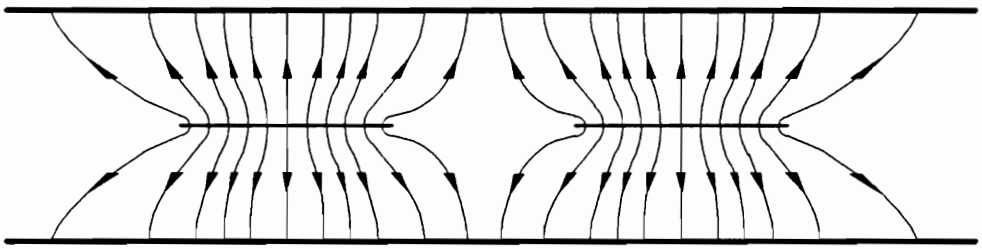

Even-mode electric field distibution

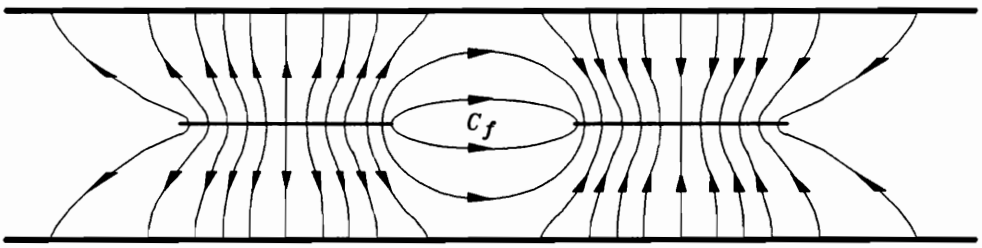

Odd-mode electric field distribution

b. Field distribution of the even and odd modes in coupled strip line

Fig. 2.2 Shielded coupled-strip transmission line. Fringing capacitance (C_f) is equivalent to mutual capacitance.

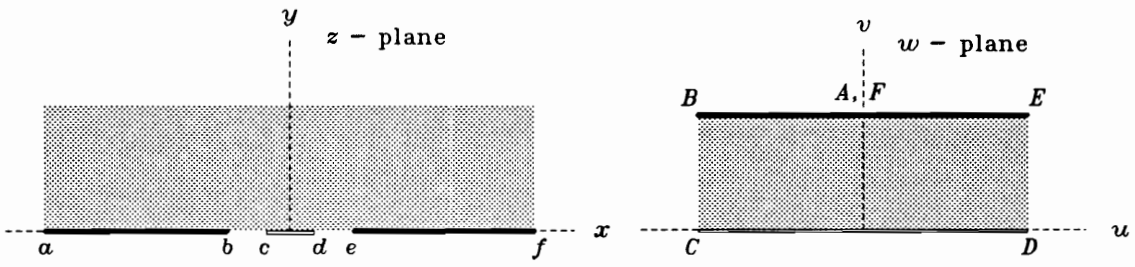

a. Conformal mapping of a surface strip line with infinite ground planes

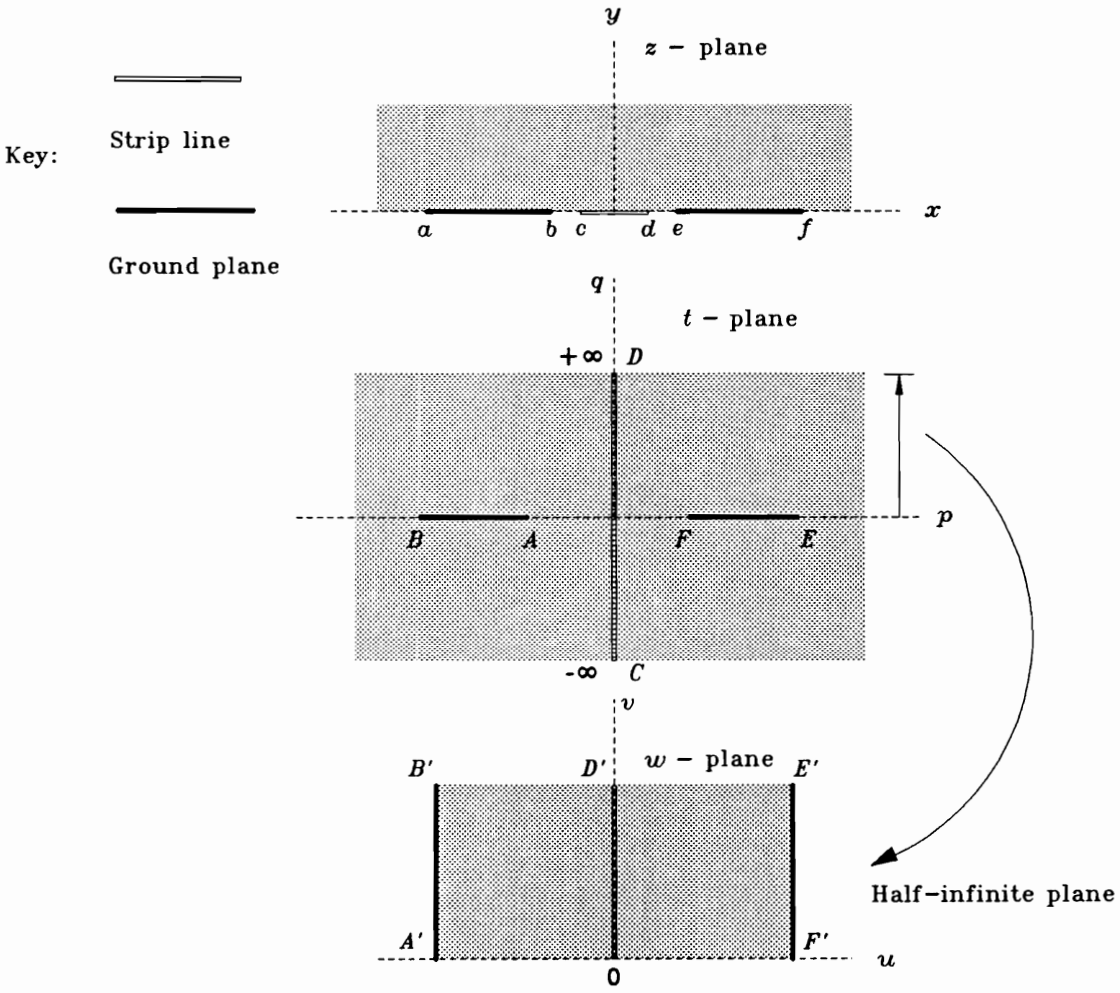

b. Conformal mapping of a surface strip line with finite ground planes

Fig. 2.3 Examples of conformal mapping for capacitance calculations

§ 2.4 Mutual inductance

Inductance calculations have been used primarily in power engineering applications. F.W. Grover provided an extensive treatment for electronic circuit geometries[36]. When cross sectional dimensions are small compared with the distance between them, it suffices to assume that mutual inductance is sensibly the same as the mutual inductance of filaments along their axes, and to use the appropriate basic formula for filaments to calculate the mutual inductance. The mutual inductance of two equal parallel straight filaments is:

$$L_m = 200 \left[\ln \left(\frac{l}{d} + \sqrt{1 + \frac{l^2}{d^2}} \right) - \sqrt{1 + \frac{d^2}{l^2}} + \frac{d}{l} \right] \quad \text{(nH/m)} \qquad (2.7)$$

where l is the filament length, and d is distance (center-to-center) between lines For conductors whose cross section is too large to use this formula directly, geometrical mean distance (GMD) is used instead of d. GMD of two parallel strips is given by (See Fig. 2.4-a):

$$\ln S = \ln na - \left(\frac{1}{12n^2} + \frac{1}{60n^2} + \frac{1}{168n^2} + \cdots\cdots \right) \qquad (2.8)$$

where S is GMD, a is the line width, and na is the line separation (center-to-center). For a multitude of conductor geometries, A.E. Ruehli developed a filament approximation which is convenient for computer implementation[37]. The concept of this technique is that the conductor cross sections are partitioned into a set of rectangles (Fig. 2.4-b), and a simple formation is obtained as the sum of partial inductances:

$$L_{kn} = \lim_{\substack{k\to\infty \\ n\to\infty}} \frac{1}{kn} \sum_{i=1}^{k} \sum_{j=1}^{n} L_{ij} \tag{2.9}$$

where k and n correspond to conductors k and n respectively. The L_{ij} can be obtained from Eq. (2.7) for each partitioned section.

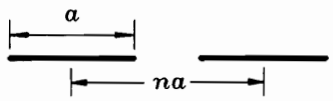

a. Cross sectional view of parallel microstrip. G.M.D. of Eq. (2.8) is used in place of distance d in Eq. (2.7) for mutual inductance.

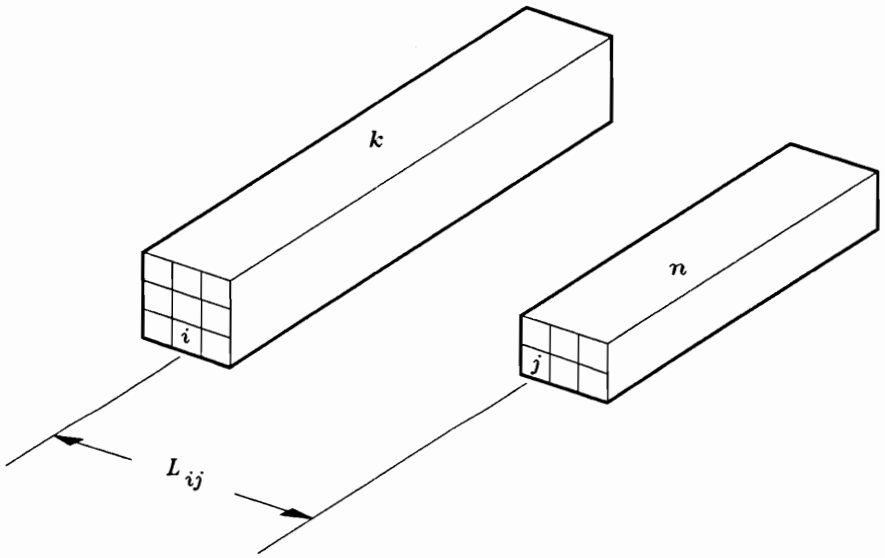

b. Partitioning of areas k and n for arbitrary line geometries.

Fig. 2.4 Mutual inductance calculation for two geometries: a. infinitely thin conductor tapes; b. conductor bars with finite thickness.

Chapter III

Theoretical Background

In this chapter, the basic theory of transmission lines, including mutual parameter calculations will be reviewed. The transverse electromagnetic (TEM) mode of propagation will be discussed and applied to microstrips of interest. In addition, basic conformal mapping techniques related to mutual capacitance calculation for microstrips will be shown. Finally, conventional inductance calculations will be reviewed in detail for use in determining mutual inductance.

§ 3.1 The transmission line equations

The electrical transmission line is an example of a one-dimensional propagating electromagnetic wave system. It is usually required that the electrical length of the line be at least several percent of a wavelength at the highest frequency of interest[27]. An ideal lossless transmission line is surrounded by electric and magnetic fields that are normal both to each other and to the direction of energy propagation. This is the common TEM mode of propagation. This is not to say, however, that a transmission line must propagate a signal in the TEM mode. For example, even though a microstrip is one form of transmission line, it cannot support TEM waves at frequencies other than zero because there is an inhomogeneous dielectric cross section of the line normal to the direction of propagation (see Fig. 1.1). However, a microstrip can be regarded as an ideal transmission line with TEM mode by introducing the *effective dielectric constant* of dielectric layer. In this case,

the microstrip is called "quasi-static microstrip line"[27]. In this section, the telegrapher's equation and crosstalk equation for lossless transmission line will be reviewed.

3.1.1 Telegrapher's equations

Fig. 3.1-a shows an ideal transmission line above a ground plane. Since charge is conserved, the following relationship can be established at distance x from the source:

$$-\frac{\partial I}{\partial x} = \frac{\partial Q}{\partial t} \tag{3.1}$$

where Q is the charge per unit length at distance x and time t on the line. If we assume that the line is a perfect conductor, we have:

$$-\frac{\partial V}{\partial x} = \frac{\partial \Phi}{\partial t} \tag{3.2}$$

where Φ represents the magnetic flux linked with unit length of the line at distance x and time t. The charge and the flux are described as:

$$Q = CV \quad , \quad \Phi = LI \tag{3.3}$$

where C is the self-capacitance (line capacitance) and L is the self-inductance (line inductance). From Eq.(3.1), (3.2), and (3.3), we obtain

$$\frac{\partial I}{\partial x} = -C\frac{\partial V}{\partial t} \tag{3.4}$$

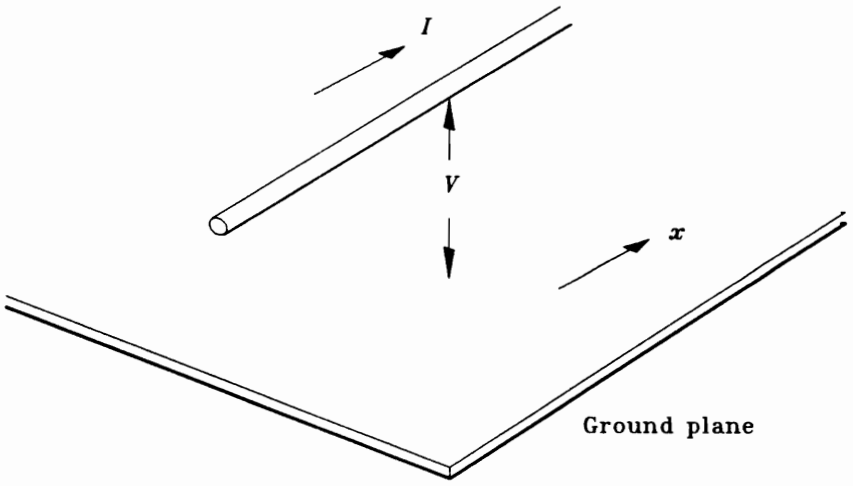

a. Single transmission line

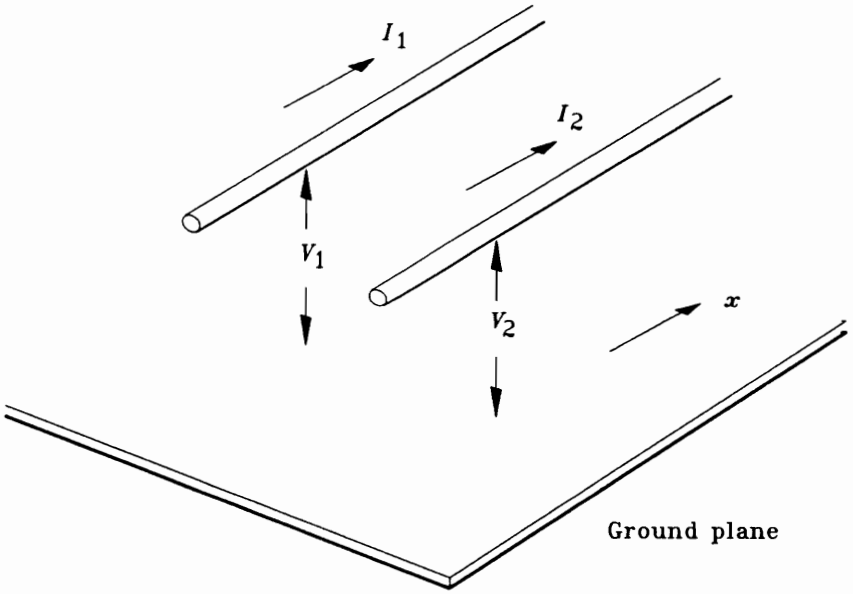

b. Coupled transmission lines

Fig. 3.1 Transmission line model on ground plane

$$\frac{\partial V}{\partial x} = -L\frac{\partial I}{\partial t} \tag{3.5}$$

Equations (3.4) and (3.5) are coupled first-order partial differential equations in V and I. Differentiating Eq.(3.4) with respect to t and Eq.(3.5) with respect to x, we have

$$\frac{\partial^2 I}{\partial x \partial t} = -C\frac{\partial^2 V}{\partial t^2} \tag{3.6}$$

$$\frac{\partial^2 V}{\partial x^2} = -L\frac{\partial^2 I}{\partial t \partial x} \tag{3.7}$$

Equating the mixed partial derivatives yields

$$\frac{\partial^2 V}{\partial x^2} = LC\frac{\partial^2 V}{\partial t^2} \tag{3.8}$$

Similarly, by reversing the order of differentiation, we obtain an equation in I alone as:

$$\frac{\partial^2 I}{\partial x^2} = LC\frac{\partial^2 I}{\partial t^2} \tag{3.9}$$

Eq.(3.8) and/or (3.9) are called the Telegrapher's equation[39, 40] for a lossless line. Maxwell's equations yield a result similar equation to the telegrapher's equation. In homogeneous space, Maxwell's equations are

$$\nabla \cdot \boldsymbol{D} = \rho \tag{3.10}$$

$$\nabla \cdot \boldsymbol{B} = 0 \tag{3.11}$$

$$\nabla \times \boldsymbol{E} = -\frac{\partial \boldsymbol{B}}{\partial t} \tag{3.12}$$

$$\nabla \times \boldsymbol{H} = \boldsymbol{J} + \frac{\partial \boldsymbol{D}}{\partial t} \tag{3.13}$$

where $\boldsymbol{D}$ = Electric displacement vector

$\boldsymbol{B}$ = Magnetic flux vector

$\boldsymbol{E}$ = Electric field intensity vector

$\boldsymbol{H}$ = Magnetic field intensity vector

$\boldsymbol{J}$ = Electric current density vector

ρ = Space charge density

When the wave is propagating through a dielectric, $\rho=0$. Also,

$$\boldsymbol{B} = \mu \boldsymbol{H} \tag{3.14}$$

$$\boldsymbol{D} = \epsilon \boldsymbol{E} \tag{3.15}$$

where μ and ϵ are the permeability and permittivity, respectively, of the material. Substituting the relationships above into Maxwell's equations, we have

$$\nabla \cdot \boldsymbol{E} = 0 \tag{3.16}$$

$$\nabla \cdot \boldsymbol{H} = 0 \tag{3.17}$$

Take the curl of both sides of Eq.(3.12) and substitute the result into Eq.(3.13),

$$\begin{aligned} \nabla \times (\nabla \times \boldsymbol{E}) &= -\mu \nabla \times \frac{\partial \boldsymbol{H}}{\partial t} = -\mu \frac{\partial}{\partial t}(\nabla \times \boldsymbol{H}) \\ &= -\mu \frac{\partial}{\partial t}\left(\boldsymbol{J} + \frac{\partial \boldsymbol{D}}{\partial t}\right) = -\mu \frac{\partial^2 \boldsymbol{D}}{\partial t^2} \\ &= -\mu e \frac{\partial^2 \boldsymbol{E}}{\partial t^2} \end{aligned} \tag{3.18}$$

By vector identity,

$$\nabla \times (\nabla \times \boldsymbol{E}) = \nabla (\nabla \cdot \boldsymbol{E}) - \nabla^2 \boldsymbol{E} = -\nabla^2 \boldsymbol{E} \tag{3.19}$$

since $\nabla \cdot \boldsymbol{E} = 0$ from Eq.(3.16). Therefore,

$$\nabla^2 \boldsymbol{E} = \mu e \frac{\partial^2 \boldsymbol{E}}{\partial t^2} = \frac{\partial^2 \boldsymbol{E}}{\partial x^2} \tag{3.20}$$

Eq.(3.20) has the same form as Eq.(3.8) and (3.9). Similarly, it can be shown that $\boldsymbol{H}$ also satisfies the same telegrapher's equation.

Now consider a wave having the form

$$\xi = \xi\left(\frac{x}{c} \pm t\right) = \frac{1}{2}\left\{g\left(\frac{x}{c} + t\right) + g\left(\frac{x}{c} - t\right)\right\} \tag{3.21}$$

where the $-$ sign indicates wave motion to the right (increasing x) and the $+$ sign indicates wave motion to the left (decreasing x). The wave has a constant velocity c. Let $f = x/c \pm t$, then

$$\frac{\partial \xi}{\partial x} = \frac{\partial \xi}{\partial f}\frac{\partial f}{\partial x} = \frac{1}{c}\frac{\partial \xi}{\partial f} \tag{3.22}$$

and

$$\frac{\partial \xi}{\partial t} = \frac{\partial \xi}{\partial f}\frac{\partial f}{\partial t} = \pm \frac{\partial \xi}{\partial f} \tag{3.23}$$

To obtain solutions to Eq.(3.22) and Eq.(3.23), it is useful to find an equation in ξ alone. Since Eq.(3.23) has both the $+$ and $-$ sign, differentiate Eq.(3.23) with respect to t and Eq.(3.22) with respect to x in order to satisfy $\pm$ properties simultaneously. Then we obtain

$$\frac{\partial^2 \xi}{\partial x^2} = \frac{1}{c^2}\frac{\partial^2 \xi}{\partial f^2} \tag{3.24}$$

and

$$\frac{\partial^2 \xi}{\partial t^2} = \frac{\partial^2 \xi}{\partial f^2} \tag{3.25}$$

or

$$\frac{\partial^2 \xi}{\partial x^2} = \frac{1}{c^2}\frac{\partial^2 \xi}{\partial t^2} \tag{3.26}$$

Eq.(3.26) is the wave equation and is equivalent to the telegrapher's equation. Thus, from Eq.(3.8), (3.20), and (3.26), we have

$$\frac{1}{c^2} = LC = \mu e \tag{3.27}$$

Now consider a semi-infinite line, extending from $x=0$ to $x=\infty$. A wave launched at $x=0$ will propagate in the $+x$ direction. Then from Eq.(3.5), (3.22), and (3.23),

$$\frac{\partial I}{\partial t} = -\frac{1}{L}\frac{\partial V}{\partial x} = -\frac{1}{L}\frac{1}{c}\frac{\partial V}{\partial f} = \sqrt{\frac{C}{L}}\frac{\partial V}{\partial t} \tag{3.28}$$

and therefore for the wave traveling only in the $+x$ direction,

$$V(x,t) = \sqrt{L/C}\, I(x,t) \tag{3.29}$$

The ratio of the voltage to the current at any point along the line is therefore a constant having the units of resistance. This resistance is defined as the *characteristic impedance*, Z_o, of the line.

$$Z_o = \sqrt{L/C} \tag{3.30}$$

3.1.2 Coupling equations for TEM mode

When we consider two parallel conductors above a ground line (Fig. 3.1-b), there is some coupling between them due to their proximity. The electrostatic formulae and steady current formulae are again used for these two lines:

$$Q_1 = C_1 V_1 - C_m V_2$$
$$Q_2 = -C_m V_1 + C_2 V_2 \tag{3.31}$$

and

$$\Phi_1 = L_1 I_1 + L_m I_2$$
$$\Phi_2 = L_m I_1 + L_2 I_2 \tag{3.32}$$

, where C_1, C_2 : Line capacitances

C_m : Mutual capacitance

L_1, L_2 : Line inductances

L_m : Mutual inductance

Eq.(3.1), (3.2), (3.31), and (3.32) can be combined to give the differential equations of the system:

$$\frac{\partial I_1}{\partial x} = -C_1 \frac{\partial V_1}{\partial t} + C_m \frac{\partial V_2}{\partial t}$$
$$\frac{\partial I_2}{\partial x} = -C_2 \frac{\partial V_2}{\partial t} + C_m \frac{\partial V_1}{\partial t}$$
$$\frac{\partial V_1}{\partial x} = -L_1 \frac{\partial I_1}{\partial t} - L_m \frac{\partial I_2}{\partial t} \tag{3.33}$$
$$\frac{\partial V_2}{\partial x} = -L_2 \frac{\partial I_2}{\partial t} - L_m \frac{\partial I_1}{\partial t}$$

The general solutions for the voltages on the two lines in terms of all four waves are rather complicated but are given by Tripathi[17]. However, when symmetric coupled lines are considered with $C_1=C_2=C$ and $L_1=L_2=L$, Eq.(3.33) reduces to

$$\begin{aligned}
\frac{\partial I_1}{\partial x} &= -C\frac{\partial V_1}{\partial t} + C_m\frac{\partial V_2}{\partial t} && (1)\\
\frac{\partial I_2}{\partial x} &= -C\frac{\partial V_2}{\partial t} + C_m\frac{\partial V_1}{\partial t} && (2)\\
\frac{\partial V_1}{\partial x} &= -L\frac{\partial I_1}{\partial t} - L_m\frac{\partial I_2}{\partial t} && (3)\\
\frac{\partial V_2}{\partial x} &= -L\frac{\partial I_2}{\partial t} - L_m\frac{\partial I_1}{\partial t} && (4)
\end{aligned} \tag{3.34}$$

To simplify the solutions, add and subtract (1) and (2), and (3) and (4) in Eq.(3.34).

$$\begin{aligned}
\frac{\partial(I_1 + I_2)}{\partial x} &= -(C - C_m)\frac{\partial(V_1 + V_2)}{\partial t}\\
\frac{\partial(I_1 - I_2)}{\partial x} &= -(C + C_m)\frac{\partial(V_1 - V_2)}{\partial t}\\
\frac{\partial(V_1 + V_2)}{\partial x} &= -(L + L_m)\frac{\partial(I_1 + I_2)}{\partial t}\\
\frac{\partial(V_1 - V_2)}{\partial x} &= -(L - L_m)\frac{\partial(I_1 - I_2)}{\partial t}
\end{aligned} \tag{3.35}$$

Two modes are defined as:

$$\begin{aligned} &\text{even mode} && V_e = V_1 + V_2 \quad (I_e = I_1 + I_2) \\ &\text{odd mode} && V_o = V_1 - V_2 \quad (I_o = I_1 - I_2) \end{aligned} \tag{3.36}$$

Thus,

$$\begin{aligned} \frac{\partial I_e}{\partial x} &= -(C - C_m)\frac{\partial V_e}{\partial t} \\ \frac{\partial I_o}{\partial x} &= -(C + C_m)\frac{\partial V_o}{\partial t} \\ \frac{\partial V_e}{\partial x} &= -(L + L_m)\frac{\partial I_e}{\partial t} \\ \frac{\partial V_o}{\partial x} &= -(L - L_m)\frac{\partial I_o}{\partial t} \end{aligned} \tag{3.37}$$

Using the same procedure as before, from Eq.(3.6) through (3.9),

$$\begin{aligned} \frac{\partial^2 V_e}{\partial x^2} &= (L + L_m)(C - C_m)\frac{\partial^2 V_e}{\partial t^2} \\ \frac{\partial^2 V_o}{\partial x^2} &= (L - L_m)(C + C_m)\frac{\partial^2 V_o}{\partial t^2} \end{aligned} \tag{3.38}$$

Then even-mode and odd-mode velocities are defined as

$$\begin{aligned} &\text{even-mode velocity} && \frac{1}{c_e^2} = (L + L_m)(C - C_m) \\ &\text{odd-mode velocity} && \frac{1}{c_o^2} = (L - L_m)(C + C_m) \end{aligned} \tag{3.39}$$

Combining Eq.(3.37), (3.39), and (3.28) gives

$$-\frac{1}{c_e}V_e = -(L + L_m)I_e$$
$$-\frac{1}{c_o}V_o = -(L - L_m)I_o \tag{3.40}$$

Therefore, even- and odd-characteristic impedances are, from Eq.(3.40):

$$\frac{V_e}{I_e} = Z_{oe} = c_e(L + L_m)$$
$$= \sqrt{\frac{L + L_m}{C - C_m}} \tag{3.41}$$
$$Z_{oo} = \sqrt{\frac{L - L_m}{C + C_m}}$$

where characteristic impedance is expressed by[27]:

$$Z_o^2 = Z_{oe}Z_{oo} \tag{3.42}$$

When there is a homogeneous medium, the two velocities must be equal to each other and to the wave propagation velocity in the homogeneous dielectric medium. Thus,

$$(L + L_m)(C - C_m) = (L - L_m)(C + C_m)$$

or
$$\frac{C_m}{C} = \frac{L_m}{L} = k_h \tag{3.43}$$

where k_h is the coupling coefficient in the homogeneous medium.

To solve Eq.(3.38), each variable is replaced by its Laplace transformation; $\mathcal{L}[V_e]=\overline{V_e}$, etc. and $\mathcal{L}\left[\frac{\partial V_e}{\partial t}\right]=s\overline{V_e}$, etc.. Then

$$\frac{\partial^2 \overline{V_e}}{\partial x^2} = (L + L_m)(C - C_m)s^2\overline{V_e} = \frac{s^2}{c_e^2}\overline{V_e}$$

$$\frac{\partial^2 \overline{V_o}}{\partial x^2} = (L - L_m)(C + C_m)s^2\overline{V_o} = \frac{s^2}{c_o^2}\overline{V_o} \qquad (3.44)$$

In the homogeneous medium, the solutions of differential equations in Eq.(3.44) are

$$\overline{V_e} = A_1 e^{sx/c_e} + A_2 e^{-sx/c_e}$$

$$\overline{V_o} = A_3 e^{sx/c_o} + A_4 e^{-sx/c_o} \qquad (3.45)$$

where A_1, A_2, A_3, and A_4 are constants to be determined. To solve for the currents, Eq.(3.45) is substituted into Eq.(3.38), with replacing I_e and I_o with their respective Laplace transformations. Hence:

$$\frac{\partial \overline{V_e}}{\partial x} = -(L + L_m)s\overline{I_e}$$

and $$\overline{I_e} = -\frac{1}{L + L_m}\left[\frac{1}{c_e}A_1 e^{sx/c_e} - \frac{1}{c_e}A_2 e^{-sx/c_e}\right]$$

or $$\overline{I_e} = \sqrt{\frac{C - C_m}{L + L_m}}\left[-A_1 e^{sx/c_e} + A_2 e^{-sx/c_e}\right] \qquad (3.46)$$

Likewise,

$$\overline{I_o} = \sqrt{\frac{C + C_m}{L - L_m}} \left[-A_3 e^{sx/c_o} + A_4 e^{-sx/c_o} \right] \tag{3.47}$$

The above solutions result from "close-coupling" theory. The effect of a wave traveling along line 1 is to induce a wave in line 2. These waves will then affect the wave in line 1. However, if the coupling is weak it is plausible to assume that the wave induced on line 2 will be small and so will have a negligible effect on the large driving wave on line 1. This assumption leads to the "loose-coupling" theory. The simplified version of Eq.(3.34) is then

$$\begin{aligned}
\frac{\partial I_1}{\partial x} &= -C\frac{\partial V_1}{\partial t} \\
\frac{\partial I_2}{\partial x} &= -C\frac{\partial V_2}{\partial t} + C_m\frac{\partial V_1}{\partial t} \\
\frac{\partial V_1}{\partial x} &= -L\frac{\partial I_1}{\partial t} \\
\frac{\partial V_2}{\partial x} &= -L\frac{\partial I_2}{\partial t} - L_m\frac{\partial I_1}{\partial t}
\end{aligned} \tag{3.48}$$

Using the same procedure as that in close-coupling theory,

$$\begin{aligned}
\frac{\partial \overline{I_1}}{\partial x} &= -sC\overline{V_1} \\
\frac{\partial \overline{I_2}}{\partial x} &= -sC\overline{V_2} + sC_m\overline{V_1} \\
\frac{\partial \overline{V_1}}{\partial x} &= -sL\overline{I_1} \\
\frac{\partial \overline{V_2}}{\partial x} &= -sL\overline{I_2} - sL_m\overline{I_1}
\end{aligned} \tag{3.49}$$

After differentiating and combining Eq.(3.49), we have

$$\begin{aligned}
\frac{\partial^2 \overline{V_1}}{\partial x^2} &= \frac{s^2}{c^2}\overline{V_1} \\
\frac{\partial^2 \overline{V_2}}{\partial x^2} &= \frac{s^2}{c^2}\left(\frac{L_m}{L} - \frac{C_m}{C}\right)\overline{V_1} + \frac{s^2}{c^2}\overline{V_2}
\end{aligned} \tag{3.50}$$

where $c^2=1/LC$.

The solution to Eq.(3.50) is then

$$\begin{aligned}
\overline{V_1} &= B_1 e^{sx/c} + B_2 e^{-sx/c} \\
\overline{I_1} &= \frac{1}{Z_o}\left[-B_1 e^{sx/c} + B_2 e^{-sx/c}\right]
\end{aligned} \tag{3.51}$$

$$\overline{V_2} = B_3 e^{sx/c} + B_4 e^{-sx/c} + \frac{s}{2c} x \left(\frac{L_m}{L} - \frac{C_m}{C} \right) \left(B_1 e^{sx/c} - B_2 e^{-sx/c} \right)$$

$$\overline{I_2} = \frac{1}{Z_o} \left(-B_3 e^{sx/c} + B_4 e^{-sx/c} \right) + \frac{1}{2Z_o} \left(3\frac{L_m}{L} + \frac{C_m}{C} \right) \left(B_1 e^{sx/c} - B_2 e^{-sx/c} \right)$$

$$- \frac{1}{2Z_o} \frac{s}{c} x \left(\frac{L_m}{L} - \frac{C_m}{C} \right) \left(B_1 e^{sx/c} + B_2 e^{-sx/c} \right)$$

$$+ \frac{1}{2Z_o} \left(\frac{L_m}{L} - \frac{C_m}{C} \right) \left(-B_1 e^{sx/c} + B_2 e^{-sx/c} \right) \tag{3.52}$$

where $Z_o = \sqrt{L/C}$.

As a particular choice of boundary conditions, suppose that the lines are terminated in their characteristic impedance Z_o and that at time $t=0$, a voltage V is applied to the input line 1. Therefore, if l is the length of each line, we obtain

$$V_N = \frac{V}{4} c \left(\frac{L_m}{Z_o} + Z_o C_m \right) \left(1 - e^{-2sl/c} \right)$$

$$V_F = -\frac{V}{2} \left(\frac{L_m}{Z_o} - Z_o C_m \right) ls e^{-sl/c} \tag{3.53}$$

The above results were derived independently (and by different means) by Jarvis[6,24] (1963), Feller et al[11] (1965), and Rainal[10] (1978), respectively.

§ 3.2 Conformal transformations

Conformal transformation is a mathematical technique that allows a particular transmission line geometry to be transformed into a new geometry in the second coordinate system, with certain rules governing the relationship between the electrical properties of the lines in the two systems. If the second system is judiciously chosen, the new geometry is more amenable to solution by Laplace's equation (in the plane) than was the original geometry. The theory of conformal transformations is a topic in the more general theory of complex variables. A complex number in z-plane has the form:

$$z = x + jy = r\cos\theta + jr\sin\theta = re^{j\theta} \tag{3.54}$$

A function $w(z)$ of the complex variable z is itself a complex number whose real and imaginary parts u and v depend on the position of z in the z-plane.

$$w(z) = u(x, y) + jv(x, y) \tag{3.55}$$

Two different graphical representations of the function $w(z)$ are useful. One is simply to plot the real and/or imaginary parts, $u(x, y)$ and $v(x, y)$ as surface above the z-plane. The other is to present the complex number $w(z)$ by a point in the complex "w-plane", so that to each point in the z-plane corresponds one (or more) points in the w-plane. In this way, the function $w(z)$ produces a mapping of the z-plane into the w-plane. It is found that Laplace's equation in the z-plane still satisfy Laplace's

equation in the w-plane (See Appedix A). In this case, a transformed solution becomes the final solution. In the following sections, some sample transformation functions will be reviewed.

3.2.1 Exponential function

Let $w=\tanh z$ and find $u(x, y)$ and $v(x, y)$. Since

$$\begin{aligned} \tanh z &= \frac{e^z - e^{-z}}{e^z + e^{-z}} \\ &= \frac{1}{2}\frac{\sinh 2x + j\sin 2y}{\cos^2 y \cosh^2 x + \sin^2 y \sinh^2 x} \\ &= u + jv \end{aligned} \tag{3.56}$$

we obtain

$$\begin{aligned} u^2 + (v - \cot 2y)^2 &= \frac{1}{\sin^2 2y} \\ (u - \cosh 2x)^2 + v^2 &= \frac{1}{\sinh^2 2x} \end{aligned} \tag{3.57}$$

Therefore, when y is confined to the region between zero and $\pm\pi/2$ (Fig.3.2-a), Eq.(3.57) forms bipolar coordinates depending on values of x and y as shown in Fig. 3.2-c. Hence, each quarter region in the z-plane can be mapped to a corresponding region in the w-plane (Fig. 3.2-b).

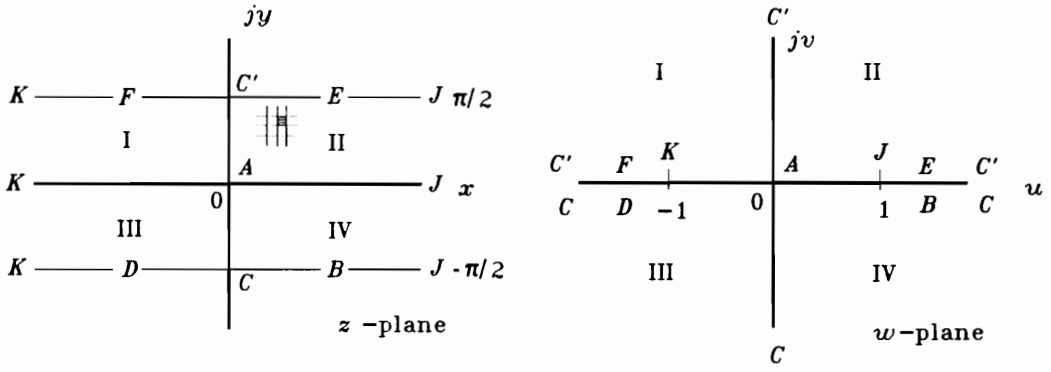

a. w=tanh$z$ mapping from z-plane to w-plane showing corresponding regions and points

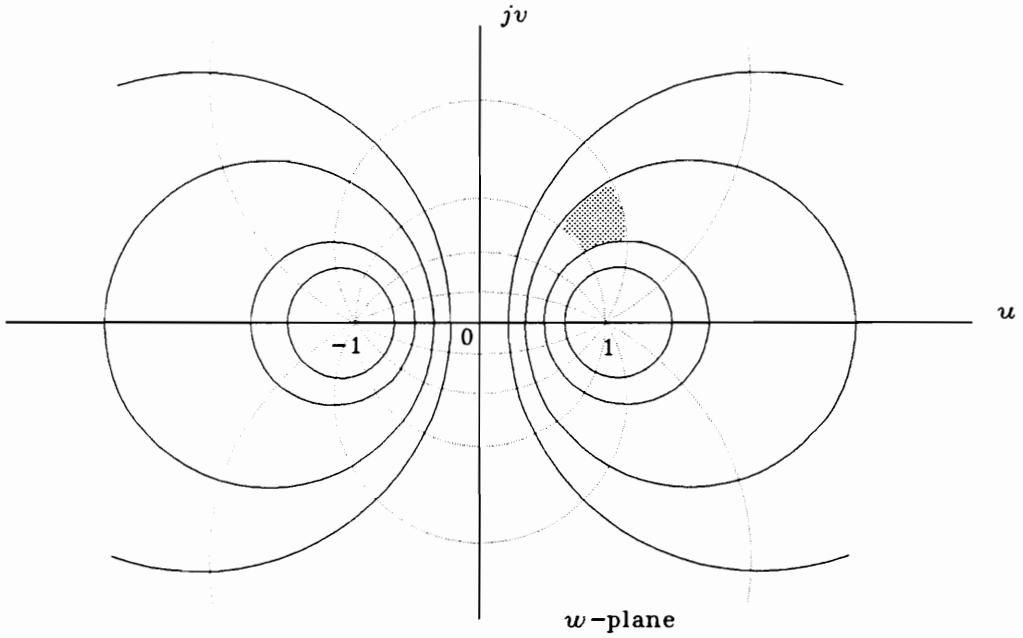

b. Grids of the above conformal transformation showing bipolar coordinates: shaded area corresponds to that in z-plane

Fig. 3.2 Conformal transformation by an exponential function

3.2.2 Schwarz-Christoffel transformation of coplanar strips

Consider two coplanar parallel strips, where the strip boundaries are given by $\pm a$ and $\pm b$. Four $\pi/2$ real axis bends take the form (See Appendix B for details)

$$w = A \int \frac{dz}{\sqrt{(z^2-a^2)(z^2-b^2)}} + B \tag{3.58}$$

which is known as an elliptic integral of the first kind. Let $w=0$ when $z=0$ for convenience, then $B=0$ and

$$w = A \int \frac{dz}{\sqrt{(a^2-z^2)(b^2-z^2)}}$$

$$= \frac{A}{ab} \int \frac{dz}{\sqrt{\left[1-\left(\frac{z}{a}\right)^2\right]\left[1-\left(\frac{a}{b}\right)^2\left(\frac{z}{a}\right)^2\right]}} \tag{3.59}$$

The inverse function of the elliptic integral, Eq.(3.59), is the elliptic function, i.e.;

$$z = a\,\mathrm{sn}\left(\frac{ab}{A}w,\ \frac{a}{b}\right) = a\,\mathrm{sn}\left(\frac{ab}{A}w,\ k\right) \tag{3.60}$$

where $k=a/b$. Special values of the elliptic signs are

$$\mathrm{sn}\,(\,K + jK',\ k\,) = k^{-1}$$
$$\mathrm{sn}\,(\,K + \frac{1}{2}jK',\ k\,) = k^{-1/2} \tag{3.61}$$

where k is the modulus, $K'=K(k')$, and $k'=\sqrt{1-k^2}$ is the complementary modulus.

K and K' are the corresponding complete elliptic integrals where K is expressed as:

$$K = \frac{\pi}{2}\left[1+\left(\frac{1}{2}\right)^2 k^2+\left(\frac{1\cdot3}{2\cdot4}\right)^2 k^4+\left(\frac{1\cdot3\cdot5}{2\cdot4\cdot6}\right)^2 k^6+\cdots\cdots\right] \tag{3.62}$$

Thus, where $z=b$, from Eq.(3.60),

$$\frac{b}{a} = k^{-1} = \mathrm{sn}\left(\frac{ab}{A}w,\ k\right) \tag{3.63}$$

and

$$\frac{ab}{A}w = K + jK' \tag{3.64}$$

Since $u = \overline{OA}$ and $v = \overline{AB}$ when $z=b$, in Fig. 2.1-b,

$$K = \frac{ab}{A}\overline{OA}$$
$$K' = \frac{ab}{A}\overline{AB} \tag{3.65}$$

The capacitance per unit length is, from Fig. 2.1-b,

$$C = \epsilon\frac{\overline{AB}}{\overline{A^*A}} = \epsilon\frac{K'}{2K} \tag{3.66}$$

Since Fig. 2.1-b is the conformal transformation for half-infinite plane of z-plane, capacitance for the whole upper- and lower-space will be

$$C = \epsilon\frac{K'}{K} \tag{3.67}$$

§ 3.3 Inductance calculation

Although the self-inductances and mutual inductances of circuit elements not associated with magnetic materials are independent of the value of the current and dependent only on the geometry of the system, it is only in the simplest cases that these constants can be calculated exactly. Fortunately, from these basic formulae for ideal cases, expressions applicable to the more important circuit elements met in practice may be built up by general synthetic methods. A brief survey of the methods employed in deriving the basic formulae will first be given and , following these, a treatment of methods of procedure for building up solutions of the problem

for actual circuits is presented.

3.3.1 Mutual inductance of two equal parallel straight filaments

Consider the two parallel filaments shown in Fig. 3.3-a. By applying the Biot-Savart law, a current I flowing in the y direction produces a magnetic flux density, $B(x, y)$, given by

$$B(x, y) = \frac{\mu I}{4\pi} \int_{-l/2}^{l/2} \frac{\sin\theta}{r^2}\, ds = \frac{\mu I}{4\pi} \int_{-l/2}^{l/2} \frac{x}{r^3}\, ds$$
$$= \frac{\mu I}{4\pi x}\left[\frac{(y+l/2)}{\sqrt{(y+l/2)^2+x^2}} - \frac{(y-l/2)}{\sqrt{(y-l/2)^2+x^2}}\right] \tag{3.68}$$

where μ is the permeability of the medium. The total flux, Φ, linking line 2 is then given by

$$\Phi = \int_{d}^{\infty} dx \int_{-l/2}^{l/2} B(x, y)\, dy$$
$$= \frac{\mu I l}{2\pi}\left[\ln\left\{\frac{l}{d} + \sqrt{1+\left(\frac{l}{d}\right)^2}\right\} - \sqrt{1+\left(\frac{d}{l}\right)^2} + \frac{d}{l}\right] \tag{3.69}$$

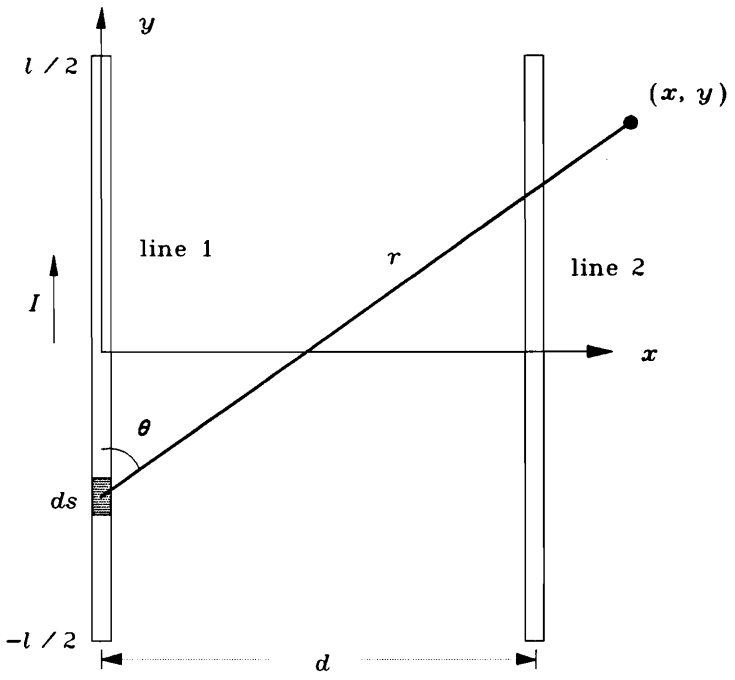

a. Coordinate system for derivation of mutual inductance

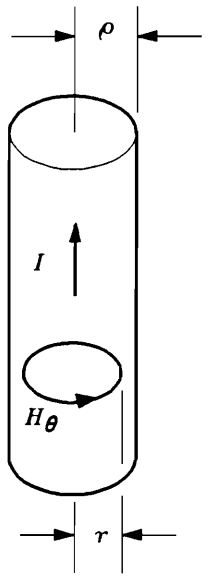

b. Notation for derivation of self-inductance

Fig. 3.3 Inductance calculation models

If the medium is a vacuum or air, then $\mu = \mu_o = 4\pi \times 10^{-7}$ H/m and the mutual inductance, L_{12}, is given by

$$L_{12} = \frac{\Phi}{l I}$$

$$= 200\left[\ln\left\{\frac{l}{d} + \sqrt{1 + \left(\frac{l}{d}\right)^2}\right\} - \sqrt{1 + \left(\frac{d}{l}\right)^2} + \frac{d}{l}\right] \quad \text{(nH/m)} \tag{3.70}$$

3.3.2 Self-inductance of a straight conductor

Consider the current element shown in Fig. 3.3-b. A basic definition of self-inductance, L, is

$$L = \frac{\Phi}{I} = \text{total number of flux linkage per ampere} \tag{3.71}$$

From Ampere's law, the magnetic intensity, internal to the conductor is given by

$$\oint H \cdot dA = \left(\frac{I}{\pi\rho^2}\right)(\pi r^2) = I\left(\frac{r}{\rho}\right)^2 \qquad 0 \le r \le \rho \tag{3.72}$$

where A is the incremental cross sectional area and ρ is the radius of the conductor. Eq.(3.72) assumes that the current density, $I/(\pi\rho)^2$, is uniform in the conductor (skin effect is neglected at low frequencies). From Eq.(3.72), H_θ is defined as:

$$H_\theta = |H| = \frac{I}{2\pi r}\left(\frac{r}{\rho}\right)^2 \qquad 0 \le r \le \rho \tag{3.73}$$

The flux density, B_θ , internal to the conductor is then

$$B_\theta = \mu H_\theta = \frac{\mu I}{2\pi r}\left(\frac{r}{\rho}\right)^2 \qquad 0 \le r \le \rho \tag{3.74}$$

A given flux line of radius $r \le \rho$ encloses a fraction $(r/\rho)^2$ of the total current I. Thus, from Eq.(3.71) and (3.74) the self-inductance, L_i, resulting from the internal magnetic field is

$$L_i = \frac{l}{I}\int_0^\rho B_\theta\left(\frac{r}{\rho}\right)^2 dr = \frac{\mu l}{8\pi} \tag{3.75}$$

The total self-inductance, L_S, of a straight conductor is obtained by adding the contributions from the external and internal magnetic fields. Thus, from Eq.(3.70) and (3.75) we have

$$L_S = L_{12}\Big|_{d=\rho} + L_i \tag{3.76}$$

for $\rho \ll l$,

$$L_S = 200\left[\ln\left(\frac{2l}{\rho}\right) - \frac{3}{4}\right] \qquad \text{nH/m} \tag{3.77}$$

3.3.3 Inductance for a multitude of geometries

In calculating the mutual inductance of two conductors whose cross sectional dimensions are small compared with their separation, it suffices to assume that the mutual inductance is practically the same as that of the filaments along their axes. One may then use the appropriate basic formula for filaments to calculate the mutual inductance. For conductors whose cross section is too large to justify this simplifying assumption it is necessary to average the mutual inductances of all the filaments of which the conductors may be supposed to consist. That is, the basic formula for the mutual inductance is to be integrated over the cross sections of the conductors. The constant terms are of course unchanged; the average of $\ln d$ is defined as $\ln S$, where distance S is called the *geometric mean distance* (GMD) of the two geometries (See Appendix C for more information). Thus, the two conductors of rectangular cross section have been replaced by two filaments whose spacing is equal to the geometric mean distance (GMD) of the two sections. For example, the GMD of two parallel strips is given by Eq.(2.8), for example. However, as the geometry becomes complicated, it is difficult to calculate GMD in closed-form. Thus, Ruehli's technique (numerical method) is used for a multitude of geometries as given in Eq.(2.9).

Since the self-inductance of a conductor is equal to the sum of the mutual inductances of all the pairs of filaments of which it is composed, it is also evident that the self-inductance of a straight conductor of any desired section is equal to the mutual inductanc of two parallel straight sub-filaments of which a conductor is composed, spaced at the geometric mean distances of all points of the section from each other. Thus is derived the idea of the *geometric mean distance of an area from*

itself. When the cross section of the conductor is rectangular, for example, the self-inductance is given by[36, 38]

$$L_S \approx 200 \left[\ln \frac{4l}{p} + \frac{1}{2} \right] \qquad \text{nH/m} \tag{3.78}$$

where p is the perimeter of cross section.

3.3.4 Loop inductance

The transmission-line model in Fig. 1.3.a assumes that ground resistance and ground inductance are zero. However, when ground is not a perfect conductor, ground resistance cannot be neglected. and/or form a ground line, both terms should be considered. In that case, lump-circuit model is useful to obtain, so called, loop inductance. When current flow directions are considered in Fig. 1.3.b, the loop inductance affecting on line 2 is expressed as[37]:

$$L_m = L_{12} - L_{1G} - L_{2G} + L_G \tag{3.79}$$

For microstrip transmission lines, L_{12}, L_{1G}, and L_G are calculated using Eq.(3.70) or (2.9), and L_G, using Eq.(3.78).

Chapter IV

Objectives and Experiments

As mentioned previously in Chapter I, the crosstalk model at low frequencies is still open to question. In order to develop a low frequency crosstalk model, a valid crosstalk equation must first be developed for given test patterns of interest. Once the crosstalk equation is established, transmission line parameters such as mutual capacitance and mutual inductance can be calculated in order to predict crosstalk by combining these parameters with the crosstalk equation.

Crosstalk equations have been developed by several investigators[6,7,10,11,12,14,15,16,17]; however, as shown in the next chapter, these equations can be derived in a simpler way for low-frequency applications. In order to understand crosstalk, its dependence on the following parameters should first be addressed and investigated:

a. Transmission line length
b. Frequency
c. Line width
d. Line thickness
e. Line separation
f. Ground distance
g. Termination resistance

The above parameters can be studied with simple side-coupled microstrips on the alumina substrate. When a multilayer system is used, broad-coupled lines can also be manufactured.

Crosstalk equations contain mutual inductance and mutual capacitance terms. Therefore it is important to develop techniques to calculate these parameters to simulate crosstalk for given geometrical structures of transmission line. As mentioned before, conventional calculations can be used for mutual inductance. As for mutual capacitance, new techniques need to be established.

§ 4.1 Test patterns

In this reseach, the following test pattern parameters were varied to test crosstalk at low frequencies:

#1 : Variations in line spacing using ground plane

#2 : Variations in ground line separation, with constant line spacing

#3 : Variations in line spacing with constant ground line separation

A : Test pattern #1 on TOS

B : Test pattern #1 at TOS-alumina substrate interface

C : Broad-coupling pattern with TOS medium on alumina substrate

Test patterns are shown in Fig. 4.1. Line spacing (D) of Pattern #1 was designed to have 5, 7, 10, 15 and 20 mils of edge-to-edge distance. Transmission line width (W) is 10 mils, with line thickness (T) of 0.8 mil. Ground line separations of Pattern #2 were 10, 20, 40, 80, and 160 mils, with constant line spacing of 10 mils. As for Pattern #3, line spacing has the same dimensions as Pattern #1 with 10 mil ground line distance. Patterns A and B are essentially the same as Pattern #1 except for an additional TOS layer. Pattern C has ground plane on the underside of the alumina substrate. Patterns A, B, and C were designed to investigate crosstalk in

multilayer circuits. TOS varies from single to triple layer. Each transmission line was terminated by a resistance of 50Ω, 61Ω (or 66Ω) and 75Ω. These resistors were chosen to study resistor dependence of crosstalk. The open termination was also tested to check crosstalk modeling.

§ 4.2 Sample preparation

Test pattern design was performed using CAD (Computer Aided Design). The test patterns were printed on an alumina substrate with DuPont 6160 (pure silver) paste and then dried for 10 min. at 150°C in a BLUE M oven and fired in a BTU furnace at 850°C with 10 min. peak time in a 60 min. cycle. For the ground plane, DuPont 6134 (Ag/Pd) was used with the same processing conditions. Once sample fabrication was finished, chip resistors were attached at each line termination using silver epoxy (Epo-Tek H20E). This epoxy was also used to connect the resistor pads and the ground plane of Pattern #1 along the edge of the alumina substrate. Curing time was 10 min. at 120°C.

§ 4.3 Measurements

A HP3325A Synthesizer/Function Generator(20 MHz max.) was used to apply the source signal, and a Tektronix 2215 60 MHz Oscilloscope was used to measure both source and output voltage at each termination. A sinusoidal voltage was applied using frequencies up to 10 MHz. Peak voltages were measured and plotted versus frequency. Voltage versus frequency was plotted on both linear and dB scales.

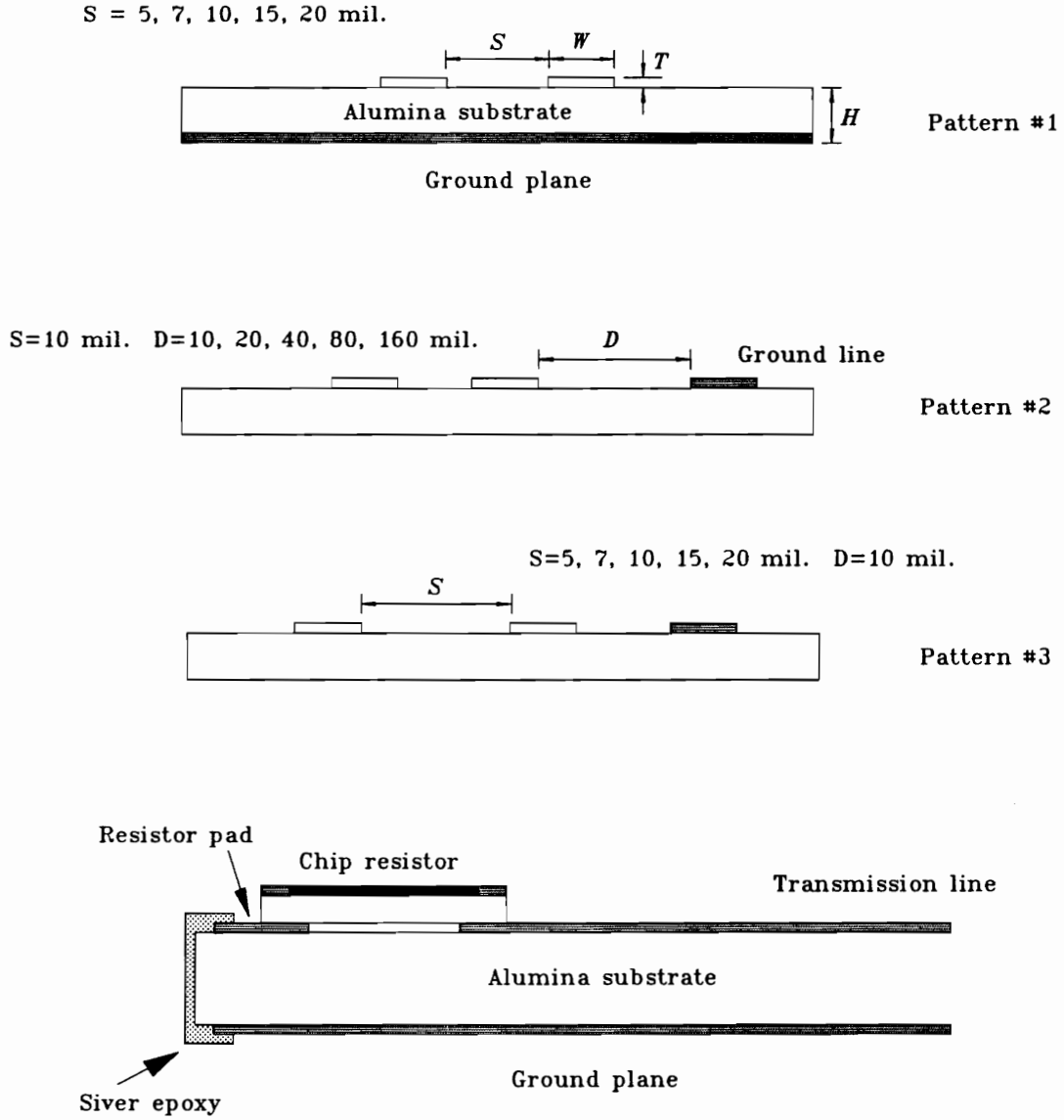

Fig. 4.1.a Test patterns #1, #2, and #3.

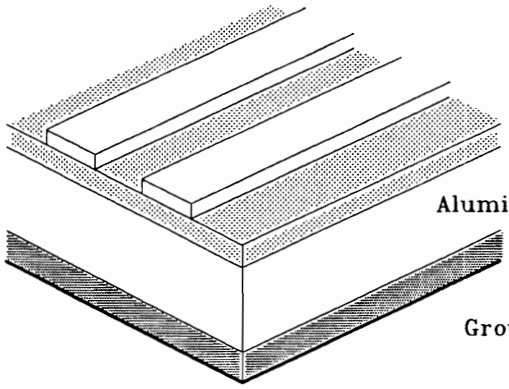

Single TOS layer

Variations in line separation

Pattern A

Variations in TOS layer

Variations in line separation

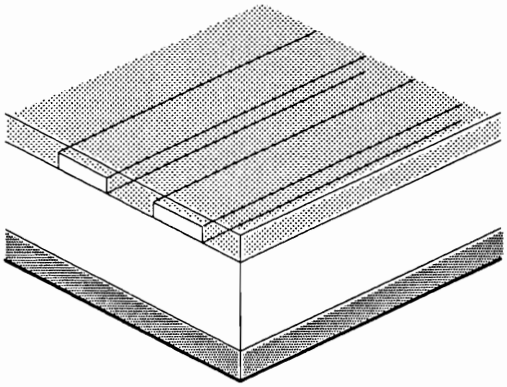

Pattern B

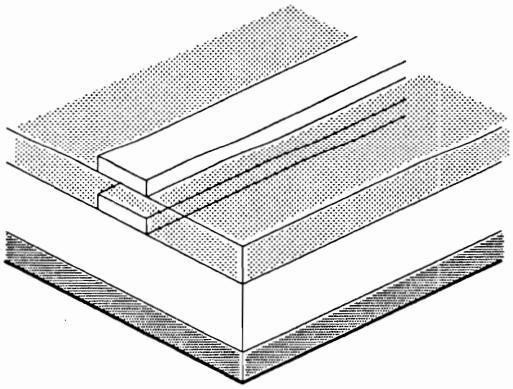

Variations in TOS layer (line separation)

Pattern C

Fig. 4.1.b TOS test patterns A, B, and C.

Chapter V

Results and Discussion

The major test results are illustrated in the Figures 5.1 to 5.9. They may be summarised as follows:

- Fig. 5.1.a Typical crosstalk of coupled transmission lines.
- Fig. 5.1.b Crosstalk in dB for the same sample as that in Fig. 5.1.a.
- Fig. 5.2 Line separation dependence of Pattern #1 crosstalk versus frequency for 75Ω termination. Patterns A and B show similar results to Pattern #1.
- Fig. 5.3.a Termination resistance dependence of crosstalk for Pattern #1 versus frequency.
- Fig. 5.3.b Line separation dependence of Pattern #1 crosstalk versus termination resistance.
- Fig. 5.4 Ground line distance dependence of Pattern #2 crosstalk versus frequency. Sign of the far-end crosstalk is considered for illustrative purposes.
- Fig. 5.5 Ground line distance dependence of Pattern #2 crosstalk versus termination resistance.
- Fig. 5.6 Line spacing dependence of Pattern #3 crosstalk versus frequency.
- Fig. 5.7 Line spacing dependence of Pattern #3 crosstalk versus termination resistance.
- Fig. 5.8 Termination resistance dependence of Pattern C crosstalk versus

frequency.

· Fig. 5.9 Line separation dependence (number of TOS layers) of Pattern C crosstalk versus termination resistance.

§ 5.1 Test results

Typical crosstalk values for Pattern #1 at both near- and far-end are shown in Fig. 5.1.a where absolute values are given in a linear scale. The input source was a sinusoidal signal and the peak voltage of each signal was recorded. Crosstalk shows good linearity between 3 MHz and 10 MHz. Crosstalk at frequencies lower than 1 MHz can be seen more easily when plotted in a dB gain scale as shown in Fig. 5.1.b. It is shown that crosstalk maintains a practically constant level in the frequency range below than 1 MHz. Fig. 5.2 shows the line separation dependence of Pattern #1 for a given termination resistance where only linear frequency dependence ranges are plotted. In Fig. 5.3.a, the frequency dependence of crosstalk for Pattern #1 is illustrated for each termination resistance for a given line separation; the open termination shows a high, constant (maximized) level of crosstalk. This will be discussed in the next section. When resistance dependence is recorded, the sign of output voltage was considered as shown in Fig. 5.3.b, because far-end crosstalk shows negative sign sometimes. Patterns A and B show similar results to Pattern #1. Figs. 5.4 – 5.7 show the crosstalk of Pattern #2 and #3 where ground line dependence (Pattern #2) and line separation dependence (Pattern #3) were recorded, respectively. The sign of far-end crosstalk is not always negative. In Fig. 5.9, it is shown that the far-end sign of Pattern C varies depending on line separation (number of TOS layers) and/or termination resistance. The near-end

crosstalk of Pattern C has a minimum value between 50Ω and 75Ω. This will be discussed in detail in the next section.

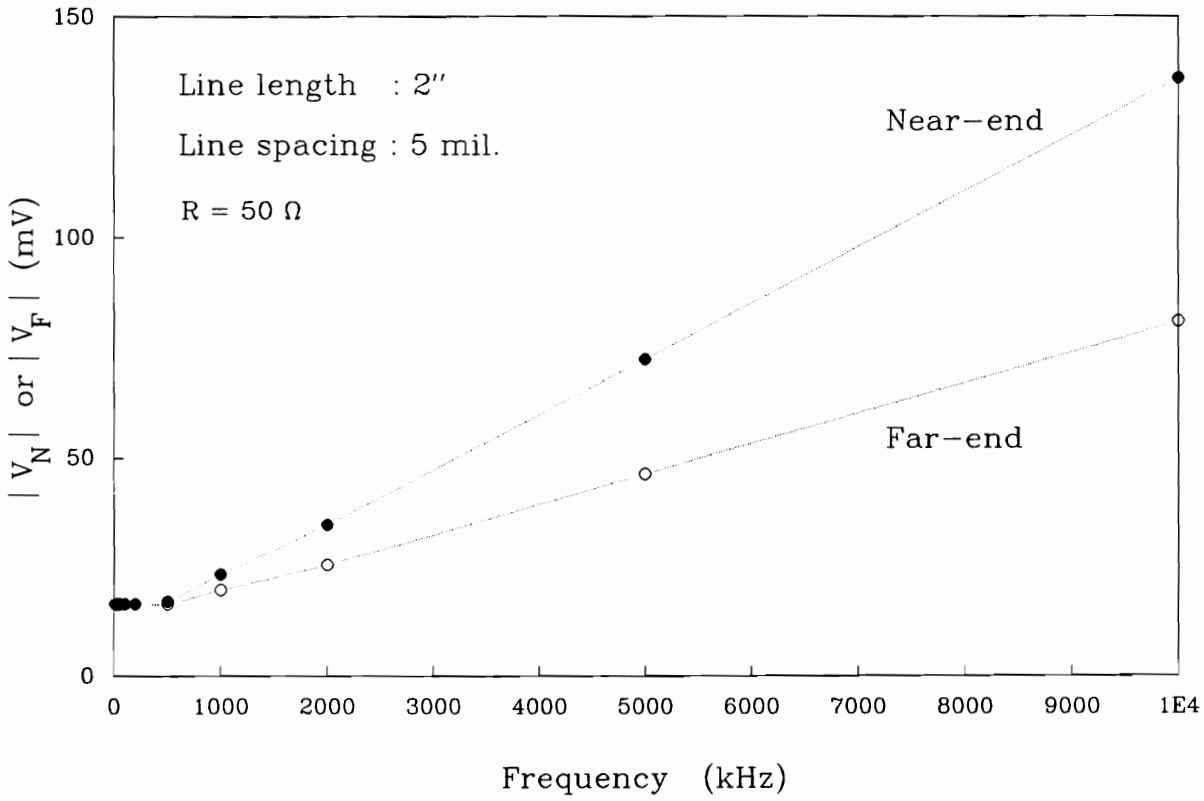

Fig. 5.1.a Typical crosstalk of coupled transmission lines for Pattern #1.

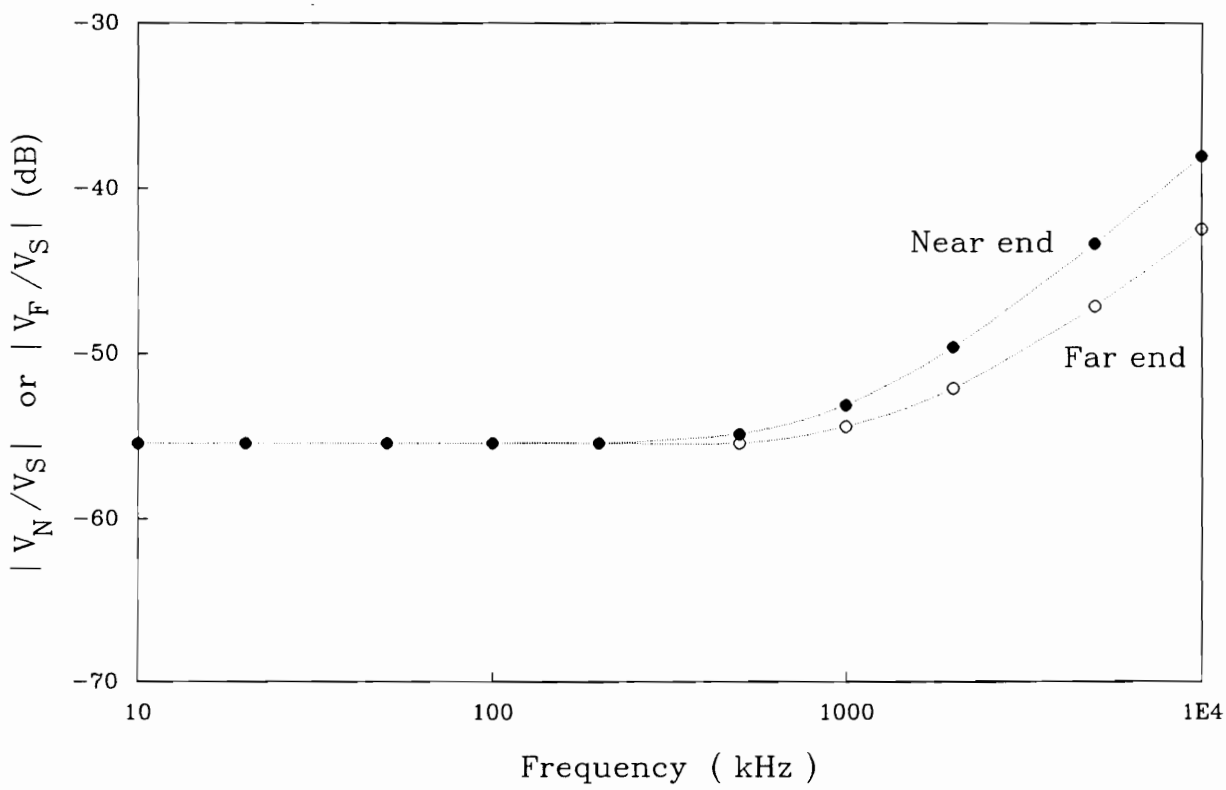

Fig. 5.1.b Crosstalk expressed in dB for Pattern #1.

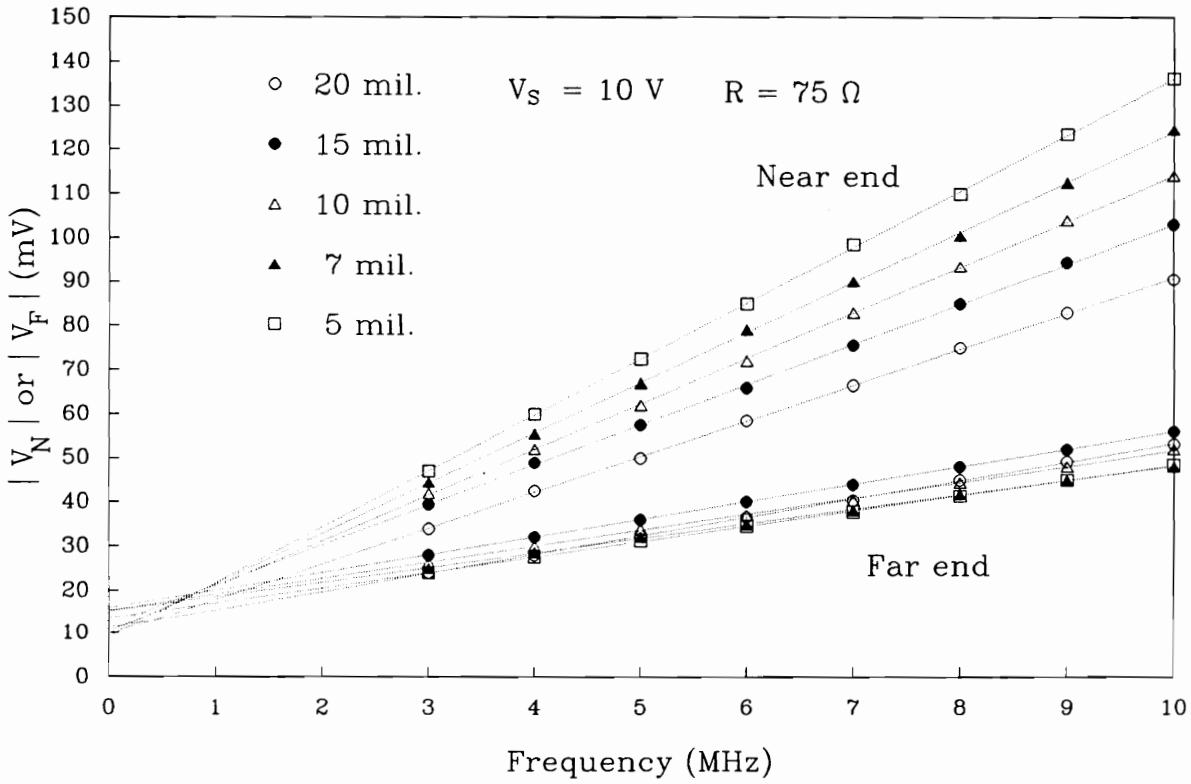

Fig. 5.2 Line separation dependence of Pattern #1 crosstalk versus frequency for 75 Ω termination. TOS Patterns A and B show similar results to Pattern #1.

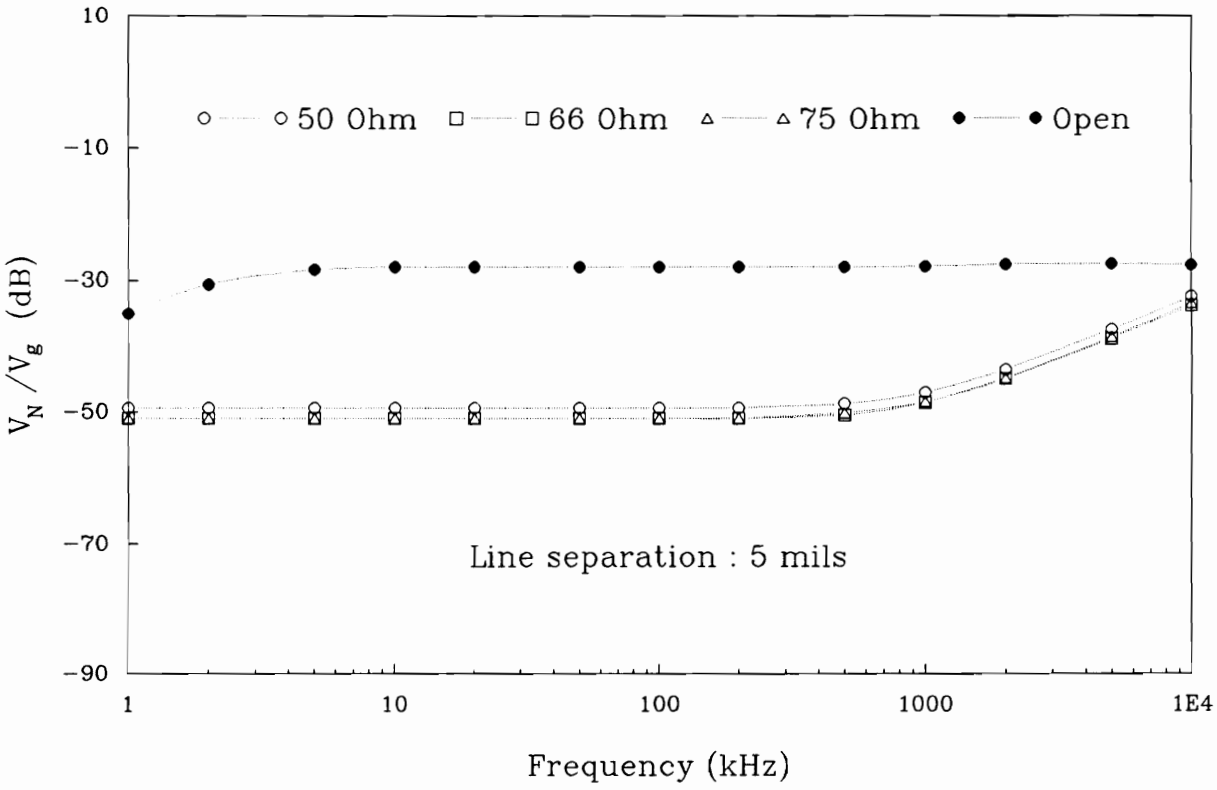

Fig. 5.3.a Terminating resistance dependence of crosstalk for Pattern #1 versus frequency

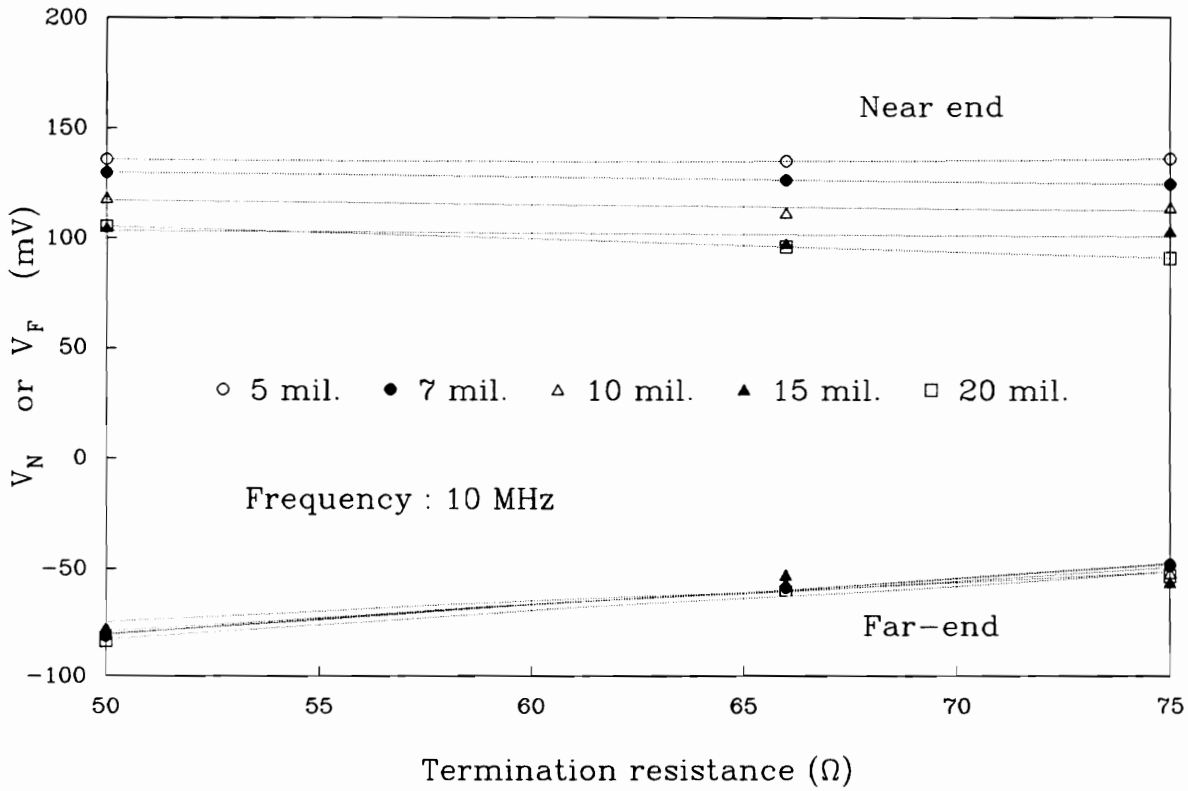

Fig. 5.3.b Line separation dependence of Pattern #1 crosstalk versus termination resistance

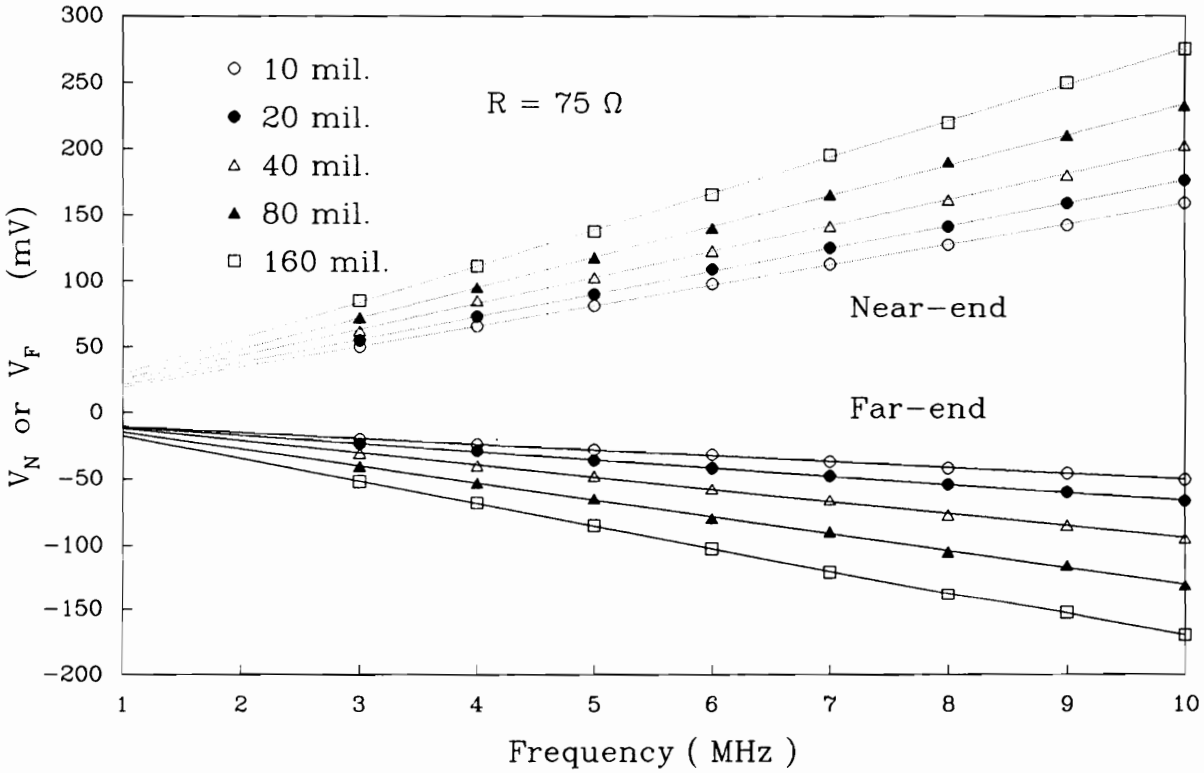

Fig. 5.4 Ground line distance dependence of Pattern #2 crosstalk versus frequency. Sign of the far−end crosstalk is considered for illustrative purposes.

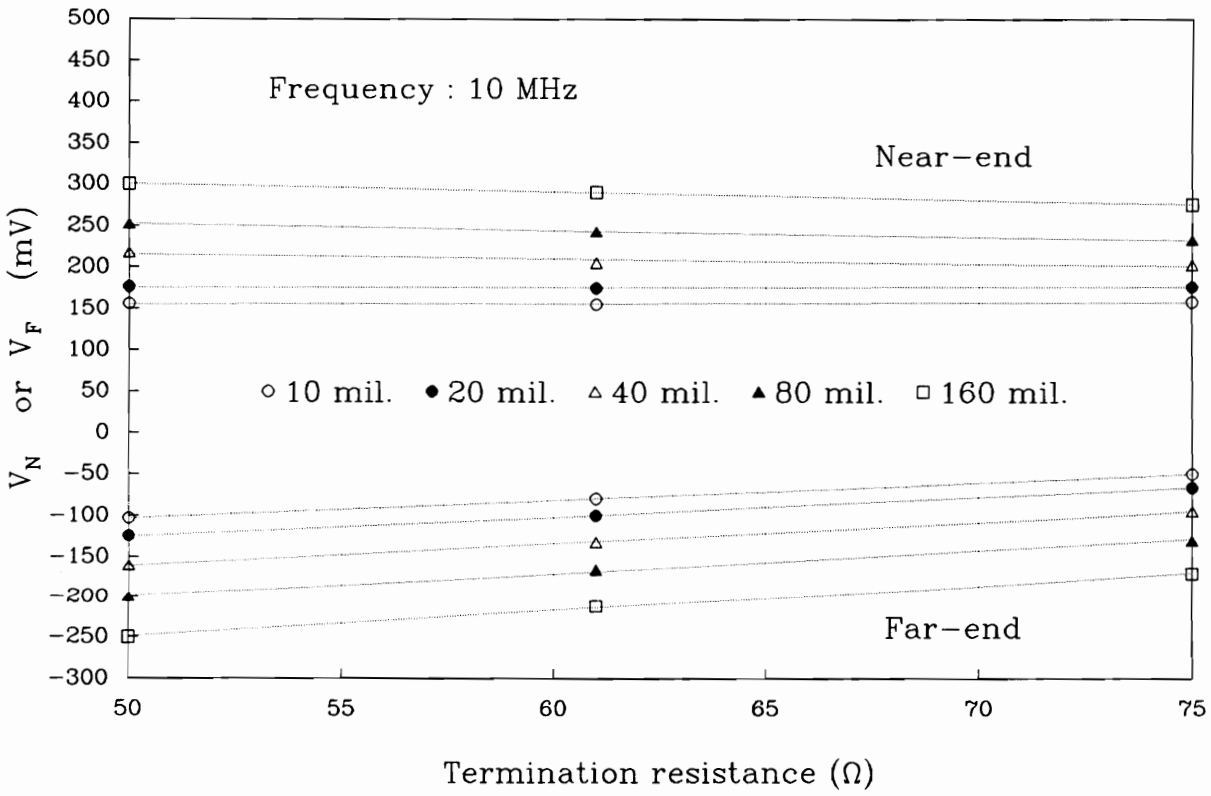

Fig. 5.5 Ground line distance dependence of Pattern #2 crosstalk versus termination resistance

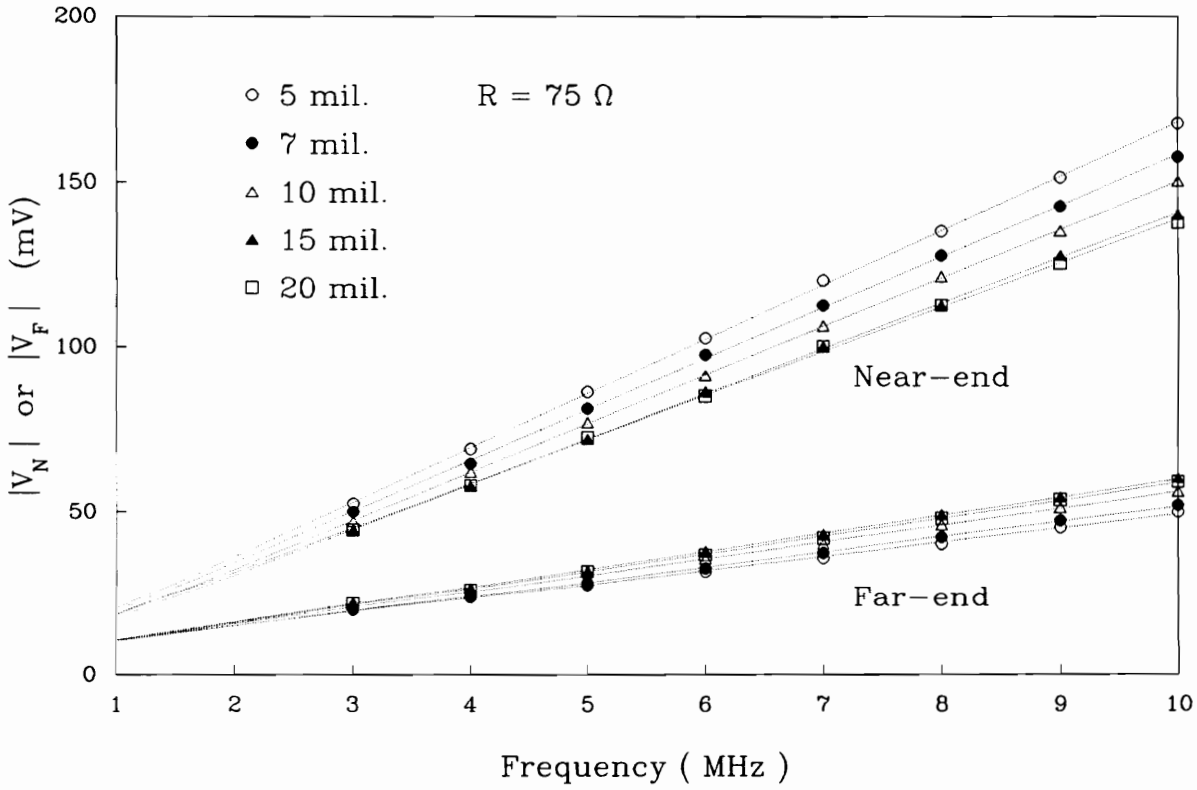

Fig. 5.6 Line spacing dependence of Pattern #3 crosstalk versus frequency

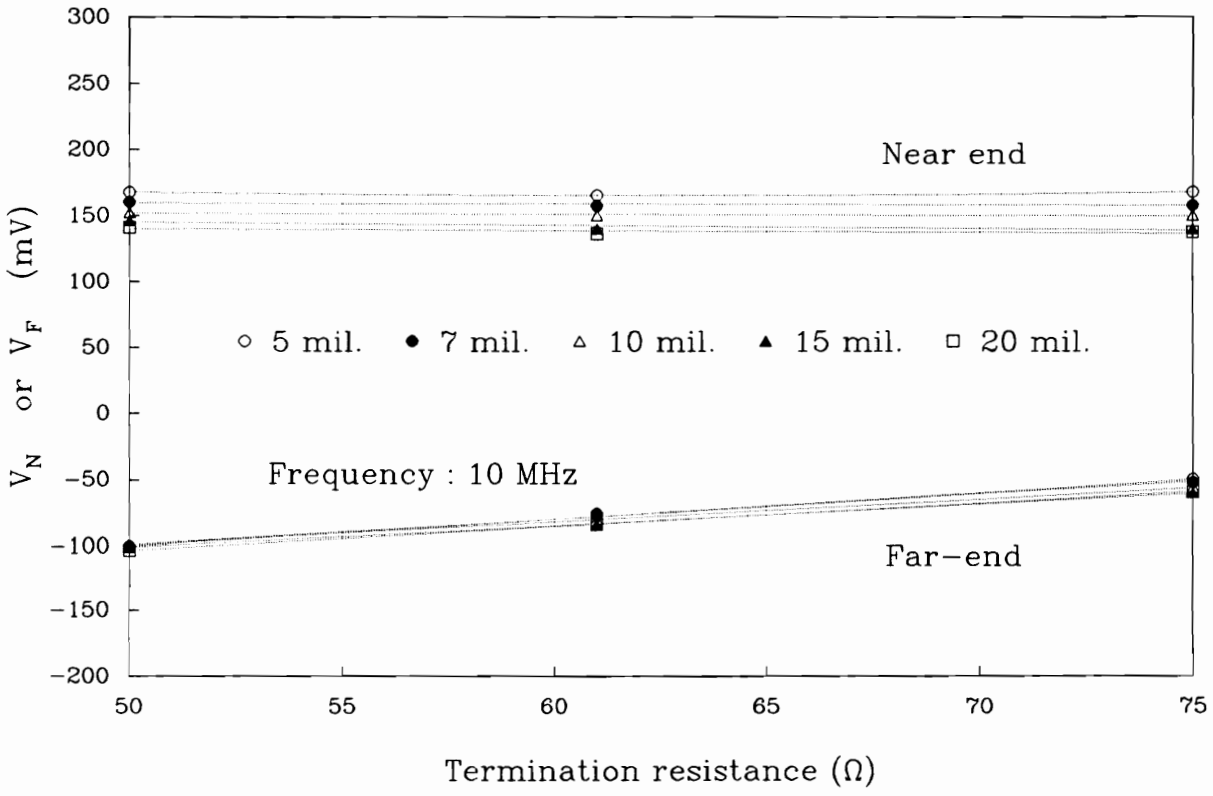

Fig. 5.7 Line spacing dependence of Pattern #3 crosstalk versus termination resistance

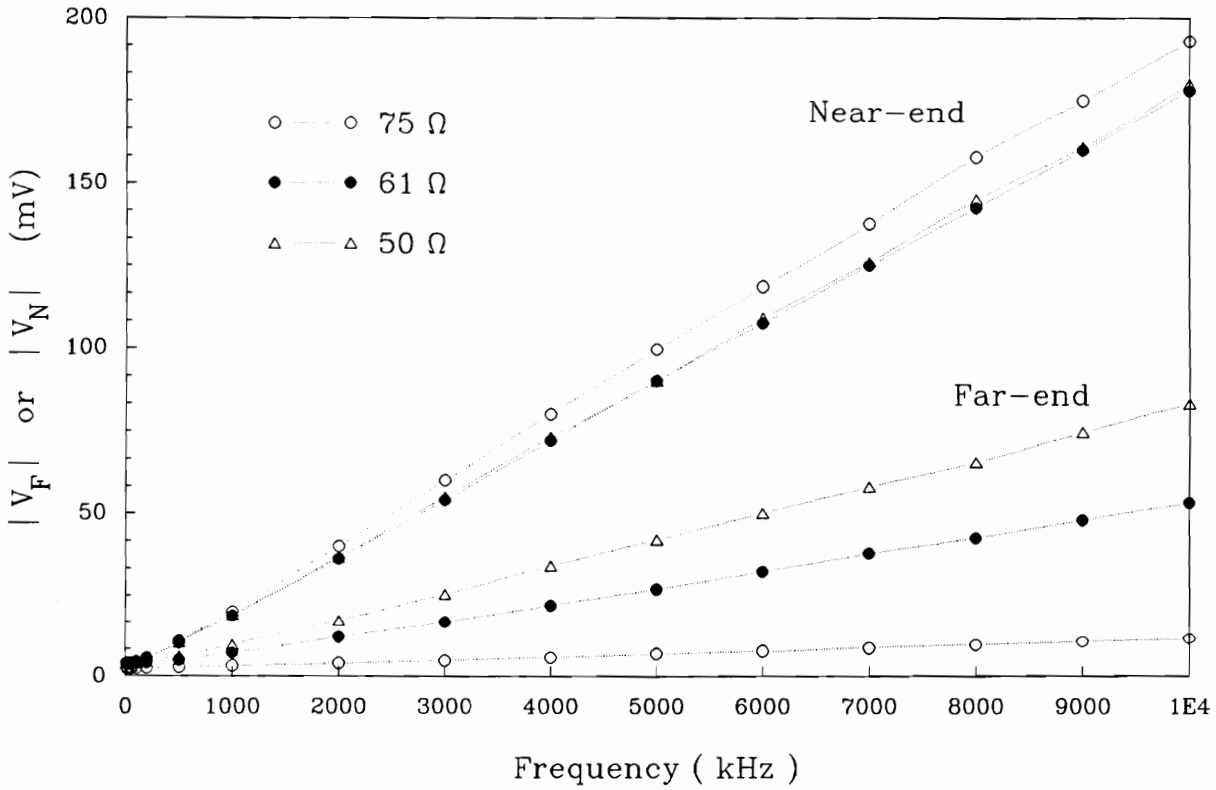

Fig. 5.8 Termination resistance dependence of Pattern C crosstalk versus frequency

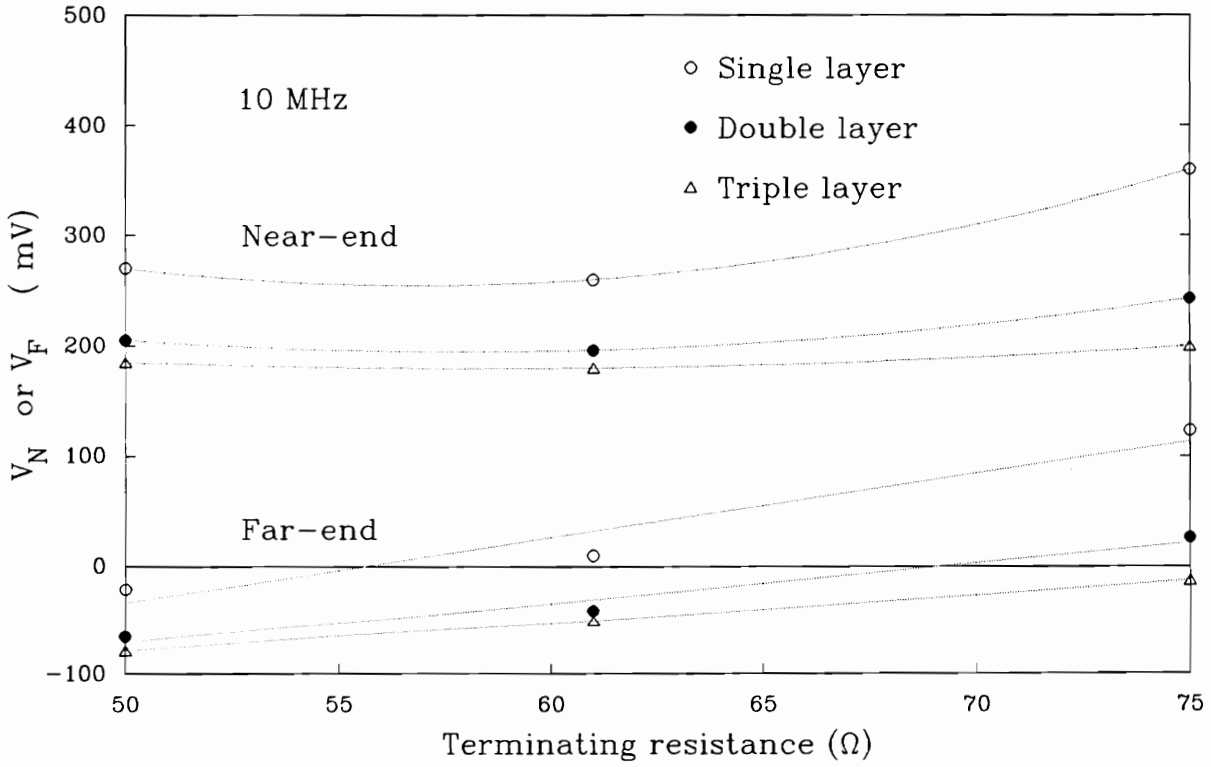

Fig. 5.9 Line separation dependence (number of TOS layers) of Pattern C crosstalk versus terminating resistance.

§ 5.2 Discussion

The goal of this study is to be able to predict crosstalk for given transmission line parameters such as line spacing, ground line distance, etc. as mentioned earlier. The first step in predicting crosstalk is to model the crosstalk itself. There are several crosstalk equations at high frequencies suitable for TEM or quasi-TEM mode applications. Paul[7] derived a low frequency approximation, as a special case, from the general high-frequency solution. In this section, a crosstalk equation will also be derived for low frequency applications.

5.2.1 Crosstalk modeling

Consider a signal propagating on line 1 as shown in Fig. 5.10. The coupling can be divided into two components; capacitive and inductive. These two coupling components are induced by the mutual capacitance C_m and the mutual inductance L_m, respectively in Fig. 5.10. The capacitively induced current, i_C, is induced in line 2 by mutual capacitance. This current divides into two currents of opposite phase which propagate toward each end of the line (i_{CN} and i_{CF}). Simultaneously, an inductive current i_L is induced in line 2 by mutual inductance and forms a loop current. As a result, near- and far-end currents are established as:

$$\begin{aligned} i_F &= i_L + i_{CF} \\ i_N &= i_{CN} - i_L \end{aligned} \tag{5.1}$$

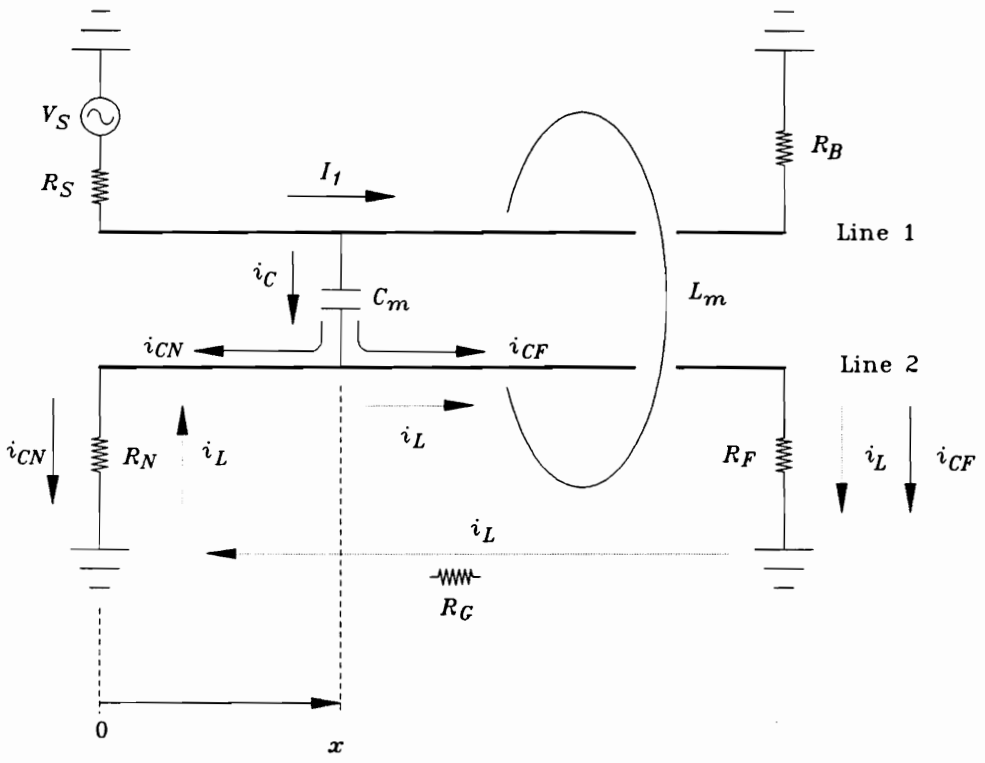

Fig. 5.10 Crosstalk model showing induced current components

and

$$\begin{aligned} V_F &= R_F i_F \\ V_N &= R_N i_N \end{aligned} \tag{5.2}$$

where

$$R_F i_{CF} = R_N i_{CN} \tag{5.3}$$

Thus, from Eq.(5.1),

$$\begin{aligned} i_F + i_N &= i_{CF} + i_{CN} \\ i_F - i_N &= 2i_L + i_{CF} - i_{CN} \end{aligned} \tag{5.4}$$

When crosstalk is discussed at low frequencies, it is plausible to apply "loose-coupling" theory. Then from Eq.(3.48),

$$\frac{\partial I_2}{\partial x} = -C\frac{\partial V_2}{\partial t} + C_m\frac{\partial V_1}{\partial t} \tag{5.5}$$

$$\frac{\partial V_2}{\partial x} = -L\frac{\partial I_2}{\partial t} - L_m\frac{\partial I_1}{\partial t} \tag{5.6}$$

Jarvis[6] combined the above two equations to find I_2 and V_2 by considering the correlation between them. However, the second term on the right hand side of each equation refers to the component induced by the mutual parameter, i.e.,

$$\frac{\partial i_C}{\partial x} = C_m\frac{\partial V_1}{\partial t} \tag{5.7}$$

$$\frac{\partial V_L}{\partial x} = -L_m \frac{\partial I_1}{\partial t} \tag{5.8}$$

where i_C is the capacitively induced current and V_L is the inductively induced potential. Integrating Eq.(5.7), considering current direction, from x to 0 (to obtain i_{CN}) and from x to l (to obtain i_{CF}) yields capacitive current at each terminal as,

$$\begin{aligned} i_C\big|_{x=0} &= i_{CN} = -\int_x^0 C_m \frac{\partial V_1}{\partial t} dx \\ i_C\big|_{x=l} &= i_{CF} = \int_x^l C_m \frac{\partial V_1}{\partial t} dx \end{aligned} \tag{5.9}$$

Thus,

$$i_C = i_{CN} + i_{CF} = \int_0^l C_m \frac{\partial V_1}{\partial t} dx \tag{5.10}$$

From Eq.(5.1) and (5.2), when considering each termination resistance R_F and R_N,

$$R_F i_F = V_F = R_F (i_L + i_{CF}) \tag{5.11}$$

$$R_N i_N = V_N = R_N (i_{CN} - i_N) \tag{5.12}$$

Multiplying Eq.(5.11) by R_N and (5.12) by R_F, and then adding them yields

$$R_N V_F + R_F V_N = R_N R_F (i_{CN} + i_{CF}) \tag{5.13}$$

From Eq.(5.9),

$$R_N V_F + R_F V_N = R_N R_F C_m \int_0^l \frac{\partial V_1}{\partial t} dx \tag{5.14}$$

Integrating Eq.(5.8) from 0 to l gives

$$\begin{aligned} V_L \Big|_l - V_L \Big|_0 &= i_L R_F - (-i_L R_N) \\ &= -\int_0^l L_m \frac{\partial I_1}{\partial t} dx \\ &= -\int_0^l \frac{L_m}{R_B} \frac{\partial V_1}{\partial t} dx \end{aligned} \tag{5.15}$$

where $V_1 = I_1 R_B$ according to loose-coupling theory.

From Eq.(5.11), (5.12), (5.3), and (5.15),

$$\begin{aligned} V_F - V_N &= (R_F + R_N) i_L + R_F i_{CF} - R_N i_{CN} \\ &= (R_F + R_N) i_L = -\int_0^l \frac{L_m}{R_B} \frac{\partial V_1}{\partial t} dx \end{aligned} \tag{5.16}$$

Combining Eq.(5.14) and (5.16), we obtain :

$$V_N = \left[\frac{R_N}{R_F + R_N} L_m \frac{1}{R_S + R_B} + \frac{R_N R_F}{R_F + R_N} C_m \frac{R_B}{R_S + R_B} \right] \int_0^l \frac{\partial V_S}{\partial t} dx$$

$$V_F = - \left[\frac{R_F}{R_F + R_N} L_m \frac{1}{R_S + R_B} - \frac{R_N R_F}{R_F + R_N} C_m \frac{R_B}{R_S + R_B} \right] \int_0^l \frac{\partial V_S}{\partial t} dx \qquad (5.17)$$

where $V_1 = \frac{R_B}{R_S + R_B} V_S$ has been substituted. When V_S is a sinusoidal signal without attenuation, Eq.(5.17) is equivalent to Paul's result in Eq.(2.5). If each termination has the condition of $R_B = R_N = R_F = R = Z_o$, Eq.(5.17) becomes

$$V_N = \frac{1}{2} \left(\frac{L_m}{Z_o} + C_m Z_o \right) \int_0^l \frac{\partial V_S}{\partial t} dx$$

$$V_F = - \frac{1}{2} \left(\frac{L_m}{Z_o} - C_m Z_o \right) \int_0^l \frac{\partial V_S}{\partial t} dx \qquad (5.18)$$

In this study, every line was terminated by resistor of the same resistance value. From the above equations, a minimum V_N occurs as R varies. Pattern C shows this minimum between 50Ω and 75Ω (Fig. 5.9). V_F also varies from negative to positive as R varies. In directional coupling condition, V_F becomes zero as discussed in § 2.2. Pattern C shows this condition as mentioned in § 5.1 (Fig. 5.9).

When V_S is an arbitrary signal with propagation delay T_d, Eq.(5.18) can be described as:

$$V_N = \frac{1}{2}\left(\frac{L_m}{Z_o} + C_m Z_o\right)\int_0^l \frac{\partial V(t-2x/c)}{\partial t}dx$$
$$V_F = -\frac{1}{2}\left(\frac{L_m}{Z_o} - C_m Z_o\right)\int_0^l \frac{\partial V(t-T_d)}{\partial t}dx \tag{5.19}$$

where C is the wave propagation velocity.

Then

$$V_N = \frac{c}{4}\left(\frac{L_m}{Z_o} + C_m Z_o\right)\left[V(t)-V(t-2T_d)\right]$$
$$V_F = -\frac{1}{2}l\left(\frac{L_m}{Z_o} - C_m Z_o\right)\frac{dV(t-T_d)}{dt} \tag{5.20}$$

Eq.(5.20) is equivalent to Eq.(3.53). Jarvis[6] and Feller et al[11] first derived the line voltage of line 2 (V_2) and then obtained V_N and V_F using boundary conditions, i.e., $V=Z_oI$ when $x=0$ and $x=l$. By contrast, Rainal[10] obtained V_N and V_F directly; all approaches yielded the same result.

5.2.2 Common ground impedance

When the ground is not a perfect conductor, resistance R_G will result in a voltage drop. Even at very low frequencies where crosstalk essentially dies off, this ground voltage still exists because it is independent of frequency. Paul[4] derived the ground voltage drop as follows.

For a sufficiently small frequency (the current is almost DC), the current in

line 1 is approximately:

$$I_1 = \frac{V_S}{R_S + R_B} \tag{5.21}$$

since R_G is small compared to R_S and R_B. The majority of this current passes through the common return conductor (ground), developing a voltage drop of

$$V_G = R_G I_1 \tag{5.22}$$

across that ground. This voltage is felt across the near- and far-end of line 2 to yield

$$\begin{aligned} V_{NG} &= \frac{R_N}{R_N + R_F} \frac{R_G}{R_S + R_B} V_S \\ V_{FG} &= -\frac{R_F}{R_N + R_F} \frac{R_G}{R_S + R_B} V_S \end{aligned} \tag{5.23}$$

which is frequency-independent. This provides a plateau for the total crosstalk as shown in Fig. 5.11. Strictly speaking, V_{NG} or V_{FG} is not crosstalk but simply a ground voltage drop generated by the common-ground resistance, R_G. V_{NG} and V_{FG} can be verified by applying a DC source voltage and measuring the output voltage at both near- and far-end positions. In this test, a DC power source without source resistance was used so that the input voltage was recorded as V_g, which is the same as V_1 in Eq.(5.17). Fig. 5.12 shows these ground drops versus input voltage. When these ground drops are recorded on a gain scale, it is found that their values are the same as those in Fig. 5.1.b.

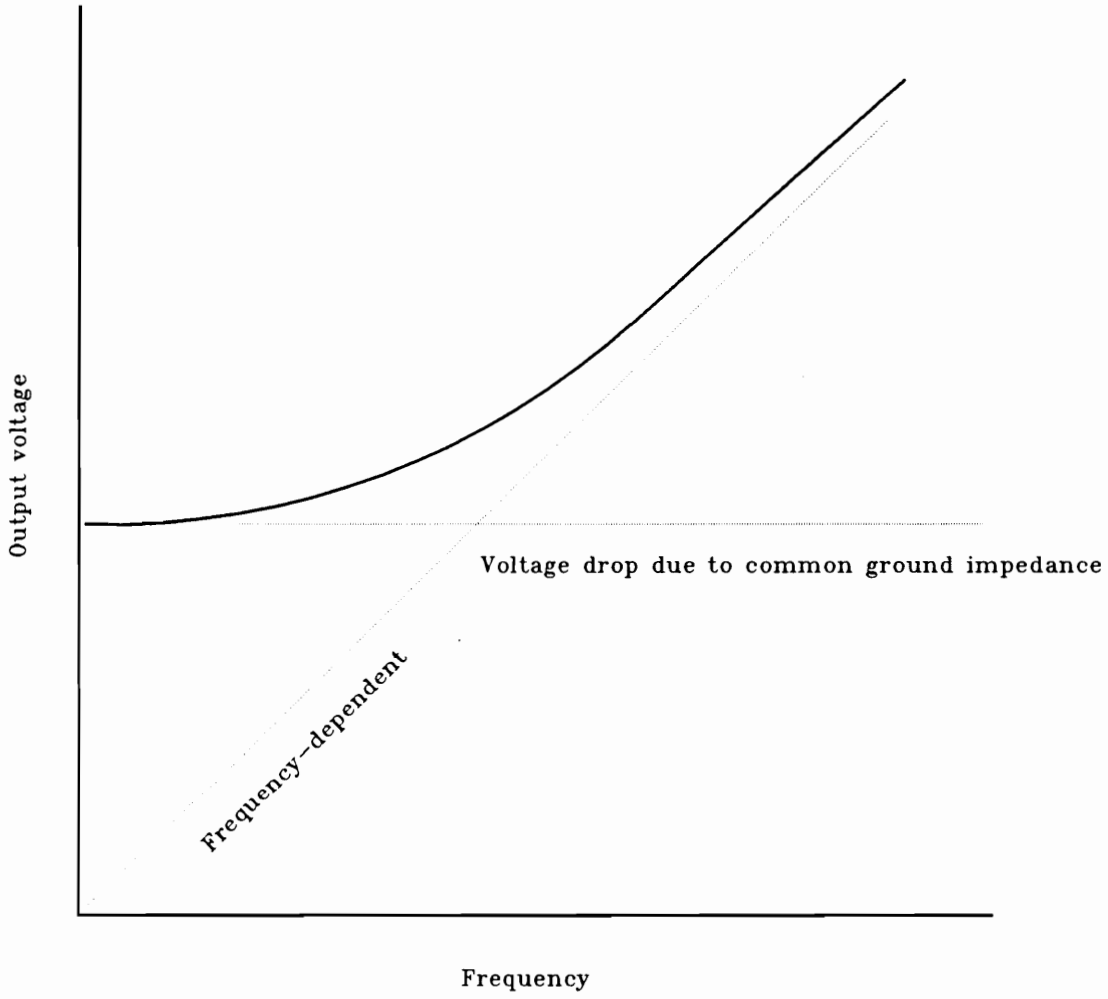

Fig. 5.11 Common ground impedance effect on frequency response of crosstalk

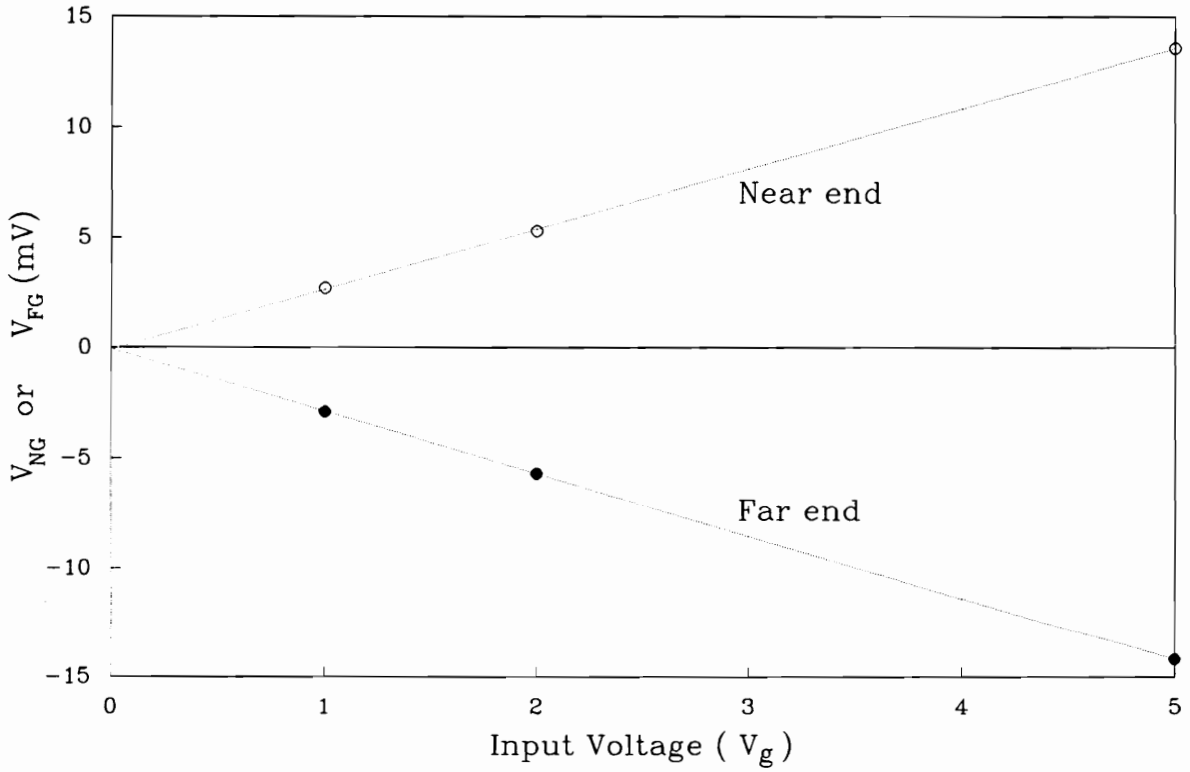

Fig. 5.12 Ground voltage drop due to common ground resistance

§ 5.3 Mutual parameters

In the previous section, mutual parameters were found to exist in the crosstalk equations. These mutual parameters can be obtained by substituting measured crosstalk values into the crosstalk equations. The measured crosstalk values can also be derived by substituting calculated mutual parameters into the crosstalk equations. In this section, experimental mutual parameters will first be discussed and, later, direct mutual parameter calculations will be shown to accurately predict crosstalk.

5.3.1 Mutual parameter data

In this study a sinusoidal signal was applied at low frequencies, leading to a crosstalk equation of the form of Eq.(2.5) as discussed earlier. Since the test pattern was terminated by $R_B = R_F = R_N = R$ at each port, the crosstalk equations become;

$$V_N = \frac{1}{2} j\omega l \left(\frac{L_m}{R} + C_m R \right) \frac{R}{R_S + R} V_S$$

$$V_F = -\frac{1}{2} j\omega l \left(\frac{L_m}{R} - C_m R \right) \frac{R}{R_S + R} V_S \qquad (5.24)$$

When the ground voltage drop is considered,

$$V_N = \frac{1}{2} j\omega l \left(\frac{L_m}{R} + C_m R \right) \frac{R}{R_S + R} V_S + \frac{1}{2} \frac{R_G}{R_S + R} V_S$$

$$V_F = -\frac{1}{2} j\omega l \left(\frac{L_m}{R} - C_m R \right) \frac{R}{R_S + R} V_S - \frac{1}{2} \frac{R_G}{R_S + R} V_S \tag{5.25}$$

At very low frequencies where $\omega \cong 0$, only the second term of each equation in Eq.(5.25) remains, resulting in constant values for V_F and V_N. As the frequency increases, the first term begins to dominate, yielding the reduced form of Eq.(5.24). However, this relationship is not applicable to the open termination because, when $R=\infty$, Eq.(5.25) results in $V_N=V_F=\infty$, which is not a possible solution. Clearly, when the termination is open, only capacitive coupling appears, and inductive coupling does not exist. Under these circumstances, current does not flow. Therefore, from Eq.(5.5), when $I_2=0$ for open termination, we have

$$C \frac{dV_2}{dt} = C_m \frac{dV_1}{dt} \tag{5.26}$$

or

$$V_2 = \frac{C_m}{C} V_1 \tag{5.27}$$

for a sinusoidal signal. Eq.(5.27) implies that the output voltage is essentially constant, which depends on mutual capacitance and line capacitance. Fig. 5.3.a verifies that V_N=V_F=constant for an open termination.

It was shown that crosstalk is linearly dependent on frequency as described in Eq.(5.24). Thus, crosstalk can be expressed as:

$$\begin{aligned} V_N &= S_N f \\ V_F &= -S_F f \end{aligned} \tag{5.28}$$

where S_N and S_F are the slopes of the crosstalk versus frequency curves. Since S_N and S_F are measurable from these experimental curves, experimental L_m and C_m are obtained from Eq.(5.24) and Eq.(5.28):

$$\begin{aligned} L_m &= \frac{R_S+R}{2\pi l V_S}(S_N+S_F) \\ C_m &= \frac{R_S+R}{2\pi l V_S R^2}(S_N-S_F) \end{aligned} \tag{5.29}$$

5.3.2 Mutual parameter calculation

As for mutual inductance, the conventional techniques discussed in § 3.3 can be used directly for each pattern. Fig.s 5.13 through Fig. 5.16 show a comparison between experimental L_m obtained from Eq.(5.29) and the calculated L_m from Eq.(3.79). As for Pattern C, the calculated curve shows a greater rate of decrease (slope) than the real data points (Fig. 5.16). Since TOS covers both the base substrate and printed conductor lines, the thickness of TOS on the conductor lines

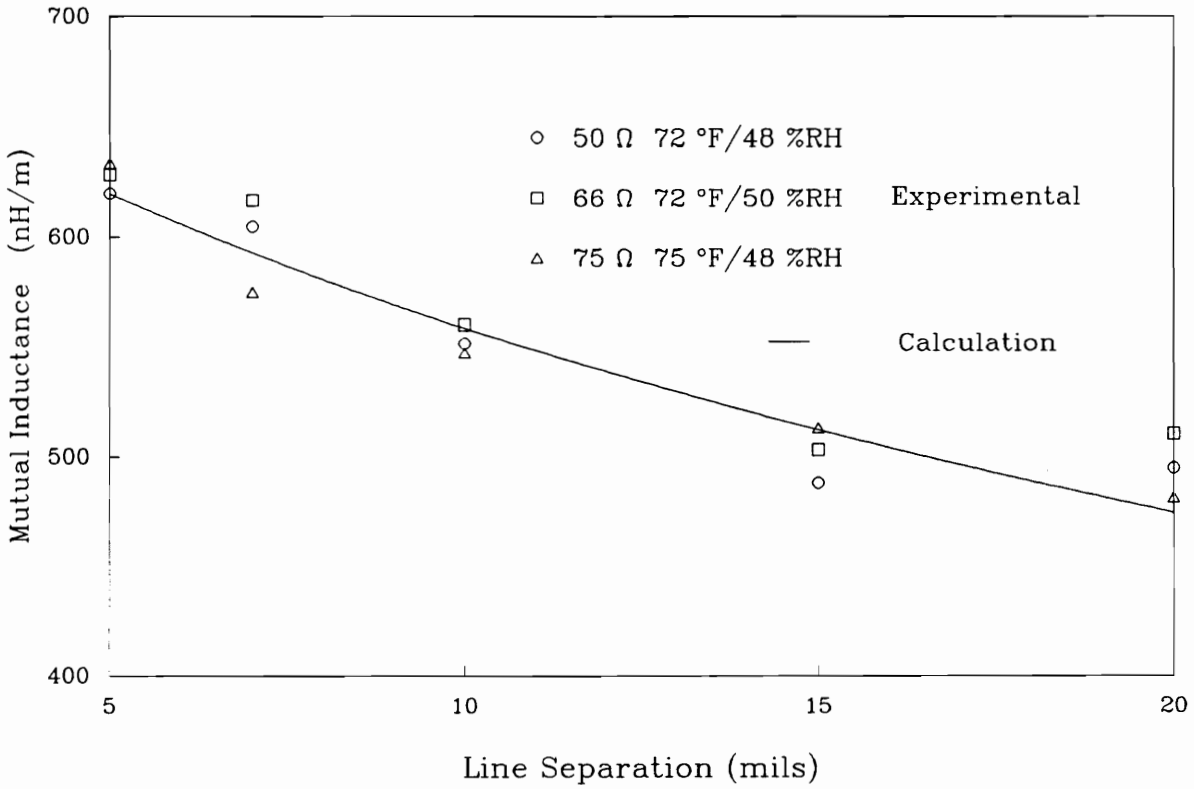

Fig. 5.13 Comparison between calculated and measured mutual inductances for Pattern #1, versus line separation (Patterns A and B show similar results to Pattern #1)

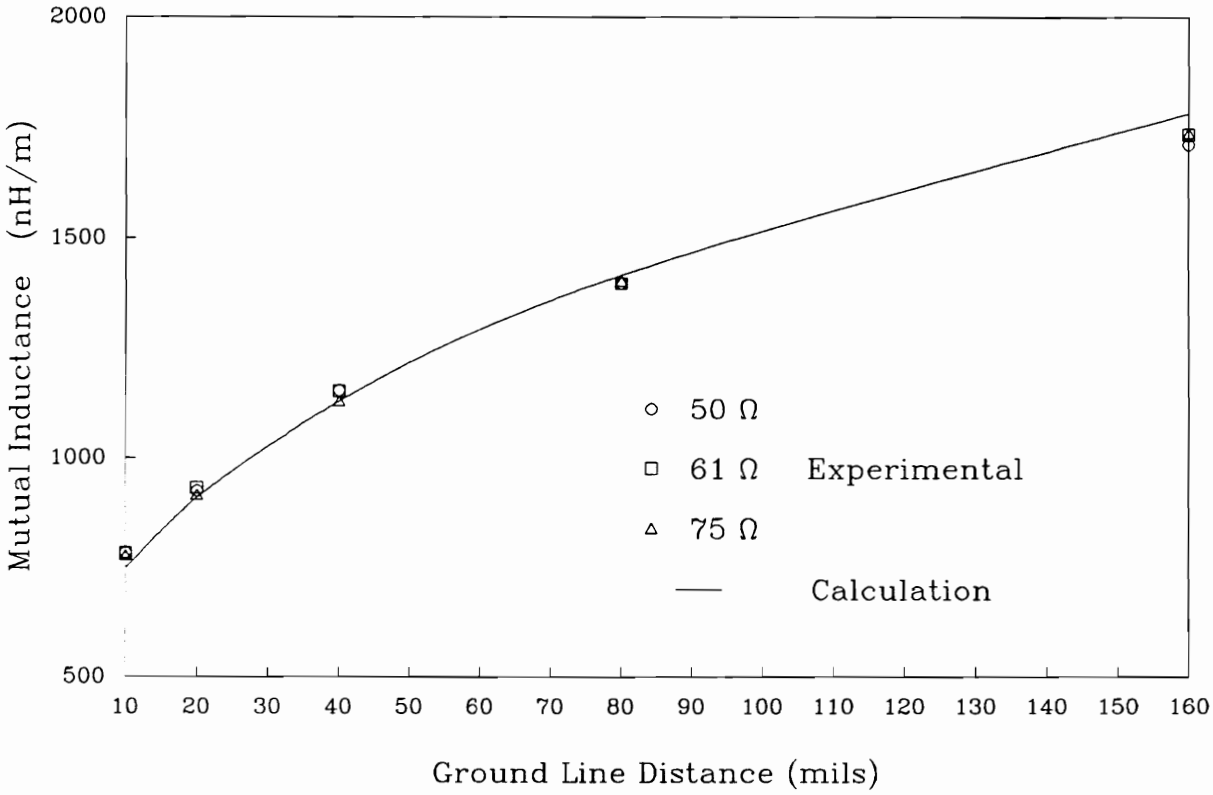

Fig. 5.14 Comparison between calculated and measured mutual inductances for Pattern #2, versus distance to ground

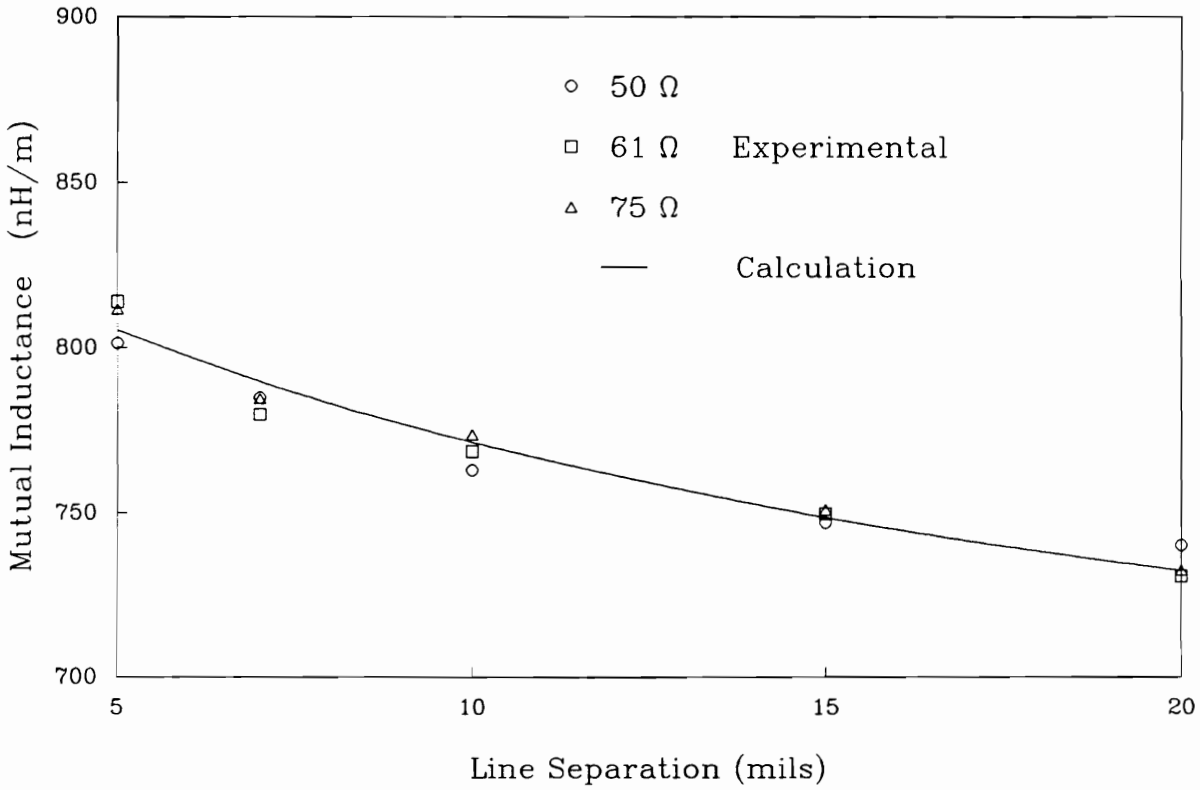

Fig. 5.15 Comparison between calculated and measured mutual inductances for Pattern #3, versus line separation

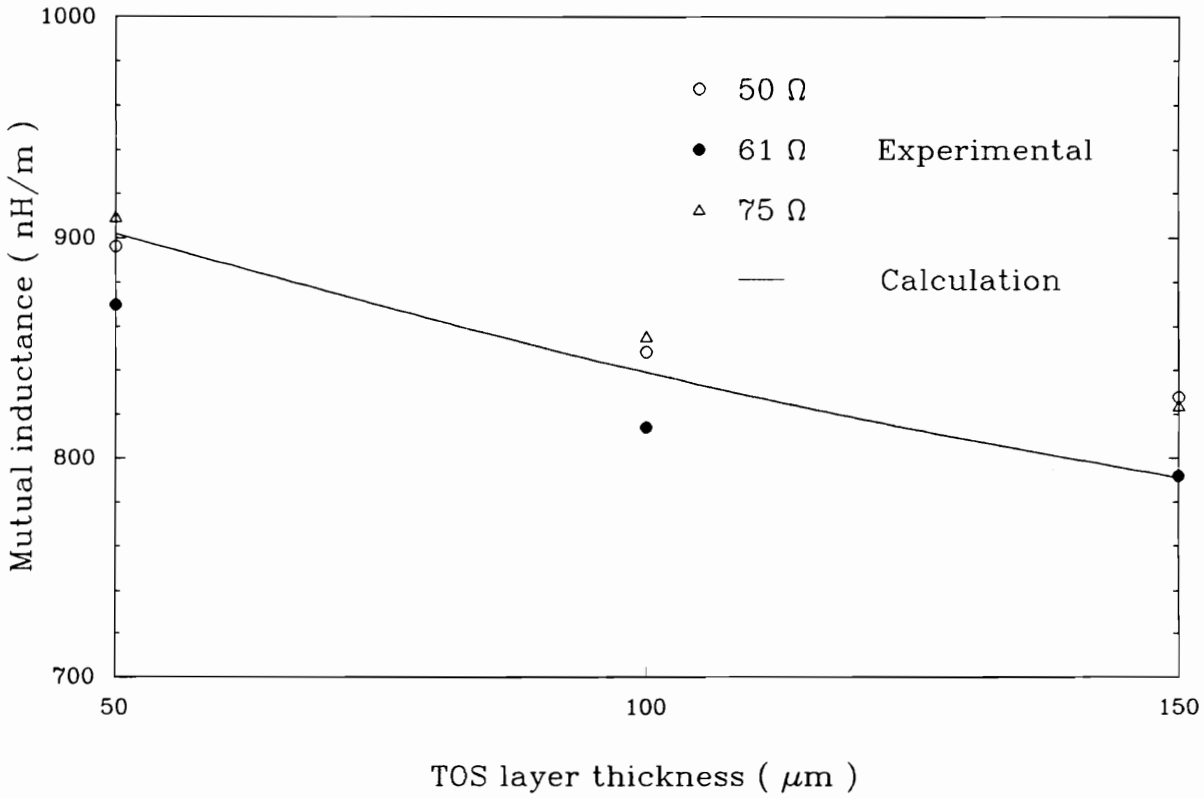

Fig. 5.16 Comparison between calculated and measured Mutual inductances for Pattern C, versus TOS thickness (line separation, i.e.; number of TOS layers)

may actually be less than the thickness on the base substrate alone.

The mutual capacitance calculations will now be discussed in detail. As the simplest case, Patterns #2 or #3 will be discussed first. A cross-sectional view of Pattern #2 (or #3) is shown in Fig. 5.17. For this structure, total mutual capacitance can be broken up into the sum of three parallel capacitances[35]; $C_m = C_1 + C_2 + C_3$.

C_1 is the capacitance calculated above the transmission line in an air medium. C_3 is the capacitance in the dielectric region only. C_2 is a capacitance that considers the conductor thickness, and is approximately given by $C_2 = e_o T/D$, where T is the conductor thickness, and D is edge-to-edge line separation. Mutual capacitance between the transmission line and ground line is neglected because the size of the ground line is so small that its effect on the electric field is assumed to be negligible. The expression for C_1 was previously discussed in § 3.2.2.

To determine C_3, first assume that all the electric field lines are concentrated in the dielectric[32,33], a reasonable assumption when the dielectric constant of the substrate is substantially higher than that of the air. Then, the following conformal mapping function is used to obtain new parallel strips on a half-infinite dielectric space;

$$t = \tanh \frac{\pi}{2H} z \tag{5.30}$$

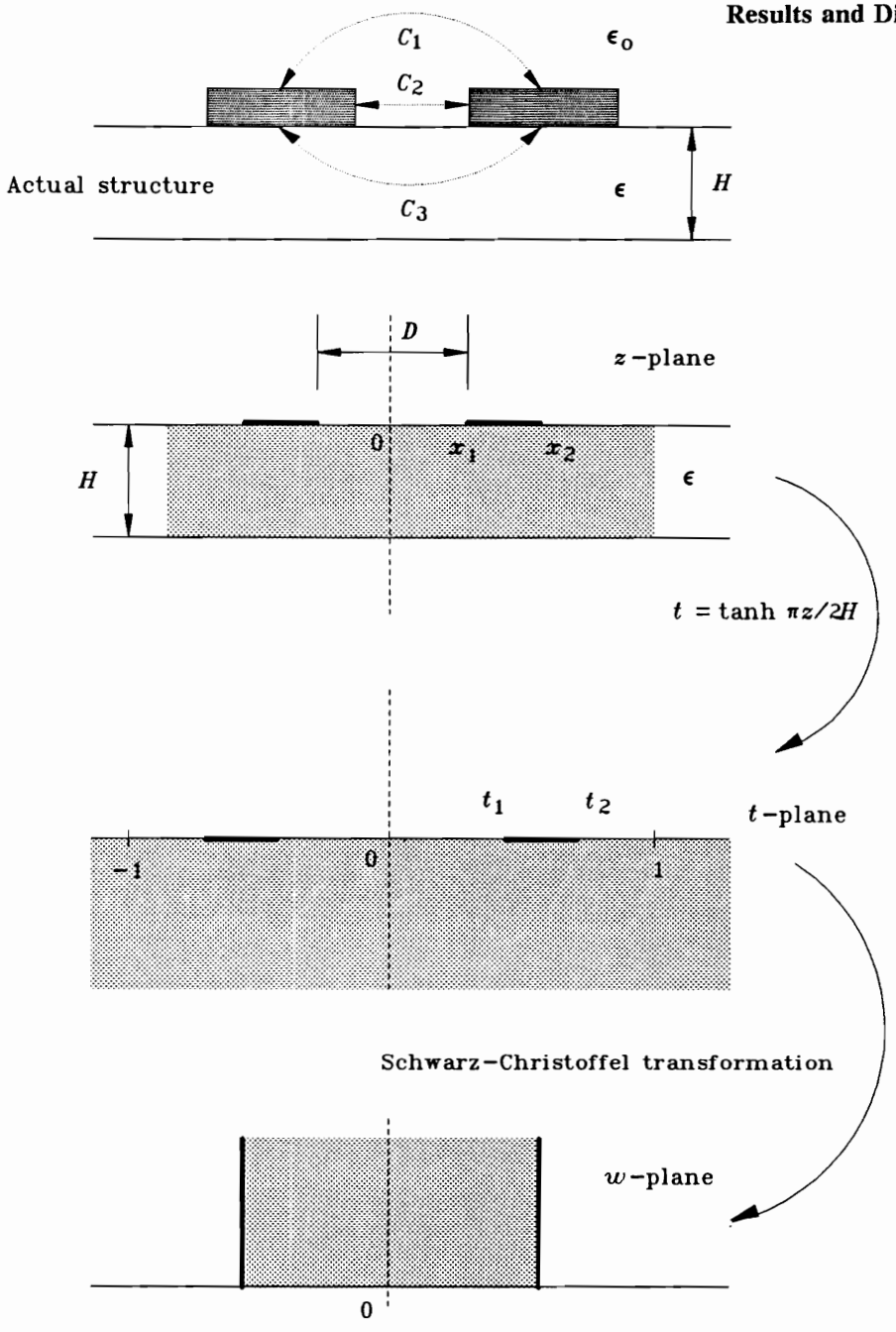

Fig. 5.17 Mutual capacitance calculation for Patterns #2 and #3 using conformal mapping

where H is substrate thickness. The above mapping function has been discussed in § 3.2.1 and gives two coplanar parallel strips with half-infinite space in the t-plane as shown in Fig. 5.17. These strips can be transformed to the w-plane using the Schwarz-Christoffel transformation, and the final capacitance calculation is obtained with parameter k_1:

$$k_1 = \frac{t_1}{t_2} = \frac{\tanh \frac{\pi}{2H} x_1}{\tanh \frac{\pi}{2H} x_2} \tag{5.31}$$

Thus, from Eq.(3.86)

$$C_3 = e \frac{K(k'_1)}{2K(k_1)} \tag{5.32}$$

where e is the permittivity of the substrate. The resultant mutual capacitance is then

$$C_m = e_o \frac{K(k'_o)}{2K(k_o)} + e_o \frac{T}{2x_1} + e \frac{K(k'_1)}{2K(k_1)} \tag{5.33}$$

where $k_o = x_1/x_2$.

Fig.s 5.18 and Fig. 5.19 show comparisons between the measured (from Eq.(5.29)) and calculated mutual capacitance for Patterns #2 and #3, respectively. The scattering of the Pattern #2 data stems from measurement error in Eq.(5.29), where C_m is expressed in pF and L_m is expressed in nH with the same error bound of ΔS_N and ΔS_F. In other words, Fig. 5.18 utilises a finer scale than Fig. 5.14, and the data appears to be more scattered. From Fig. 5.19, it can be verified that ground line

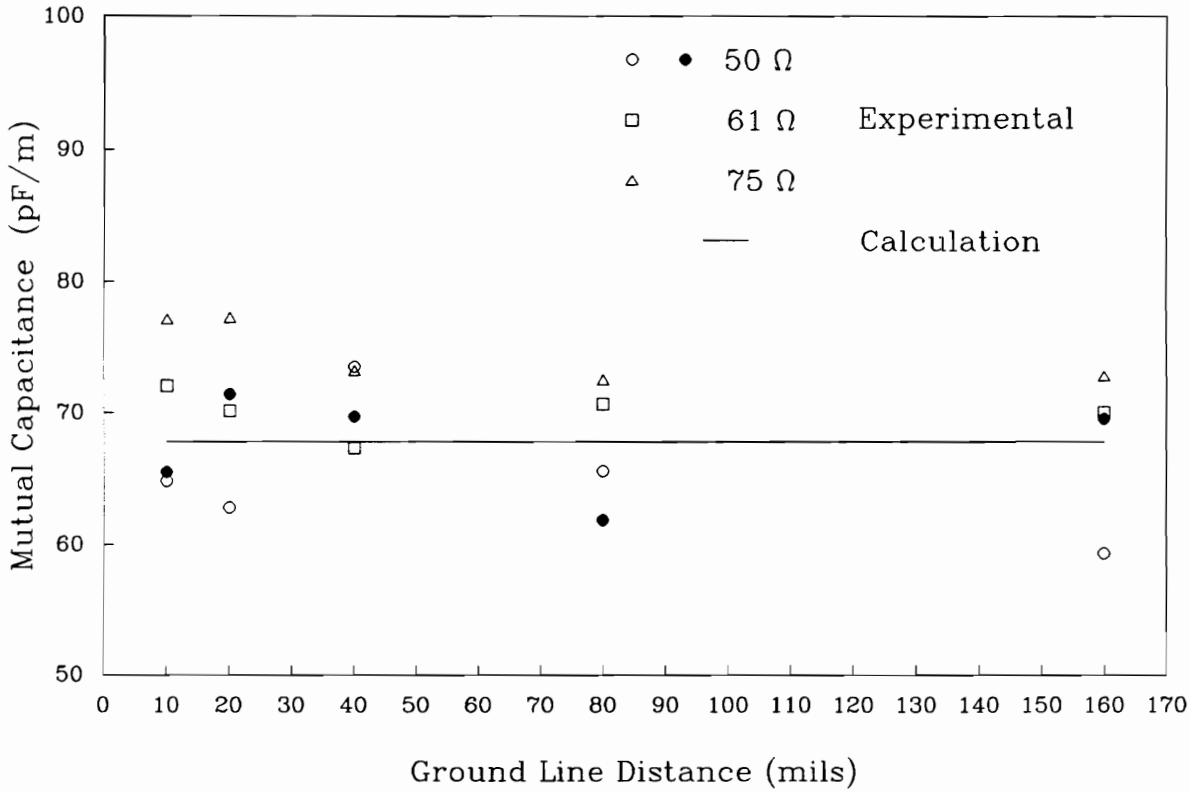

Fig. 5.18 Comparison between calculated and measured mutual capacitances for Pattern #2, versus distance to ground line.

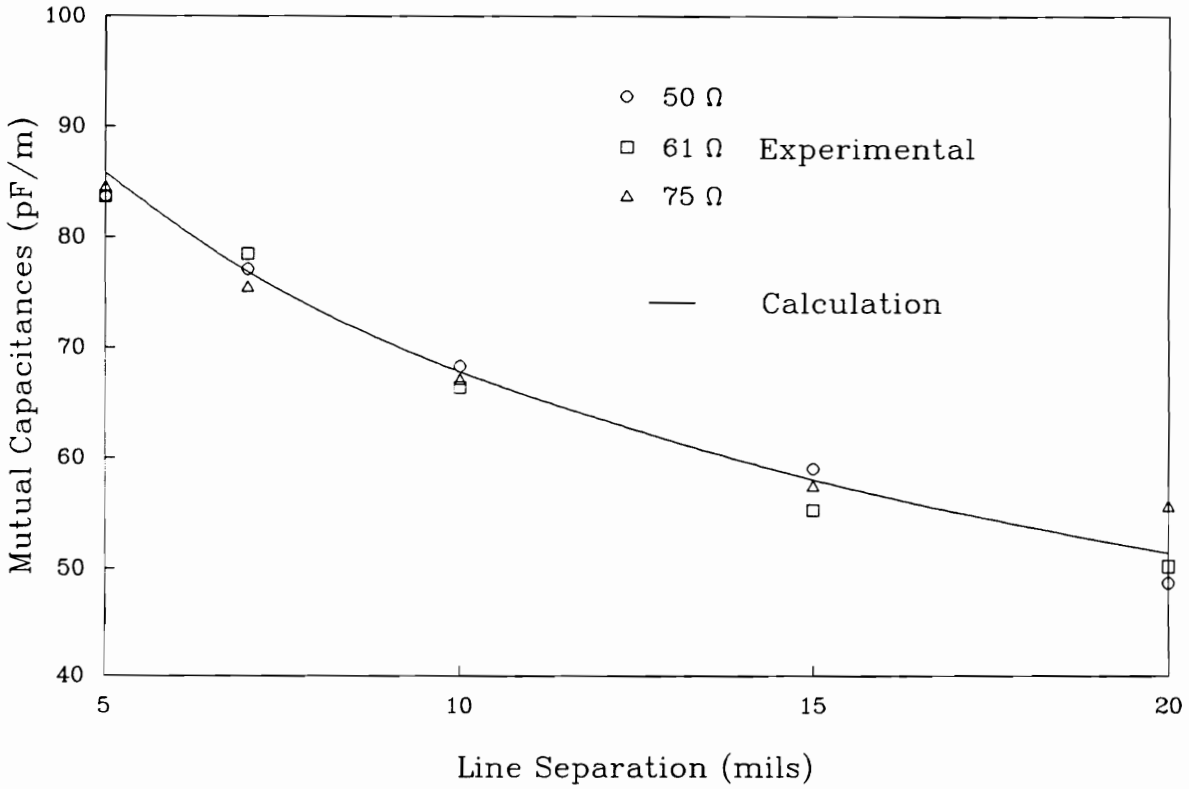

Fig. 5.19 Comparison between calculated and measured mutual capacitances for Pattern #3, versus line separation

effect on the mutual capacitance is negligible.

Now consider Pattern #1 structure which has a bottom ground plane. As a result, two sets of electric field lines exist, forming C'_3 and C_G in the dielectric. Clearly, this structure can be related to the stripline structure of Fig. 2.2.b, where the half-section of the odd-mode stripline is similar to the Pattern #1 structure (Fig. 5.20.a). Cohn's technique can then be used to calculate C_f which is essentially the same as C_m. Direct calculation from the real structure can be also tried; C'_3 can be calculated by subtracting C_G from C_3, which has been calculated in Eq.(5.32):

$$C'_3 = C_3 - \frac{C_G}{2} \tag{5.34}$$

The following transformation function may be used to obtain coplanar strips in the t-plane:

$$t = \coth \frac{\pi}{2H} z \tag{5.35}$$

This function is actually an inverse transformation function of Eq.(5.30) and can also be used to calculate C_3 of Pattern #2 (or #3). For Pattern #1, Eq.(5.35) should be used for subsequent transformations. As shown in Fig. 5.20.b, the ground plane is confined to the region between 1 and -1 on the real axis of the t-plane. The Veyres' mapping transforms the t-plane into the s-plane where only C_G exists (Fig. 5.20.c). Hence:

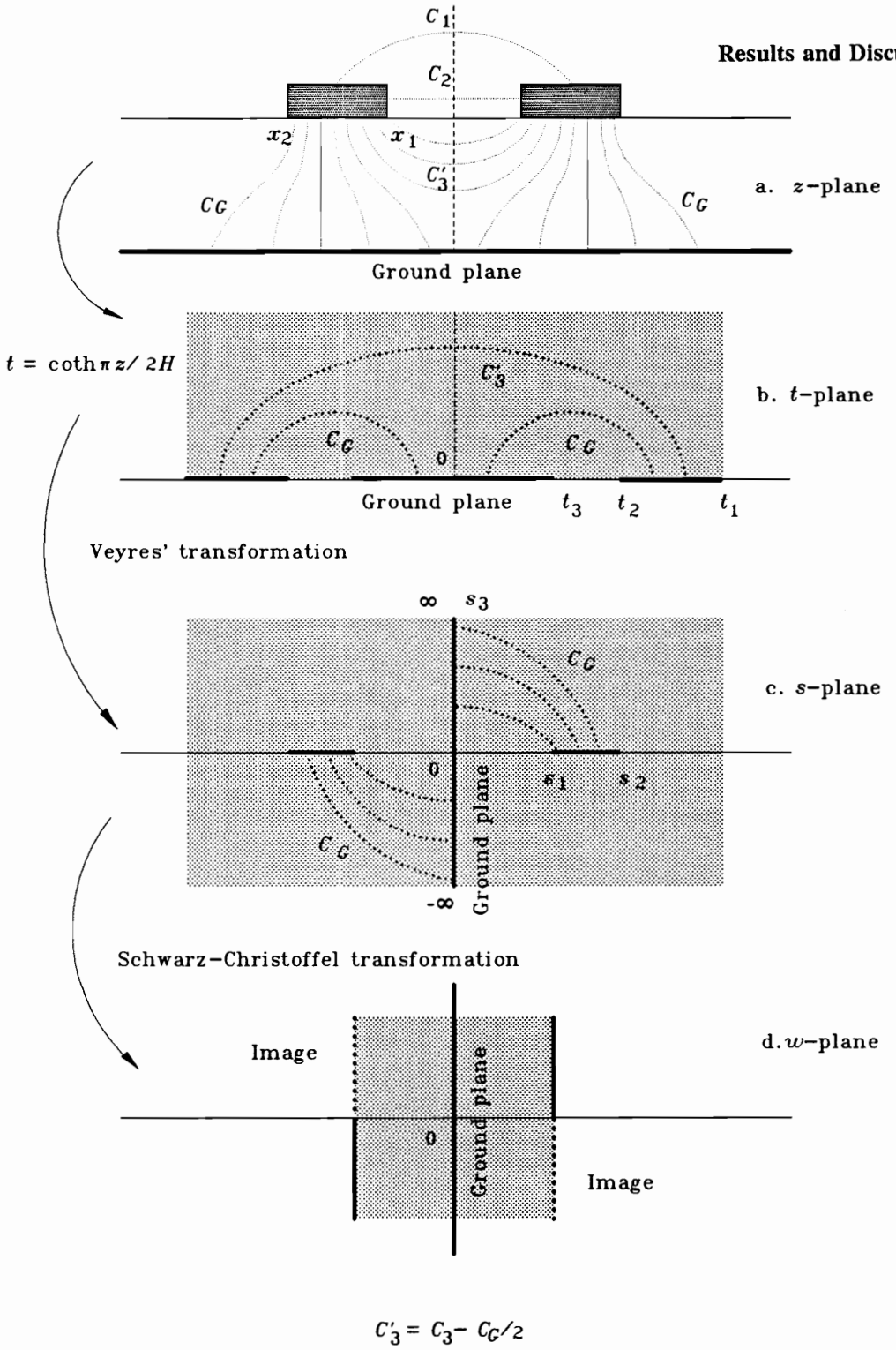

Fig. 5.20 Mutual capacitance calculation for Pattern #1

$$s = \frac{t}{t_1}\sqrt{\frac{t_1^2 - 1}{t^2 - 1}} \tag{5.36}$$

Thus, using the Schwarz-Christoffel transformation again, C_G may be calculated (Fig. 5.20.d). When a ground plane exist, the capacitance between the ground plane and transmission line is calculated using imaginary transmission line. Simultaneously, this C_G is in series in the actual structure. Therefore, the total line capacitance is:

$$\frac{C_G}{2} = \frac{1}{2}\frac{K(k'_2)}{2K(k_2)} \tag{5.37}$$

where

$$k_2 = \frac{s_1}{s_2} = \frac{1}{s_2} = \frac{t_1}{t_2\sqrt{\frac{t_1^2 - 1}{t_2^2 - 1}}} = \frac{\coth\frac{\pi}{2H}x_1}{\coth\frac{\pi}{2H}x_2\sqrt{\frac{\coth^2\frac{\pi}{2H}x_1 - 1}{\coth^2\frac{\pi}{2H}x_2 - 1}}}$$

Therefore, the mutual capacitance of interest is given by:

$$C_m = C_1 + C_2 + C'_3$$
$$= e_o \frac{K(k'_o)}{2K(k_o)} + e_o \frac{T}{D} + e \frac{K(k'_1)}{2K(k_1)} - e \frac{K(k'_2)}{4K(k_2)} \quad (5.38)$$

Fig. 5.21 shows a comparison between Cohn's mapping and the new conformal mapping. It is seen that the new conformal mapping yields a better fit, especially as line separation increases.

Since Pattern A has an anisotropic dielectric (TOS layer on the alumina substrate) it is not easy to find a closed-form solution for this case. However, considering the structural situation, an approximation can be used. When the line separation is very narrow, electric fields between two the transmission lines will be concentrated at the subsurface of the dielectric substrate (Fig. 5.22.a). When a ground plane exists, some of the electric field flux will be attracted to the ground plane. Thus, an approximation can be carried out in such a way that the dielectric constant of the TOS is used for pure mutual capacitance between two lines (C_3) before obtaining the resultant mutual capacitance C'_3. As the line separation increases, the electric field between the two transmission lines will occupy a larger portion of the substrate if the ground plane does not exist. With the ground plane pesent, however, most of electric flux is attracted, leaving only a small portion at the subsurface (Fig. 5.22.d). Therefore, the second approximation can be applied in such a manner that the dielectric constant of the TOS is used to determine C'_3. Fig. 5.23 shows the two approximations and the measured mutual capacitance of Pattern A where the dielectric constant 7.5 was used for TOS (dielectric constant of

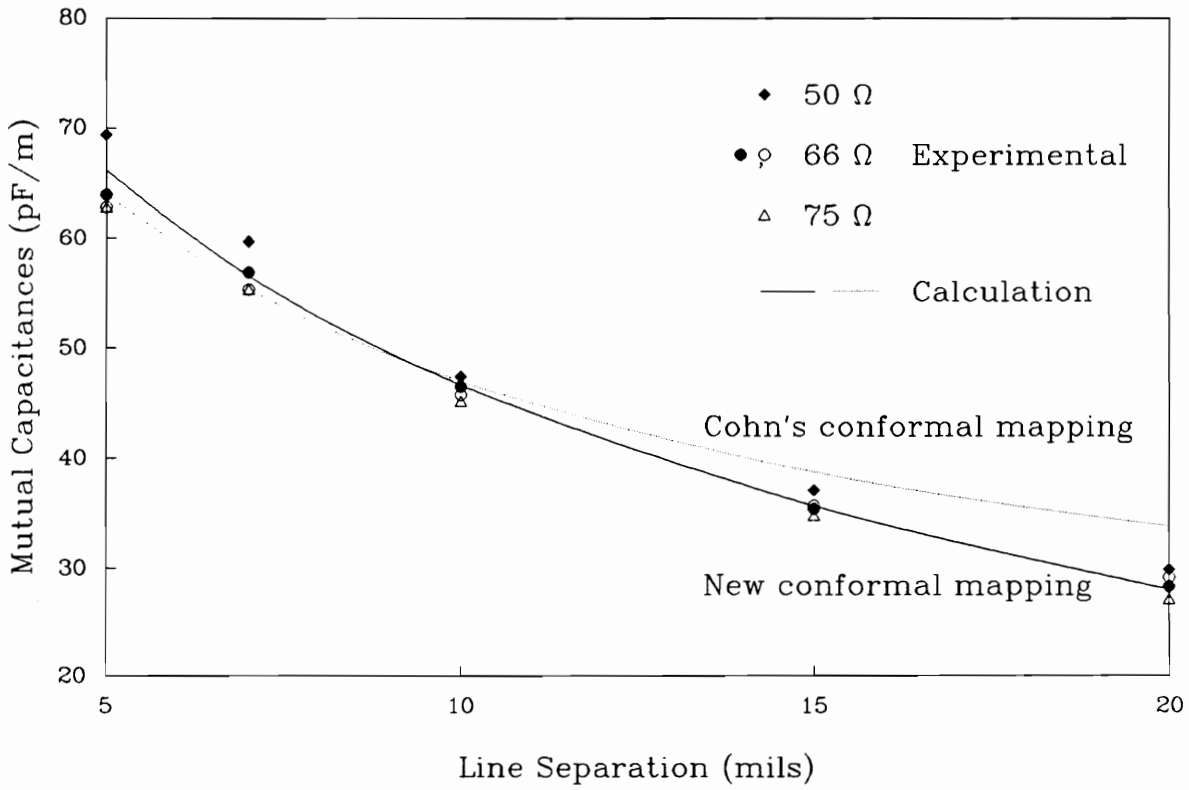

Fig. 5.21 Comparison between calculated and measured mutual capacitances for Pattern #1(with ground plane), versus line separation

a. Narrow line spacing without ground plane
The original electric fields are concentrated at subsurface.

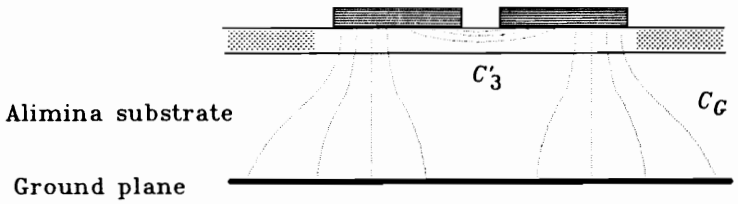

b. Narrow line spacing with ground plane

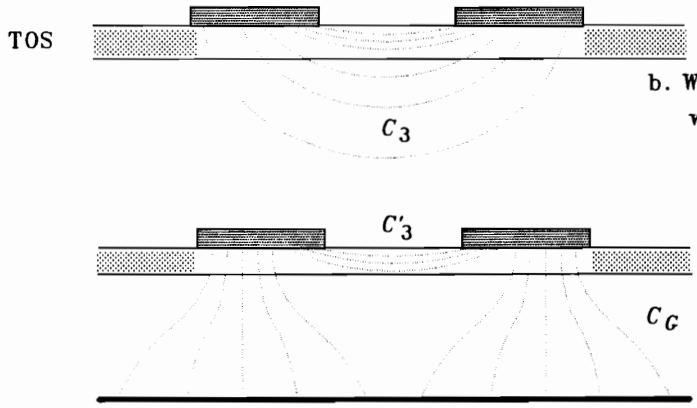

b. Wide line spacing without ground plane

d. Wide line spacing with ground plane.
The resultant electric fields remain at subsurface.

Fig. 5.22 Mutual capacitance calculation for Pattern A. The following approximation can be applied, depending on line separation: Use dielectric constant of TOS for C_3 (mutual capacitance without ground plane) in case of narrow line spacing, and that for C'_3 (mutual capacitance with ground plane) in case of wide spacing.

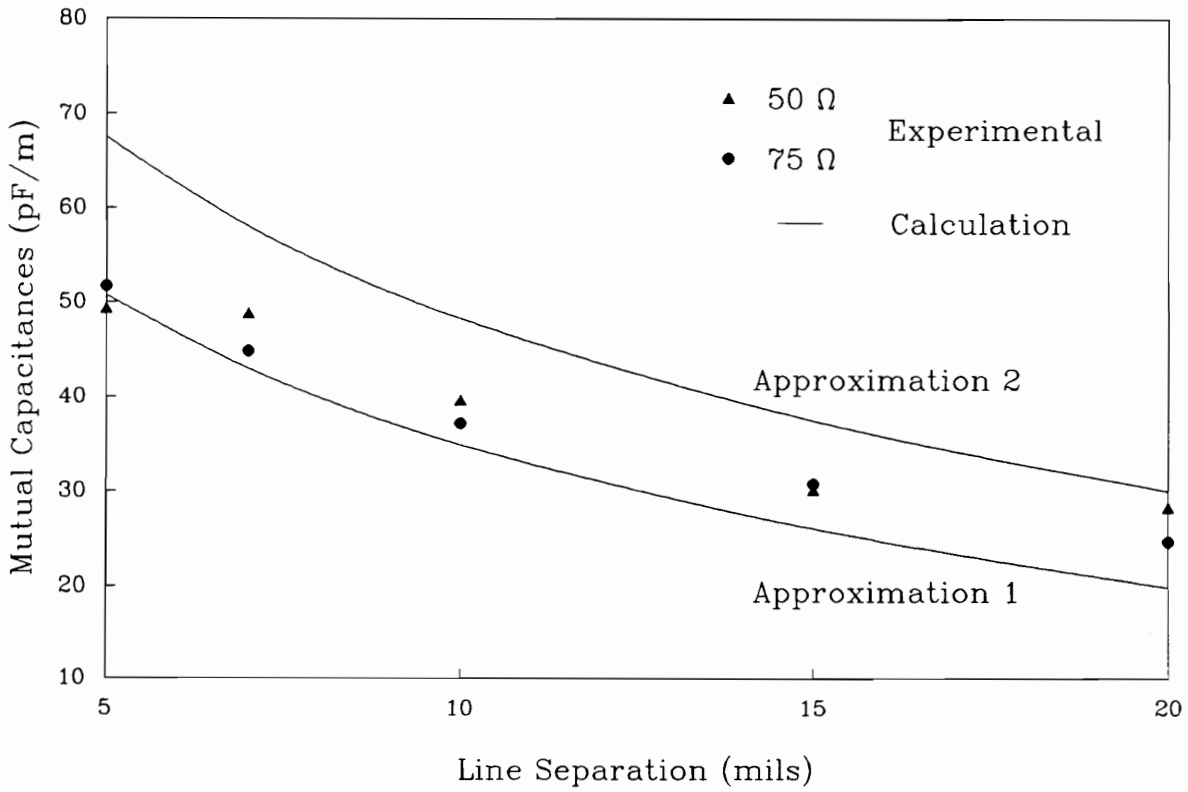

Fig. 5.23 Comparison between calculated and measured mutual capacitance versus line separation for Pattern A.

5 mils for example, the first approximation shows good agreement, while the second

of TOS known to be in the range 7-8[1]). When the line separation is narrow, 5 mils for example, the first approximation shows good agreement, while the second approximation fits quite well for wide line separations.

In Pattern B, transmission lines screened onto an alumina substrate have been covered by TOS dielectric. It is assumed again that electric flux lines between the two transmission line are stored in the TOS layer, regardless of its thickness since the dielectric constant of TOS is still large compared to that of air (Fig. 5.24). When mutual capacitance is calculated with this assumption, the result gives fairly good agreement, as shown in Fig. 5.25.

The mutual capacitance of Pattern C can be obtained by combining techniques described above. Hence, the mutual capacitance can be expressed as[4]:

$$C_m = C_{12} - \frac{C_1 C_2}{C_1 + C_2} \tag{5.39}$$

where C_{12} is the mutual capacitance without ground, and C_1, C_2 are self-capacitances with ground. Thus, each capacitance is calculated independently and the resultant mutual capacitance is obtained from Eq.(5.39). Fig. 5.26 shows each conformal transformation for Pattern C. The calculated and measured mutual capacitance of Pattern C versus line separation (number of TOS layers) are shown in Fig. 5.27.

5.3.3 Crosstalk prediction

The crosstalk model was developed in § 5.2 including ground voltage drop. The mutual parameter calculation was performed in § 5.3 showing comparison between calculation and experimental data. If the crosstalk model is combined with

the mutual parameter calculation, arbitrary crosstalk can be predicted. An example of such crosstalk prediction for Pattern #3 is illustrated in Fig. 5.28.

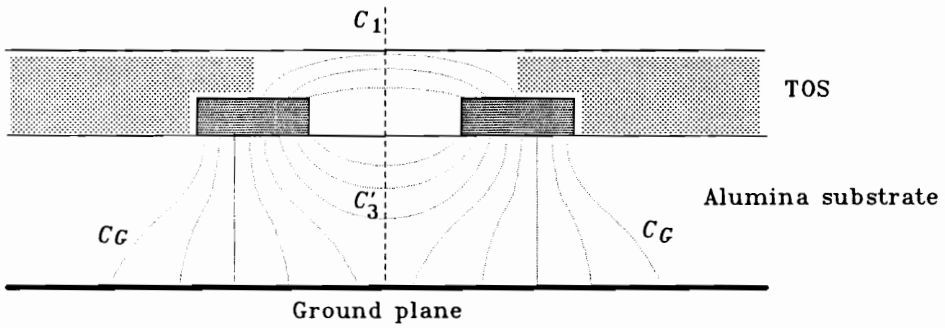

Fig. 5.24 Mutual capacitances of Pattern B. Electric fields are assumed to be stored in TOS layer.

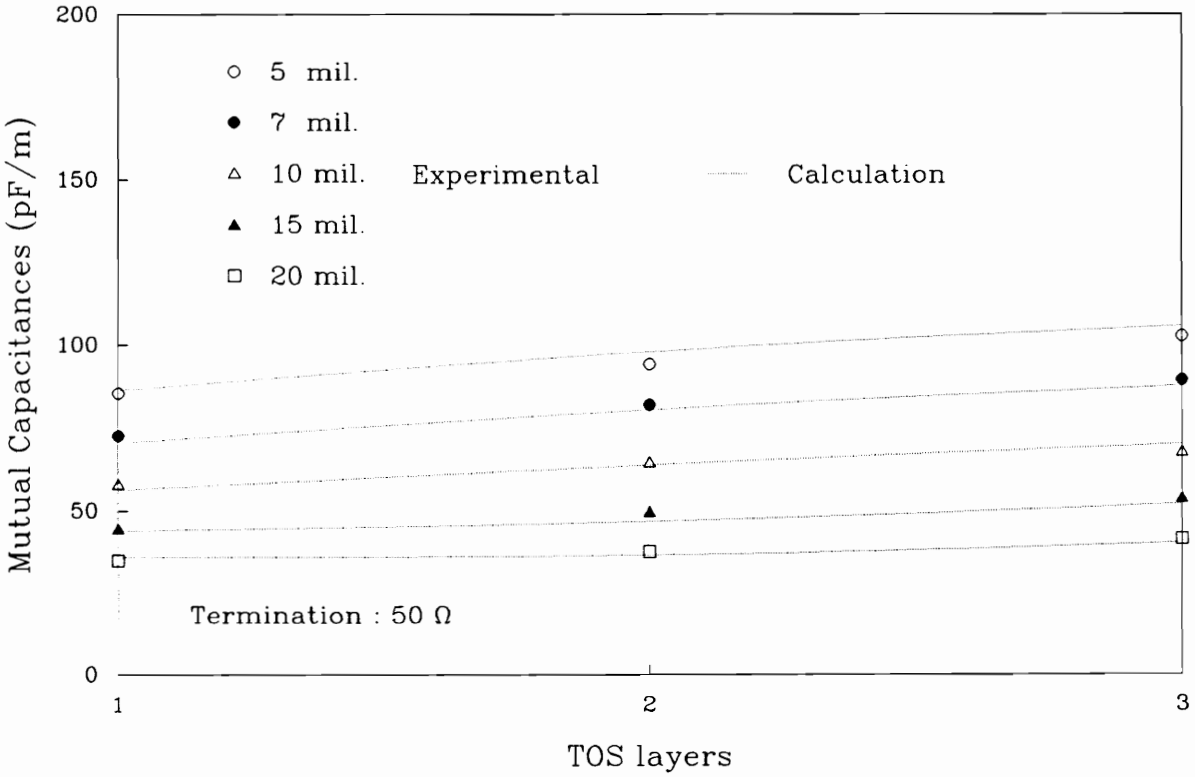

Fig. 5.25 Comparison between calculated and measured mutual capacitance of Pattern B versus number of TOS layers.

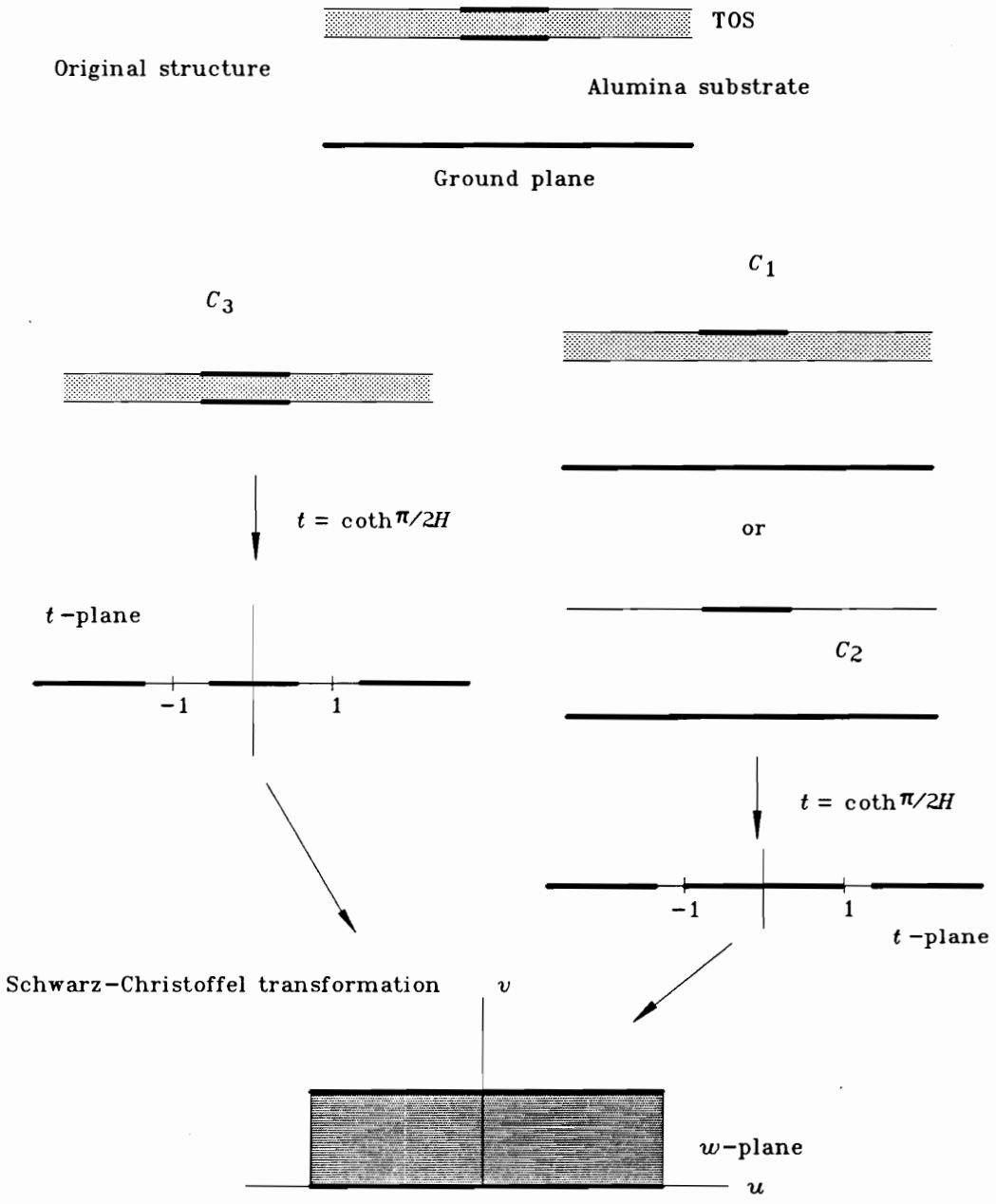

Fig. 5.26 Mutual capacitance calculation of Pattern C.
$C_1 \approx C_2 = C_G$ and $C'_3 = C_3 - C_1 C_2 / (C_1 + C_2)$.

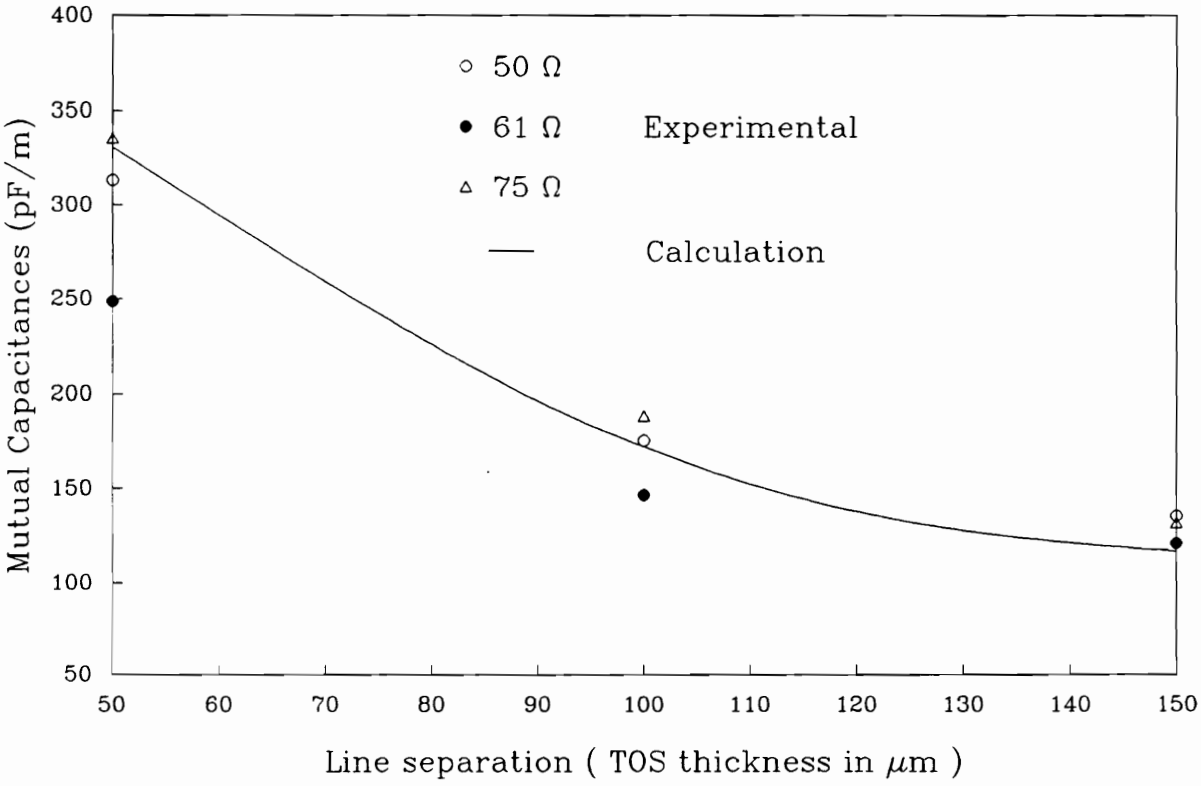

Fig. 5.27 Comparison between calculated and measured mutual capacitance for Pattern C, versus TOS thickness

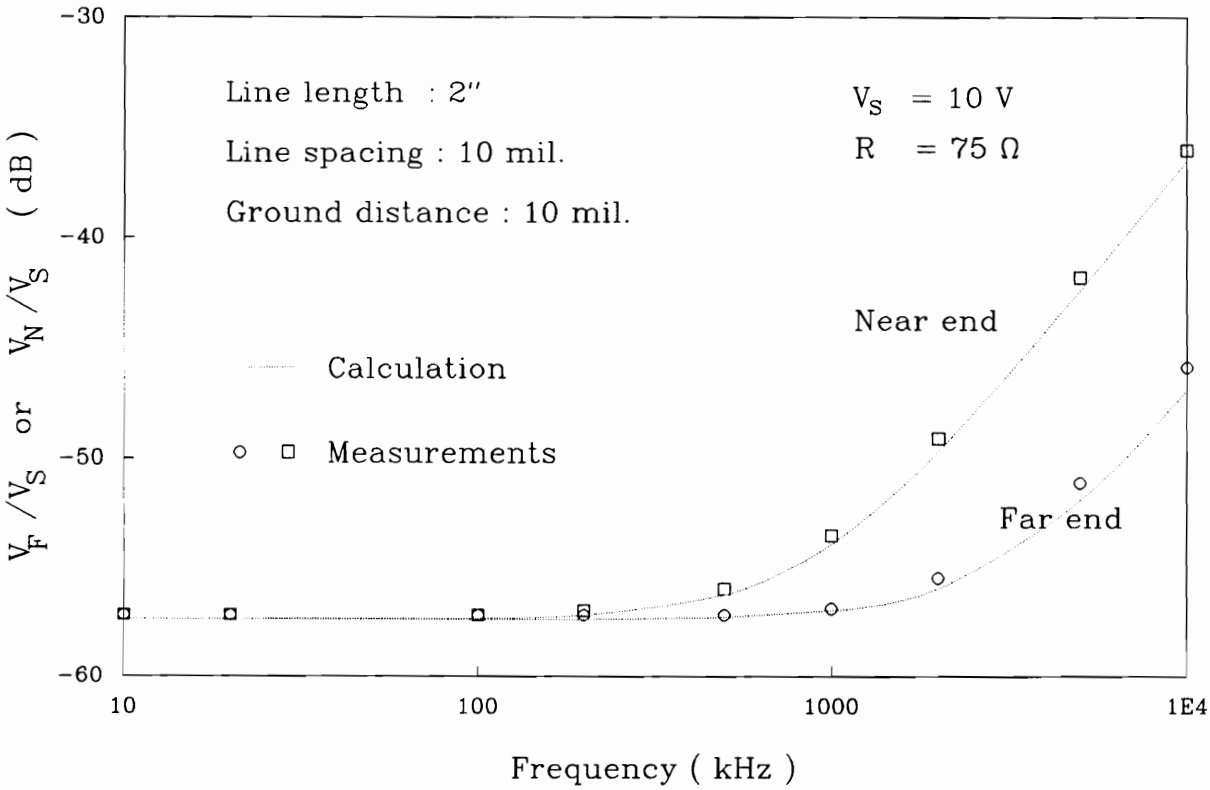

Fig. 5.28 Comparison between simulation and measurements for crosstalk of Pattern #3 versus frequency.

§ 5.4 Miscellaneous

On the assumption that termination resistance was much larger than line resistance, line resistance was not considered in crosstalk analysis. Transmission line resistance may contribute to crosstalk; however, as long as it is negligibly small compared to termination resistance, the crosstalk equations in Eq.(5.17) are still valid since transmission line is essentially lossless at low frequencies. However, when termination resistances are comparable to the line resistance, Eq.(5.17) needs modification due to line voltage changes along the transmission line.

The input source was sinusoidal in this research. When the source signal becomes digital (a trapezoidal signal, for instance) rather than analog, output crosstalk will show results given by Eq.(5.20). But when the rise time is not so short, a trapezoidal input signal can be approximated in such a way that the time derivative term $\frac{\partial V_s}{\partial t}$ in Eq.(5.17) is expressed as $\frac{\Delta V_s}{\Delta t}$ where Δt is equivalent to the rise time of the trapezoidal signal. In general, at frequencies higher than 1 GHz, Eq.(5.20) is valid[25]. But depending on line length, the time derivative approximation given above can be applied for a resonable frequency range.

Chapter VI

Conclusions

Crosstalk concerns are not confined to high frequency applications. It is necessary to study low-frequency crosstalk when considering recent trends in multilayer circuits, especially as line separations shrink. Crosstalk prediction is therefore critical to circuit design in order to reduce such interference. In this research, the following results were obtained:

a. Frequency dependence of crosstalk was confirmed.

b. Simple low-frequency crosstalk equations were derived, which agree with published equations.

c. New conformal mapping techniques were developed to calculate mutual capacitance between coupled transmission lines.

d. The effect of a ground line on mutual capacitance is not significant.

e. In a multilayer system, when transmission lines are printed on TOS, mutual capacitance can be calculated with good accuracy for both narrow and wide line separation. In this case, it was assumed that electric flux between two transmission lines exist at the subsurface of the dielectric when a ground plane exists.

f. In a multilayer system, when the transmission lines are covered with TOS, the mutual capacitance can be calculated by assuming the electric fields are stored in the TOS, regardless of the number of layers.

g. Crosstalk prediction was carried out by combining crosstalk equations with calculated mutual parameters.

A new conformal mapping technique has shown an exact closed-form solution for Pattern #1, #2, and #3 which have a single dielectric substrate. Even though reproducibility was not proven in this research, repeatability (Fig. 5.18, for example) and good agreement between data and theory with many variations support this reproducibility indirectly.

It was possible to assume that every electric field is stored in the substrate or TOS because of their high dielectric constants compared to that of the air medium. When a substrate or TOS with low permittivity is used, the above assumption is no longer acceptable. In addition to this limitation, more than two layers of different materials in a multilayer arrangement will also require modification in the conformal mapping techniques. In conclusion, the above results can be applied, as a design guideline, to areas such as mutilayers with conductors at many different depths and two sided substrates. But future work is needed for more complicated fields such as crossover metal strips, three dimensional crosstalk (when long vertical via lines exist), etc..

Appendix

A. Conformal mapping (§ 3.2)

When $w=f(z)$ is an analytic function, we can define

$$\frac{dw}{dz} = \lim_{\Delta z \to 0} \arg \frac{\Delta w}{\Delta z} \tag{A.1}$$

where arg stands for the phase of a complex function.

Assuming that this equation is in polar form,

$$\begin{aligned} &\arg \lim_{\Delta z \to 0} \frac{\Delta w}{\Delta z} = \lim_{\Delta z \to 0} \arg \frac{\Delta w}{\Delta z} \\ &= \lim_{\Delta z \to 0} \arg \Delta w - \lim_{\Delta z \to 0} \arg \Delta z = \alpha \end{aligned} \tag{A.2}$$

where α, the argument of the derivative, may depend on z but is a constant for a fixed z, independent of the direction of approach. To see the significance of this, consider two curves, C_z in the z-plane and the corresponding curve C_w in the w-plane (Fig. A.1). The increment Δz is shown at an angle of θ relative to the real x-axis whereas the corresponding increment Δw forms an angle ϕ with the real u-axis. From Eq.(A.2)

$$\phi = \theta + \alpha \tag{A.3}$$

or any line in the z-plane is rotated through an angle α in the w-plane as long as w is an analytic transformation and the derivative is not zero.

Let us consider a transmission line cross section that is defined by equi-potential surfaces in the z-plane. To find the line parameters, we shall solve Laplace

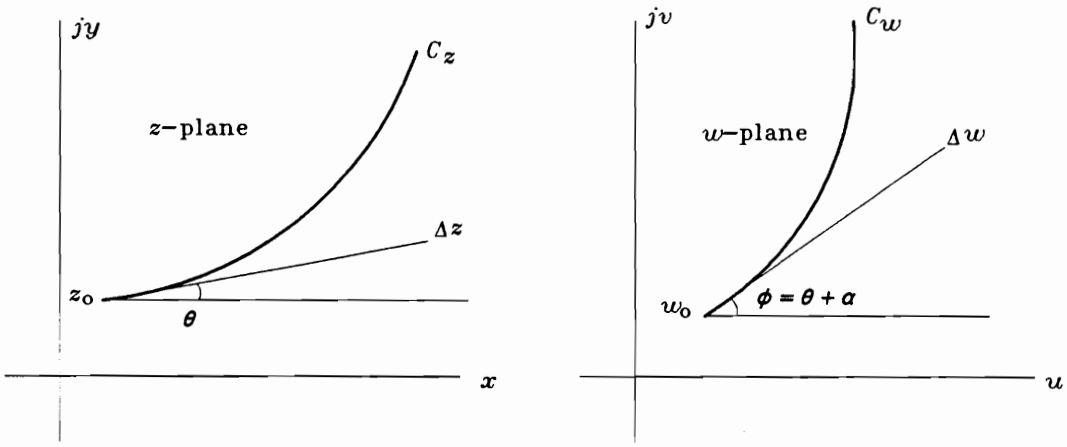

Fig. A.1 Conformal transformation: angles are preserved.

$$\Delta\phi = \phi_2 - \phi_1 = (\theta_2 + \alpha) - (\theta_1 + \alpha) = \theta_2 - \theta_1 = \Delta\theta$$

equation on the plane,

$$\nabla^2 \varphi = \frac{\partial^2 \varphi}{\partial x^2} + \frac{\partial^2 \varphi}{\partial y^2} \tag{A.4}$$

subject to the boundary conditions $\varphi = \varphi_1$ on line 1 surface and $\varphi = \varphi_2$ on line 2 surface. If one starts in the z-plane, and if a solution of the Laplace equation in the w-plane is still a solution in the z-plane when transformed back into z-plane, the new geometry in the w-plane can be used to solve the original geometry in the z-plane. In the w-plane,

$$\Psi(u, v) = \Psi[u(x, y), v(x, y)] = \varphi(x, y) \tag{A.5}$$

Differentiating $\Psi(u, v)$ with respect to x, we obtain

$$\begin{aligned} \frac{\partial \Psi(u, v)}{\partial x} &= \frac{\partial \Psi}{\partial u}\frac{\partial u}{\partial x} + \frac{\partial \Psi}{\partial v}\frac{\partial v}{\partial x} \\ \frac{\partial^2 \Psi}{\partial x^2} &= \frac{\partial \Psi}{\partial u}\frac{\partial^2 u}{\partial x^2} + \frac{\partial^2 \Psi}{\partial u^2}\left(\frac{\partial u}{\partial x}\right)^2 + 2\frac{\partial^2 \Psi}{\partial u\,\partial v}\frac{\partial u}{\partial x}\frac{\partial v}{\partial x} \\ &\quad + \frac{\partial \Psi}{\partial v}\frac{\partial^2 v}{\partial x^2} + \frac{\partial^2 \Psi}{\partial v^2}\left(\frac{\partial v}{\partial x}\right)^2 \end{aligned} \tag{A.6}$$

A similar result holds for $\frac{\partial^2 \Psi}{\partial y^2}$. Then

$$\frac{\partial^2 \varphi}{\partial x^2} + \frac{\partial^2 \varphi}{\partial y^2} = \frac{\partial^2 \Psi}{\partial x^2} + \frac{\partial^2 \Psi}{\partial y^2} - \left(\frac{\partial^2 u}{\partial x^2} + \frac{\partial^2 u}{\partial y^2} \right) \frac{\partial \Psi}{\partial u}$$

$$+ \left(\frac{\partial^2 v}{\partial x^2} + \frac{\partial^2 v}{\partial y^2} \right) \frac{\partial \Psi}{\partial v} + 2 \left(\frac{\partial u}{\partial x} \frac{\partial v}{\partial x} + \frac{\partial u}{\partial y} \frac{\partial v}{\partial y} \right) \frac{\partial^2 \Psi}{\partial u \partial v} \qquad \text{(A.7)}$$

$$+ \left[\left(\frac{\partial u}{\partial x} \right)^2 + \left(\frac{\partial u}{\partial y} \right)^2 \right] \frac{\partial^2 \Psi}{\partial u^2} + \left[\left(\frac{\partial v}{\partial x} \right)^2 + \left(\frac{\partial v}{\partial y} \right)^2 \right] \frac{\partial^2 \Psi}{\partial v^2}$$

On the right-hand side of Eq.(A.7), the first two parentheses vanish, for u and v both satisfy Laplace's equation when w is analytic. The expression in the third set of parentheses yields zero from the Cauchy-Riemann conditions, and the same conditions show that the two square brackets are equal[42]. The result is then

$$\nabla^2 \varphi(x, y) = \left[\left(\frac{\partial u}{\partial x} \right)^2 + \left(\frac{\partial u}{\partial y} \right)^2 \right] \nabla^2 \Psi(u, v) = 0 \qquad \text{(A.8)}$$

because $\Psi(u, v)$ is known to satisfy Laplace's equation in the w-plane. Therefore, when a solution of Laplace's equation is subject to an analytic transformation, it remains a solution of Laplace's equation. Finally, a solution of Laplace's equation satisfying a complete set of boundary conditions is unique. Our transformed solution (satisfying our boundary conditions) is the final solution.

B. Schwarz-Christoffel Transformation (§ 3.2.2)

To develop the Schwarz-Christoffel transformation, first consider the function:

$$\frac{dw}{dz} = A (z - a)^{-\alpha/\pi} \qquad \text{(B.1)}$$

in which A is a complex constant, α is a real constant, and a is a point on the real x-axis (Fig. B.1).

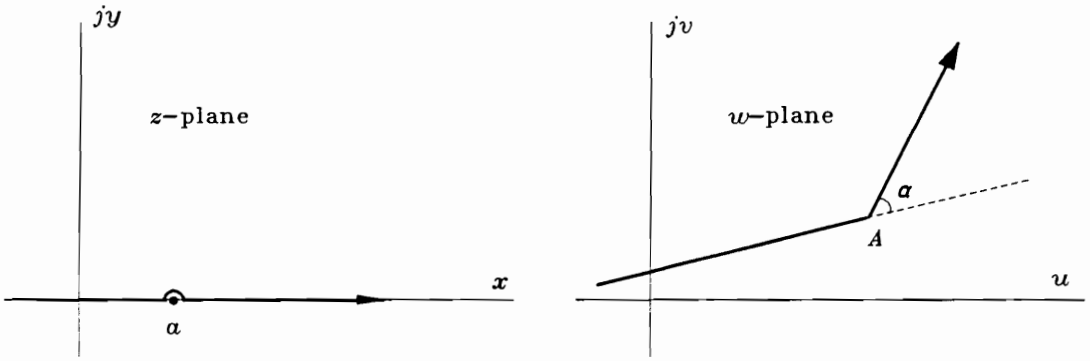

Fig. B.1 Schwarz–Christoffel transformation

Thus, when $z>a$,

$$\arg \frac{dw}{dz} = \arg A \tag{B.2}$$

and when $z<a$,

$$\frac{dw}{dz} = A(z - a)^{-\alpha/\pi}(-1)^{-\alpha/\pi} \tag{B.3}$$

Since $e^{j\pi/2} = \cos \pi/2 + j\sin \pi/2 = j$, $(-1)^{-\alpha/\pi} = e^{-j\alpha}$ and

$$\frac{dw}{dz} = A(z - a)^{-\alpha/\pi} e^{-j\alpha} \tag{B.4}$$

We can say,

$$\arg \frac{dw}{dz} = \arg A - \alpha \qquad z < a \qquad \text{(B.5)}$$

Since A is a constant, $\arg A$ is a constant and w therefore is represented by a pair of straight-line segments which form an exterior angle α. From the factor $e^{-j\alpha}$, in Eq.(B.4), we obtain one vertex of a polygon. By including n factors of this form we may construct an n vertex polygon represented by:

$$\frac{dw}{dz} = A(z-a)^{-\alpha/\pi}(z-b)^{-\beta/\pi}(z-c)^{-\gamma/\pi} \cdots (z-n)^{-\nu/\pi} \qquad \text{(B.6)}$$

with the constraint on the angles

$$\alpha + \beta + \gamma + \cdots + \nu = 2\pi \qquad \text{(B.7)}$$

By integrating Eq.(B.6) we obtain

$$w = A \int^{z} (z-a)^{-\alpha/\pi}(z-b)^{-\beta/\pi}(z-c)^{-\gamma/\pi} \cdots (z-n)^{-\nu/\pi} dz + B \qquad \text{(B.8)}$$

where B is a constant.

C. Geometric mean distance (§ 3.3.3)

In calculating the mutual inductance between straight conductors of any given cross sections, the following integral is necessary[41]:

$$\int\int\int\int \ln d \; dxdydx'dy' \qquad \text{(C.1)}$$

where $dx\,dy$ is an element of the area of the cross section of the first conductor, $dx'dy'$, an element of the second section, and d,the distance between these elements. The above integral is extended first over every element of the first section, and then over every element of the second. A distance S can be defined such that integral of Eq.(C.1) is equal to

$$A_1 A_2 \ln S \tag{C.2}$$

when A_1 and A_2 are the areas of the two cross sections. Here S may be considered as the geometrical mean of the distances between pairs of elements. It is evident that the value of S must be intermediate between the greatest and the least values of d.

Bibliography

1. "Processing and Performance Data," DuPont Green Tape System Manual, E.I. DuPont De Nemours & Co., Inc., 1988.

2. "Computing Device," Federal Communications Commission Rules and Regulations, Vol. 2, Part 15, Subpart J, pp. 160-176, July 1981.

3. C. Wei, R.F. Harrington, J.R. Mautz and T.K. Sarkar, "Multiconductor Transmission lines in Multilayered Dielectric Media," *IEEE Transactions on Microwave Theory and Techniques*, Vol. MTT-32, pp. 439-450, April 1984.

4. C.R. Paul, "Modeling Electromagnetic Interference Properties of Printed Circuit Boards," *IBM J. Develop.*, Vol. 33, No. 1, pp. 33-50, January 1989.

5. R.E. Matick, "Transmission Lines for Digital and Communication Networks," New York: McGraw-Hill, pp. 270, 1969.

6. D.B. Jarvis, "The Effects of Interconnections High-Speed Logic Circuits," *IEEE Trans. Electron. Comp.*, Vol. EC-12, No. 10, pp. 476-487, Oct., 1963.

7. C.R. Paul, "Solution of the Transmission-Line Equations for Three-Conductor Lines in Homogeneous Media," *IEEE Trans. Electromagnetic Compatibility*,

Vol. EMC-20, No. 1, pp. 216-222, Feb., 1978.

8. C.S. Meyer, D.K. Lynn, and D.J. Hamilton, "Analysis and Design of Integrated Circuits," McGraw-Hill Book Co., pp. 341-356, 1968.

9. N. Schibuya and K. Ito, "Crosstalk Noise Analysis of Wiring on the Printed Circuit Board," *Electronics and Communications in Japan*, Part 1, Vol. 70, No. 4, pp. 63-72, 1987.

10. A.J. Rainal, "Transmission Properties of Various Styles of Printed Wiring Boards," *The Bell System Technical Journal*, Vol. 58, No. 5, pp. 995-1013, May-June, 1979.

11. A. Feller, H.R. Kaupp and J.J. Digiacomo, "Crosstalk and Reflections in High-Speed Digital Systems," *AFIPS Conf. Proc.*, Fall Jt., Computer Conf., Vol. 27, pp. 511-525, 1965.

12. R.J. Mohr, "Coupling Between Open and Shielded Wire Lines Over a Ground Plane," *IEEE Trans. Electromagnetic Compatibility*, Vol. EMC-9, No. 2, pp. 34-45, Sept., 1967.

13. D.J. Riley and L.D. Bacon, "On the Limitation of the Weak-Coupling Assumption for Crosstalk Analysis Based on Quasi-TEM Propagation," *IEEE Trans. Electromagnetic Compatibility*, Vol. 32, No. 1, pp. 28-37, Feb. 1990.

14. M. Cotte, "Théorie de la propagation d'ondes de choc sur deux lignes parallèles," *Rev. Gen. Elec.*, Vol. 56, pp. 343, 1947.

15. L.J. Greenstein and H.G. Tobin, "Analysis of Cable-Coupled Inteference," *IEEE Trans. Radio Freq. Interference*, Vol. RFI-5, pp. 43-55, March 1963.

16. I. Catt, "Crosstalk (Noise) in Digital Systems," *IEEE Trans. Electronic Computers,* Vol. EC-16, No. 6, pp. 743-763, Dec. 1967.

17. V.K. Tripathi, "Asymmetric Coupled Transmission Lines in an Inhomogeneous Medium," *IEEE Trans. Microwave Theory and Techniques*, Vol. MTT-23, No. 9, pp. 734-739, Sept. 1975.

18. C.R. Paul, "Useful Matrix Chain Parameter Identities for the Analysis of Multiconductor Transmission Lines," *IEEE Trans. Microwave and Theory Techniques.*, Vol. MTT-23, No. 9, pp. 756-760, Sept. 1975.

19. S.B. Cohn, "Shielded Coupled-Strip Transmission Line," *IRE Trans. Microwave Theory and Techniques*, Vol. MTT-3, pp. 29-38, Oct. 1955.

20. T.G. Bryant and J.A. Weiss, "Parameters of Microstrip Transmission Lines and of Coupled Pairs of Microstrip Lines," *IEEE Trans. Microwave Theory and Techniques*, Vol. MTT-16, NO. 12, pp. 1021-1027, Dec. 1968.

21. W.T. Weeks, "Calculation of Coefficients of Capacitance of Multiconductor Transmission Lines in the Presence of a Dielectric Interface," *IEEE Trans. Microwave Theory and Techniques*, Vol. MTT-18, No. 1, pp. 35-43, Jan. 1970.

22. C. Wei and R.F. Harrington, "Computation of the Parameters of Multiconductor Transmissiion Lines in Two Dielectric Layers above a Ground Plane," Dept. Electrical Computer Eng., Syracuse Univ., Rep. TR-82-12, Nov. 1982.

23. C. Wei, R.F. Harrington, J.R. Mautz, and T.K. Sarkar, "Multiconductor Transmission Lines in Multilayered Dielectric Media," *IEEE Trans. Microwave Theory and Techniques*, Vol. 32, No. 4, pp. 439-450, Apr. 1984.

24. S. Okugawa, "Analysis and Computation of Crosstalk Noise between Microstrip Transmission Lines," *Electronics and Communications in Japan*, Vol. 53-C, No. 7, pp. 128-136, 1970.

25. A. Djordjević, R.F. Harrington, T. Sarkar and M. Baždar, "Matrix Parameters for Multiconductor Transmission Lines : Software and User's Manual," Artech House, 1989.

26. W.T. Weeks, A.J. Jimenez, G.W. Mahoney, D. Mehta, H. Qassemzadeh, and T. Scott, "Algorithms for ASTAP-A Network-Analysis," *IEEE Trans. Circuit Theory*, Vol. CT-20, No. 6, pp. 628-634, Nov. 1973.

27. L.N. Dworsky, "Modern Transmission Line and Theory and Applications," John Wiley & Sons, pp. 1-136, 1979.

28. H.A. Schwarz, "Mathematische Abhandlungen," Vol. II, 2nd Ed. Chelsea Publishing Co., NY, pp. 84-100, 1972.

29. K.G. Black and T.J. Higgins, "Rigorous Determination of the Parameters of Microstrip Transmission Lines," *IRE Trans. Microwave Theory and Techniques*, Vol. MTT-3, No. 2, pp. 93-113, March 1955.

30. A.A. Oliner, "Equivalent Circuits for Discontinuities in Balanced Strip Transmission Line," *IRE Trans. Microwave Theory and Techniques*, Vol. MTT-3, No. 2, pp. 134-143, March 1955.

31. H.A. Wheeler, "Transmission-Line Properties of Parallel Wide Strips by a Conformal-Mapping Approximation," *IEEE Trans. Microwave Theory and Techniques*, Vol. MTT-12, pp. 280-289, May 1964.

32. C.P. Wen, "Coplanar Waveguide: A Surface Strip Transmission Line Suitable for Nonreciprocal Gyromagnetic Device Applications," *IEEE Trans. Microwave Theory and Techniques*, Vol. MTT-17, No. 12, pp. 1087-1090, Dec. 1969.

33. C. Veyres and V.F. Hanna, "Extension of the Application of Conformal Mapping Techniques to Coplanar Lines with Finite Dimensions," *Int. J. Electronics*, Vol. 48, No. 1, pp. 47-56, 1980.

34. G. Ghione and C. Naldi, "Parameters of Coplanar Waveguides with Lower Ground Plane," *Electronic Letters*, Vol. 19, No.18, pp. 733-734, 1st Sept. 1983.

35. S.M. Wentworth, D.P. Neikirk, and C.R. Brahce, "The High-Frequency Characteristics of Tape Automated Bonding (TAP) Interconnects," *IEEE Trans. Components, Hybrids, and Manufacturing Technology*, Vol. 12, No. 3, pp. 340-347, Sept. 1989.

36. F.W. Grover, "Inductance Calculations," D. Van Nostrand Co., Inc., 1947.

37. A.E. Ruehli, "Inductance Calculations in a Complex Integrated Circuit Environment," *IBM J. Res. Develop.*, Vol. 16, No. 5, pp. 470-481, Sept. 1972.

38. A.J. Rainal, "Computing Inductive Noise of Chip Packages," *AT&T Bell Lab. Technical Journal*, Vol. 63, No. 1, pp. 177-195, Jan. 1984.

39. W.C. Johnson, "Transmission Lines and Networks," McGraw-Hill Book Co., Inc., pp. 1-26, 1950.

40. C.R. Chester, "Techniques in Partial Differential Equations," McGraw-Hill Book Co., pp. 11-62, 1971.

41. J.C. Maxwell, "A Treatise on Electricity and Magnetism," Part IV, Chapter XIII, Dover Publications, Inc., pp. 691-692, 1954.

42. G. Arfken, "Mathematical Methods for Physicists," 2nd Ed., Academic Press., International Edition, pp. 330-333, 1970.

Vita

I. K. Yoo was born in Korea in 1953. He received a B.S. degree in Metallurgical Engineering from Hanyang University, Seoul, Korea in 1975. He joined the Army service from 1975-1977, and worked at Hyundai Heavy Industries Co., Korea, from 1978-1984 where he received the Level III Certificate for non-destructive examination and Superviser's License for radiation handling. In 1983, he also received the Presidential Award in management education. He married Kyesook in 1979 and had his first child, a son, in 1981. He decided in 1984 to continue his study and attended Virginia Tech, where he received M.S. and Ph.D. degrees in Materials Engineering in 1986 and in Materials Engineering Science in 1990, respectively. His primary research interest is in the field of thick film dielectric materials.